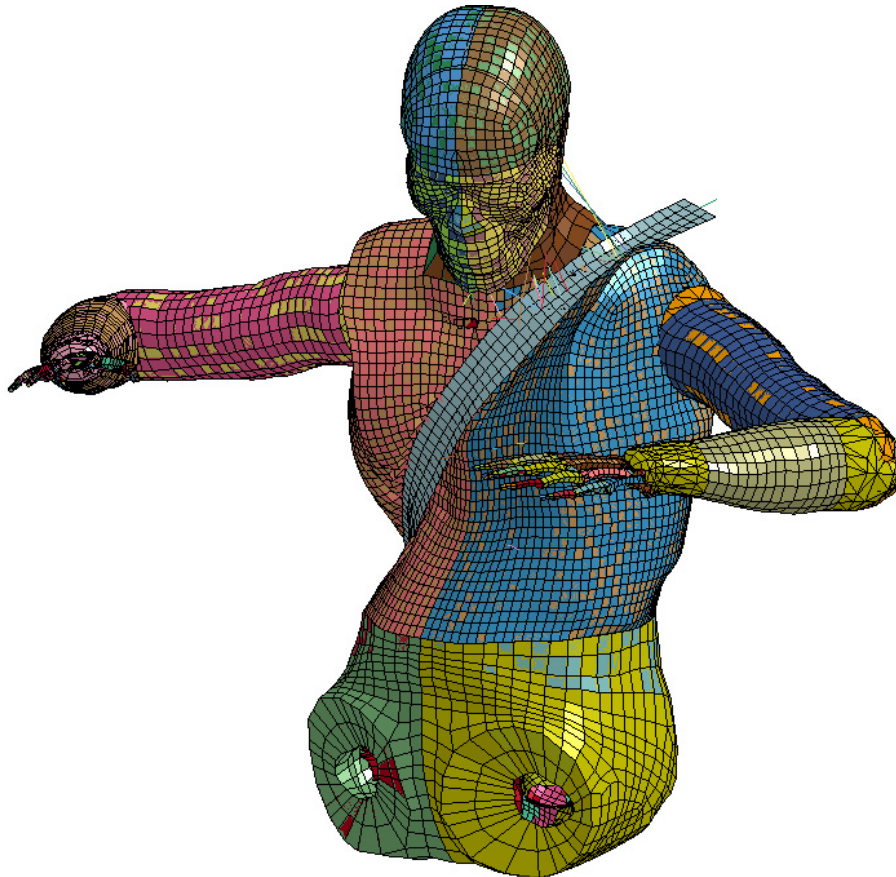


# CHALMERS



## Thorax soft tissue response for validation of human body models and injury prediction

*Master's Thesis in Applied Mechanics*

JAN-FREDERIK RATER

Vehicle Safety Division  
Department of Applied Mechanics  
CHALMERS UNIVERSITY OF TECHNOLOGY  
Gothenburg, Sweden, 2013  
Master's Thesis 2013:07



THESIS FOR THE DEGREE OF A GRADUATED ENGINEER

in

MECHANICAL ENGINEERING

Thorax soft tissue response for validation  
of human body models and injury  
prediction

by

JAN-FREDERIK RATER

Vehicle Safety Division  
Department of Applied Mechanics  
CHALMERS UNIVERSITY OF TECHNOLOGY  
Gothenburg, Sweden, 2013

**Thorax soft tissue response for validation of human body models and injury prediction**

JAN-FREDERIK RATER

© JAN-FREDERIK RATER, 2013

MASTER'S THESIS IN APPLIED MECHANICS no 2013:07  
ISSN 1652-8557

Department of Applied Mechanics  
Chalmers University of Technology  
SE-412 96 Gothenburg  
Sweden  
Telephone + 46 (0)31-772 1000

Cover:  
THUMS v3-M under single belt loading conditions in simulated table top tests by Kent et al. (2004)

Department of Applied Mechanics  
Gothenburg, Sweden, 2013

Thorax soft tissue response for validation of human body models and injury prediction  
Master's Thesis in Applied Mechanics  
JAN-FREDERIK RATER  
Department of Applied Mechanics  
Vehicle Safety Division  
Chalmers University of Technology

## Abstract

Thoracic injuries like rib fractures and lung injuries are the most frequently occurring injuries in Road Traffic Collisions (RTCs). These injuries are severe and can be life-threatening. 81 % of all car occupants in fatal car accidents have thoracic injuries with an Abbreviated Injury Scale (AIS) score of 3+.

Seatbelt use and air bags reduce the fatality risk by 61 % compared to unbelted car occupants of vehicles without air bags. Nevertheless according to the National Highway Traffic Safety Administration (NHTSA) more than 30 000 people die each year due to RTCs in the USA.

For the validation of new restraint systems and for injury prediction Anthropomorphic Test Devices (ATDs) were traditionally used. ATDs are only gross mechanical representations of the human body and thus the information to predict injuries accurately is limited. A second tool for the investigation of restraint systems and injury prediction are Finite Element Human Body Models (FE-HBMs). They offer a more detailed description of the anatomy of the human body, e.g. viscera are represented. The quality of Human Body Models (HBMs) is limited by the amount of details and the validation level of particular parts.

Lungs are, besides ribs, the most frequently and severely injured part of the body in RTCs. Despite this no investigations to validate human lung models under frontal car crash like conditions have been carried out and experimental data for the dynamic behaviour and injury mechanism are an exception.

In this study, the state of the art of HBMs, models of the thorax and currently used material models for simulating thoracic viscera were identified.

To rate and validate these material models for lungs, impact experiments on swine lungs were simulated with LS-DYNA. The time and force response of the models were compared to the experimental results at an impact speed of  $5.4 \frac{m}{s}$ .

Coefficient studies with the parameter of different material models were accomplished to enhance the model response. For the best material model, low density foam, a new stress versus strain curve was also implemented, because the model tuning due to parameter optimization was limited.

The deformation behaviour of the final model was close to the experimental results. Only the force response for the first part of deformation was higher than compared to the experiments. For rating the model quality the deformation and force response were compared

---

to the experimental data based on the Mean Square Error (MSE). Finally, the MSE of the optimized material model was only half of the MSE of the best model from literature.

The final material model was implemented as material properties in the thoracic viscera of the Total HUMAN Model for Safety version 3.0 Modified (THUMS v3-M). The influence of the modified material model to the thoracic response and the biofidelity were proved against table top tests. The tuned material did not influence the thoracic response within the first 20 mm of chest deflection. Afterwards higher reaction forces occurred as thoracic response with the tuned model, but the forces stayed clearly inside the experimental corridor.

**KEYWORDS:** Frontal crash, thoracic injury criteria, lung injury, Human Body Model, Finite Element, model validation, THUMS, lungs modelling

# Acknowledgement

This thesis was carried out at SAFER for Chalmers University of Technology, Applied Mechanics department, Traffic Safety division under the supervision of Manuel Mendoza-Vazquez and Johan Davidsson.

I would like to thank several people for their encouragement, support, and patience during the work on this thesis.

At Chalmers University of Technology in the Vehicle Safety Division I gratefully thank my supervisor M.Sc. Manuel Mendoza-Vazquez for the support he provided me throughout the research. Without his academic guidance, numerical knowledge and moral support this project may never have been completed.

I would also especially like to thank Ph.D. Johan Davidsson that he provided me with the opportunity to carry out my work in SAFER - Vehicle and Traffic Safety Centre during an ERASMUS internship at Chalmers University of Technology.

I wish to thank Ingrid Middleton for her help with her perfect English skills and endless patience whenever it was needed.

I also would particularly like to thank my wonderful girlfriend Hanna for her support, love and help from the beginning until the end. You motivate me each day anew with your backing and encouraging words.

Finally, I would like to thank my parents, Bärbel and Hans-Joachim, as well as my sisters, Juliane and Katharine, who endlessly encourage me in everything I do. I am eternally grateful for your support, encouragement and patience without which my accomplishments would not have been possible.

Many thanks.

# Table of Contents

<b>List of Figures</b>	<b>X</b>
<b>List of Tables</b>	<b>XIII</b>
<b>List of Acronyms</b>	<b>XIV</b>
<b>1 Introduction</b>	<b>1</b>
1.1 Background and Research Justification . . . . .	1
1.2 Research Objectives and Scope . . . . .	2
<b>2 Literature Research</b>	<b>4</b>
2.1 Introduction . . . . .	4
2.2 Anatomy of the Thorax . . . . .	4
2.3 Car Crash Information . . . . .	6
2.3.1 Abbreviated Injury Scale . . . . .	6
2.3.2 Frontal Car Crashes . . . . .	6
2.3.3 Seatbelt Related Injuries . . . . .	7
2.4 Human Body Models . . . . .	9
2.4.1 History . . . . .	10
2.4.2 Thoracic Modelling . . . . .	12
2.4.3 Total Human Model for Safety . . . . .	13
2.5 ATDs and Injury Prediction . . . . .	15
2.6 Lung Parenchyma Experiments . . . . .	17
2.6.1 Hoppin 1975 - Properties of Lung Parenchyma in Distortion . . .	17
2.6.2 Vawter 1978 - Elasticity of Excised Dog Lung Parenchyma . . .	18
2.6.3 Zeng 1987 - Measurement of the Mechanical Properties of the Human Lung Tissue . . . . .	20
2.7 Validation Experiments . . . . .	20
2.7.1 Hayamizu 2003 - Measurement of Impact Response of Pig Lung .	21
2.7.2 Kent 2004 - Thoracic Response to Dynamic, Non-Impact Load- ing from a Hub, Distributed Belt, Diagonal Belt and Double Di- agonal Belts . . . . .	23
2.8 Material Models . . . . .	23
2.8.1 Strain-Energy Function . . . . .	24
2.8.2 Viscoelastic Material Behaviour . . . . .	26
2.8.3 Low Density Foam . . . . .	26
<b>3 Methods</b>	<b>27</b>
3.1 Model . . . . .	27
3.1.1 THUMS . . . . .	27
3.1.2 Thoracic Organs . . . . .	27
3.2 Impact Response Tests following Hayamizu . . . . .	28
3.2.1 Experimental Modelling . . . . .	29

## Table of Contents

---

3.2.2	Contact Conditions . . . . .	31
3.2.3	Material Models . . . . .	31
3.2.4	Coefficient Study . . . . .	32
3.2.5	Load Curve Study . . . . .	33
3.3	Model Validation - Table Top Tests . . . . .	34
<b>4</b>	<b>Results</b>	<b>35</b>
4.1	Material Models . . . . .	35
4.1.1	Strain-Energy Function . . . . .	35
4.1.2	Viscoelastic Material Behaviour . . . . .	35
4.1.3	Low Density Foam . . . . .	36
4.1.4	Impact Speed Variation . . . . .	38
4.2	Coefficient Studies . . . . .	39
4.2.1	Strain-Energy Function . . . . .	39
4.2.2	Viscoelastic Material Behaviour . . . . .	41
4.2.3	Low Density Foam . . . . .	43
4.3	Load Curve Study . . . . .	44
4.4	Final Model Response . . . . .	47
4.5	Model Validation . . . . .	48
<b>5</b>	<b>Discussion</b>	<b>51</b>
5.1	Experimental Discussion . . . . .	51
5.1.1	Lung Tissue Experiments . . . . .	51
5.1.2	Impact Response Tests . . . . .	53
5.1.3	Table Top Tests . . . . .	54
5.2	Discussion of the Simulations . . . . .	54
5.2.1	Strain-Energy Function . . . . .	55
5.2.2	Viscoelastic Material Behaviour . . . . .	56
5.2.3	Low Density Foam . . . . .	56
5.2.4	Model Validation . . . . .	57
5.2.5	Summary . . . . .	58
5.3	Classification of the Results . . . . .	59
5.3.1	Comparability Between Human Lungs, Swine Lungs and the Lungs Model . . . . .	59
5.3.2	THUMS v3.0 Lung Model . . . . .	60
5.4	Injury Prediction . . . . .	60
<b>6</b>	<b>Conclusions</b>	<b>62</b>
6.1	Summary . . . . .	62
6.2	Future Work . . . . .	63
	<b>References</b>	<b>XV</b>
	<b>Appendix A</b>	<b>XXI</b>
	<b>Appendix B</b>	<b>XXII</b>

# List of Figures

2.1	Thoracic organs without muscles, ribs and sternum (a); lungs with pulmonary segments, anterior view (b); modified from Schuenke et al. (2006)	5
2.2	Injury regions and severe for drivers in frontal car crashes, Cuerden et al. (2007)	8
2.3	Seatbelt signs by Hayes et al. (1991)	9
2.4	An overview of recent FE-HBMs, Yang et al. (2006)	11
2.5	Stress versus strain curves from experiments and modified curves for low density foam, Mendoza-Vazquez et al. (2012); Vawter et al. (1978); Wang (1995)	13
2.6	THUMS v4: AF05, AM50 and AM95, Toyota (2011)	14
2.7	AIS injury severity depending to the velocity and compression for lungs and soft tissue, Lau and Viano (1986)	16
2.8	Rat lung model with maximum strain (a) and best correlation metric (b) for $\epsilon_{max} * \dot{\epsilon}_{max}$ , Gayzik et al. (2007)	18
2.9	Schematic drawing of the tissue testing set-up (a); extension ratio under symmetrical loading for all axes against normalized tensile force (b), Hoppin Jr. et al. (1975)	19
2.10	Slabs specimen testing under uni- or biaxial loading conditions Fung (1993) (a); stress versus strain curve for eleven specimens under uniaxial loading condition (b) Vawter et al. (1978)	19
2.11	Stress versus strain curve for a human lung tissue specimen subjected to a fixed load in x-direction and sinusoidally varied stretch in the y-direction, Zeng et al. (1987)	20
2.12	High speed impact pictures of a swine lung after different times for $5.4 \frac{m}{s}$ , Hayamizu et al. (2003)	21
2.13	Experimental results for lung impact experiments by Hayamizu et al. (2003)	22
2.14	Load cases for table top tests, Kent et al. (2004)	23
2.15	Force versus deflection and the corridors for hub, single and double diagonal belts and distributed loading conditions; the coefficients shown in each plot refer to the quadratic equation $y = \alpha x^2 + \beta x$ , Kent et al. (2004)	24
2.16	Kelvin-Maxwell model (a), Wang (1995); behaviour of the low density foam model and the influence of the shape and decay factor (b), Livermore (2012)	26
3.1	THUMS v3-M and isolated thoracic viscera	28
3.2	Load curve for low density foam following Mendoza-Vazquez et al. (2012) for thoracic organs	29
3.3	Model of the experimental set-up by Hayamizu et al. (2003) (isometric view)	30
3.4	Time versus displacement curve adjusted to the impact time and scaled to the model size	31
3.5	Schematic drawing of curve optimization with LS-OPT	33

## List of Figures

---

3.6	Experimental set-up of the table top tests by Kent et al. (2004) with a single belt; the arrow points to the place where the displacement was recorded . . . . .	34
4.1	Simulated experiments for different values of the strain-energy function at the moment of error termination . . . . .	36
4.2	Simulated experiments for different values of the viscoelastic material model at the moment of error termination (a) and (b) and after some particular elapsed time for normal termination by Roberts et al. (2005) (c) and (d) . . . . .	37
4.3	Thoracic volume deformation behaviour with the low density foam material model after different times with an impact speed of $5.4 \frac{m}{s}$ . . . . .	38
4.4	Experimental data by Hayamizu et al. (2003) and simulation data for an impact speed of $5.4 \frac{m}{s}$ . . . . .	38
4.5	Model response and experimental data for different impact speeds for low density foam material model . . . . .	39
4.6	MSE sensitivity study for the strain versus energy function with $a = \alpha$ and $b = \beta$ . . . . .	40
4.7	Model response for a coefficient study for the material model strain-energy function . . . . .	40
4.8	Stiffest ((a) and (b)) and softest ((c) and (d)) material models from the strain-energy function parameter study shown in Figure 4.7 . . . . .	41
4.9	MSE sensitivity study for the viscoelastic material model, with $g_0 = G_S$ , $g_i = G_L$ and $b = \beta$ . . . . .	41
4.10	Model response for a coefficient study of viscoelastic material behaviour . . . . .	42
4.11	Simulated thoracic volume with viscoelastic material model with the lowest MSE at the state of highest deformation . . . . .	43
4.12	MSE sensitivity study for the viscoelastic material model with: decay constant $b = \beta$ , density $\rho = \rho$ , viscous coefficient $d = DAMP$ , young's modulus $e = E$ , shape factor for unloading $s = SHAPE$ and the hysteretic unloading factor $hu = HU$ . . . . .	43
4.13	Model response for a coefficient study of the material model low density foam; colours depending to the viscous coefficient d. . . . .	44
4.14	Model response for the the material model low density foam at the moment of highest compression ((a) and (b)) and model response plots ((c) and (d)) for the best results of the coefficient study . . . . .	45
4.15	Model responses for different load curves . . . . .	46
4.16	Stress versus strain curves from curve optimization and from literature . . . . .	46
4.17	Model response for the final material model . . . . .	47
4.18	Model response of the viscus for the final material model . . . . .	48
4.19	THUMS v3-M with the modified lung material model under single belt loading conditions, the left part of the body had been removed . . . . .	49
4.20	Force versus compression response for THUMS v3-M . . . . .	49
5.1	Stress versus strain curves from experiments, Hoppin Jr. et al. (1975); Radford and Remington (1957); Vawter et al. (1978); Zeng et al. (1987) . . . . .	52

## List of Figures

---

6.1	Force versus compression response for THUMSv3-R and THUMS v3-M, Mendoza-Vazquez et al. (2012), and the experimental table top corridors by Kent et al. (2004) . . . . .	XXI
-----	---	-----

# List of Tables

2.1	Lungs volume and linear dimension for male and female data sets with standard deviation, Kramer et al. (2012) . . . . .	5
2.2	Abbreviated injury scale, States (1990) . . . . .	6
2.3	AIS for rib cage and thoracic injuries, States (1990) . . . . .	7
2.4	Number of frontal impacts for different EES, Carroll (2009) . . . . .	7
3.1	Low density foam material variables from LS-DYNA for thoracic viscera from THUMS v3-M, Mendoza-Vazquez et al. (2012) . . . . .	28
3.2	Impactor densities for adjusted masses . . . . .	30
3.3	Values for the different material models from literature, Mendoza-Vazquez et al. (2012); Plank et al. (1998); Roberts et al. (2005); Ruan et al. (2003); Stitzel et al. (2005); Vawter (1980); Zhao and Norwani (2004) . . . . .	32
4.1	Viscoelastic material parameter for the best MSE obtained from parameter studies . . . . .	42
4.2	Parameter for low density foam from parameter and curve studies and the corresponding MSE . . . . .	46
5.1	Kinetic energy for different impact speeds . . . . .	53
6.1	Material properties for lung tissue . . . . .	XXII

# List of Acronyms

<b>ATD</b>	Anthropomorphic Test Device
<b>AIS</b>	Abbreviated Injury Scale
<b>CCIS</b>	UK Co-operative Crash Injury Study
<b>CDC</b>	Collision Deformation Classification
<b>C<sub>max</sub></b>	Maximum Chest Compression
<b>CT</b>	Computer Tomography
<b>DC</b>	Combined Deflection Criterion
<b>EES</b>	Energy Equivalent Speed
<b>FE</b>	Finite Element
<b>FEM</b>	Finite Element Method
<b>FE-HBM</b>	Finite Element Human Body Model
<b>GHBMC</b>	Global Human Body Models Consortium
<b>HBM</b>	Human Body Model
<b>NHTSA</b>	National Highway Traffic Safety Administration
<b>HUMOS</b>	HUman MOdel for Safety
<b>LDT</b>	Linear Differential Transducer
<b>MSE</b>	Mean Square Error
<b>MSE<sub>dis</sub></b>	Mean Square Error for displacement
<b>MSE<sub>force</sub></b>	Mean Square Error for force
<b>PMHS</b>	Post Mortem Human Subjects
<b>THOR</b>	Test device for Human Occupant Restraint
<b>THUMS</b>	Total HUman Model for Safety
<b>THUMS v3.0</b>	Total HUman Model for Safety version 3.0
<b>THUMS v3-M</b>	Total HUman Model for Safety version 3.0 Modified
<b>PC</b>	Pulmonary Contusion
<b>RTC</b>	Road Traffic Collision
<b>VC</b>	Viscous Criterion
<b>WHO</b>	World Health Organization

# 1 Introduction

## 1.1 Background and Research Justification

According to the World Health Organization (WHO) nearly 1.2 million people die yearly in the world due to traffic accidents and up to fifty million people retain permanent disabilities, Peden et al. (2004).

During the last forty years the amount of fatal car crashes has decreased continuously. In Germany in the year 1970 there were nearly 1.4 million Road Traffic Collisions (RTCs) with 19 193 fatalities. Despite increasing RTCs up to 2.4 million the amount of fatal accidents reached an all-time low of 3 648 in the year 2010, Bundesamt (2012).

The introduction of modern restraint systems like seatbelts and air bags contributed to this significant decline in fatal accidents, Bean et al. (2009). A statistical analysis of accidental data of the National Highway Traffic Safety Administration (NHTSA) by Bean et al. (2009) showed that seatbelt use and air bags reduce the fatality risk by 61 % compared to unbelted car occupants of a vehicle without air bags. In frontal impacts the fatality risk is actually reduced by up to 74 %, NHTSA (2009). Despite this in the USA in the year 2010 11 628 restraint car occupants died in RTCs, NHTSA (2010).

A study of UK Co-operative Crash Injury Study (CCIS) data by Cuerden et al. (2007) revealed that in the UK frontal car impacts are responsible for one third of all fatal car accidents. Klanner (2001) reported that in Europe even 40 % of all fatal car accidents are frontal impacts.

Rib fractures and lung injuries are the most frequently occurring injuries in car crashes with a serious or more severely (Abbreviated Injury Scale (AIS)  $\geq 3$ ) injured torso, Carroll (2009). At 81 % thoracic injuries with an AIS score of 3+ are the most frequent injuries of drivers who die in frontal car accidents, Cuerden et al. (2007). Thus, thoracic injuries are the most life-threatening injuries due to RTCs in the sample studied by Cuerden et al. (2007).

Despite the immense safety improvements due to restraint systems seatbelts do not completely prevent severe or fatal injuries and can themselves cause injuries. To reduce the number of rib fractures and the severity of lung injuries it is necessary to improve current restraint systems.

A benchmark is required to evaluate improvements of restraint systems. A common tool for the evaluation of restraint systems are Anthropomorphic Test Devices (ATDs). They are used e.g. in simulated vehicle impacts. However, ATDs are only a gross mechanical representation of the human body, e.g. organs are not represented. To predict injuries of the thoracic cage the deformation, acceleration, velocity and force can be recorded with ATDs.

A reliable prediction of injuries car occupants may suffer due to RTCs is a desirable goal. Hence, a validated injury criterion is a prerequisite. Current criteria like the Maximum Chest Compression ( $C_{\max}$ ) or the Viscous Criterion (VC) are based on the deformation

measurement with ATDs. These criteria do not fulfil the injury mechanism of lung injuries, Gayzik et al. (2007). The issue is that the detection of stresses and strains related to lung injuries in experiments is difficult, if not impossible, Ruan et al. (2003).

Next to ATDs Finite Element Human Body Models (FE-HBMs) are a second tool to evaluate restraint systems. The advantage of FE-HBMs is that they offer a more detailed description of the human anatomy and stresses and strains can be calculated. A reliable prediction of injuries requires a validated Human Body Model (HBM) next to an injury metric.

The most important part for the prediction of life-threatening injuries is the thorax. The model of the thorax is usually validated against pendulum impact tests, sled tests or table top tests with Post Mortem Human Subjects (PMHS). Several investigations concerning mechanical properties, injury prediction and modelling of hard tissue like ribs are available. In contrast, investigations concerning soft tissue like lungs are rare. The mechanical behaviour and injury prediction of lungs are not well researched, Gayzik et al. (2007); Ruan et al. (2003).

Since the beginning of thoracic modelling several material models for the simulation of lungs were developed. The material models of presently used HBMs were mainly adjusted to validate the thoracic response against PMHS experiments. Despite the relevance of lung injuries due to RTCs particular validations of the lung models under frontal car crash conditions were not carried out.

## 1.2 Research Objectives and Scope

The objective of the research in this thesis is outlined with four main goals. The first goal is to identify the state of the art of lung modelling and to figure out material models that are used for the simulation of thoracic organs in general and lungs in particular. Furthermore experiments which are suitable for the validation of a lung model are determined as input for the following part of the thesis.

To modify the thoracic response of HBMs the material properties of the thoracic organs have often been used. No investigations have been done in particular to validate human lung models under conditions similar to frontal crashes. Therefore, the second goal is to rate and to compare currently used material models for lung modelling. For the rating of the material models an experiment suitable for lung validation has to be identified and to be simulated with Finite Element Methods (FEMs) with different material models. The results will be used as input for the next part of the thesis.

The third goal is to improve the simulated model response against the experiments by modifying the material model. The biofidelity of a modern HBM with the modified material model has to be proved against PMHS experiments to investigate the influence of the modification to the thoracic response.

The fourth and final goal of the thesis is to identify the state of the art of lung injury prediction and the lack of knowledge for lung validations. These information have to be discussed and suggestions for future work and experiments have to be developed.

# 2 Literature Research

## 2.1 Introduction

The aim of this thesis is to compare, to evaluate and to enhance current material models of lung tissue for FE-HBMs. These models are used for automotive safety investigations. Therefore, in the first part of this chapter a short introduction to the anatomy of the thorax and important information of thoracic injuries due to RTCs will be given.

Afterwards an overview of past and current human body and thoracic models will be given. Furthermore, experiments with the aim to figure out mechanical properties of lung parenchyma as well as experiments suiting for the validation of a human lung model and of the thoracic response will be summarized. The literature research is completed by presenting common material models of lung models which were used for the model validation in the further thesis.

## 2.2 Anatomy of the Thorax

Since knowledge of the anatomy of the thoracic organs in general and the lungs in particular are essential for further investigations about the lungs, the following will provide it. The heart and lungs are next to the brain two central organs of human beings and located in the thorax. The thorax is in the body between the abdomen and the neck (Figure 2.1 (a)). The thoracic cage consists of the thoracic vertebrae, the sternum and the ribs (removed in Figure 2.1) and protects the lungs and the heart against hits and contusion.

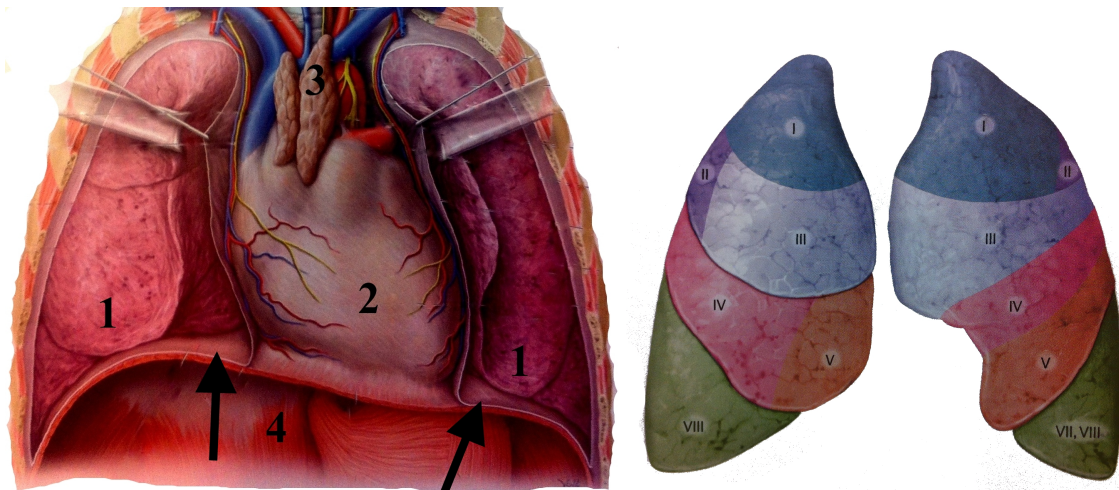
The chamber inside the thoracic wall contains the principal organs of respiration (the trachea, bronchi and lungs (1)) and circulation (the heart (2) and great vessels (3)) (Figure 2.1 (a)).

As it can be seen in Figure 2.1 the parietal pleura separates the chamber again into two closed chambers for the lungs and separates the thoracic cage from the abdominal organs (4). The organs of the circulation system are located between the two lung chambers, Schuenke et al. (2006); Schulte and Schumacher (2012); Standing et al. (2005).

### Lungs

The lungs are the essential respiration organ of humans. The human lungs consist of the right and the left lung. The basic structural unit of each lung is the lobe. The right lung has three lobes, the upper, middle and lower lobe (cf. Figure 2.1 (b)). The left lung only has an upper and a lower lobe.

Each lobe is further subdivided in segment wedges. The pulmonary segments are only incompletely separated from each other and they are not discernible as separate units on the lung surface. Each lung basically consists of ten segments (cf. Figure 2.1 (b)). The segments then consist of segmental bronchus which get divided up to the pulmonary alveoli where the actual gas exchange happens, Schuenke et al. (2006); Schulte and Schumacher (2012).



(a) (1) lungs, (2) heart, (3) great vessels and (arrows) pleural space (b) Right and left lung with pulmonary segments

**Figure 2.1:** Thoracic organs without muscles, ribs and sternum (a); lungs with pulmonary segments, anterior view (b); modified from Schuenke et al. (2006)

With a volume of 1.5 l the deflated right lung is slightly bigger than the left lung with a volume of 1.4 l. This is caused by the non-symmetric position of the heart, Schulte and Schumacher (2012).

Kramer et al. (2012) analysed Computer Tomography (CT) images of 166 patients with the aim to measure the linear dimension and volume of human lungs. Contrary to the volume of deflated lungs mentioned before, these values relate to inflated lungs inside the body. The results of their study can be found in Table 2.1.

**Table 2.1:** Lungs volume and linear dimension for male and female data sets with standard deviation, Kramer et al. (2012)

		Male	Female	Combined
Height [cm]	Left	21.0 ± 2.1	19.9 ± 2.5	19.8 ± 2.6
	Right	21.0 ± 2.1	19.0 ± 2.5	20.6 ± 2.6
Max height [cm]	Left	28.2 ± 2.2	26.0 ± 2.7	26.1 ± 2.6
	Right	21.0 ± 2.1	26.0 ± 2.7	26.9 ± 2.7
Width [cm]	Left	12.3 ± 1.1	11.1 ± 1.0	10.0 ± 1.0
	Right	12.3 ± 1.1	11.1 ± 1.0	11.6 ± 1.2
Depth [cm]	Left	18.0 ± 1.5	16.2 ± 1.7	17.1 ± 2.0
	Right	18.0 ± 1.5	16.2 ± 1.7	16.9 ± 1.8
Volume [ $cm^3$ ]	Left	2738 ± 533	1968 ± 505	2301 ± 636
	Right	3121 ± 605	2300 ± 547	2663 ± 667
	Total	5858 ± 1094	4268 ± 1028	

## 2.3 Car Crash Information

One key aspect of this paper are the simulations of restraint systems under frontal impact loading conditions. Therefore it should shortly be mentioned what a frontal car crash is, which injuries occur and why an investigation of these accidents is so important.

### 2.3.1 Abbreviated Injury Scale

The intention behind developing the AIS was to get a universal and widely accepted injury scale which describes and classifies the injury level for automotive accident investigations. It was first developed and introduced by the Association for the Advancement of Automotive Medicine in 1969.

As it is shown below in Table 2.2 the AIS divides injuries into seven levels from 0 (no injury) to 6 (maximum injury) which is also often termed virtually lethal, Forbes (2005); Nahum and Melvin (2002); States (1990).

A higher AIS level means a greater life-threatening injury but it should be noted that the scale is not continuous. This means an AIS level of 4 is much more severe than two AIS level of 2, Cuerden et al. (2007).

**Table 2.2:** Abbreviated injury scale, States (1990)

AIS Score	Description
0	No Injury
1	Minor
2	Moderate
3	Serious
4	Severe
5	Critical
6	Maximum

Since its first publication the AIS has undergone several revisions and also various scales for specific regions of the body were published. These are e.g. scales for vascular injuries or for skull fractures. The AIS for injuries to the rib cage and the thoracic soft tissue which is shown below in Table 2.3, States (1990).

### 2.3.2 Frontal Car Crashes

A car crash is called frontal car crash if the car hits a barrier or another car in a frontal collision between eleven and one o'clock impact direction. More than 66 % of all car impacts occur in this area, Cuerden et al. (2007)

An study of CCIS data by Cuerden et al. (2007) revealed that in the UK frontal car impacts are responsible for one third of all fatal car accidents. The data were collected from June 1998 and only accidents with cars built later than 1996 were used.

**Table 2.3:** AIS for rib cage and thoracic injuries, States (1990)

AIS Level	Rib Cage Injury	Thoracic Soft Tissue Injury
1	1 rib fracture	Contusions of the bronchus
2	2-3 rib fractures; sternum fracture	Partial thickness bronchus tear
3	4 or more rib fractures on one side; 2-3 rib fractures with hemothorax or pneumothorax	Lung contusion; minor heart contusion
4	Flail chest; 4 or more rib fractures on each of two sides; 4 or more rib fractures with hemothorax or pneumothorax.	Bilateral lung laceration; minor aortic laceration; major heart contusion
5	Bilateral flail chest	Major aortic laceration; lung laceration with tension pneumothorax
6		Aortic laceration with hemorrhage not confined to mediastinum

Table 2.4 below shows the absolute frequency and the percentage of car crashes in relation to the Energy Equivalent Speed (EES). The EES is the equivalent speed at which a particular vehicle would need to contact any fixed rigid object in order to dissipate the deformation energy corresponding to the observed vehicle residual damage.

**Table 2.4:** Number of frontal impacts for different EES, Carroll (2009)

EES (km/h)	Number of front impact accidents	Percentage [%]
< 15	4	1
16 - 25	37	7
26 - 35	98	18
36 - 45	121	23
46 - 55	108	20
56 - 65	120	23
66 - 75	31	6
> 75	11	2

As it can be seen in Table 2.4 two third of all accidents happen between  $36 \frac{km}{h}$  and  $65 \frac{km}{h}$  EES. The risk of a moderate thorax injury (AIS 2+) is for an EES speed of  $56 \frac{km}{h}$  to  $65 \frac{km}{h}$  already nearly 30 %, Carroll (2009). In a sled test with  $48 \frac{km}{h}$  the chest compression rate measured with PMHS is  $1 \frac{m}{s}$ , Kent et al. (2004).

### 2.3.3 Seatbelt Related Injuries

Thoracic injuries due to car accidents are severe and life-threatening and often caused through seatbelts. Therefore it is important to know what kind of injuries occur in RTCs and why injuries of the thorax are so severe.

Bean et al. (2009) showed that the use of seatbelts reduced the mortality risk in RTCs by 61 %. Seatbelts were designed to prevent occupants from hitting the interior of the car

or getting ejected out of the car. Seatbelts scatter the kinetic energy from the rapid deceleration through the body skeleton, however seatbelts can also cause injuries themselves, Abbas et al. (2011).

The first seatbelts that were implemented in cars were lap belts. Holding a body only at two points had the disadvantage that major forces are transferred directly through the lumbar spine and lap belts did not prevent the head and chest from moving forward against the steering wheel and the windscreen. The basics of the presently used three point belt were developed in 1968 by Volvo. This seatbelt prevents the upper body from bending forward against the interior, Abbas et al. (2011).

Incorrect seatbelt usage and wrong seatbelt application influence the injury severity in RTC, but the major influence on the injury severity is the velocity. There is a clear association between high speed accidents and fatal injuries. The formula for the energy (E) (Equation 2.1) explains the relationship between high velocity (v) and fatal injuries. The energy increases exponentially with increasing velocity. High energy leads to severe injuries, Abbas et al. (2011).

$$E = \frac{1}{2} * m * v^2 \tag{2.1}$$

As it is shown in Figure 2.2, 81 % of the drivers dying due to frontal car accidents had a thoracic injury AIS score of 3+ and only 37 % survived. In contrast 72 % of the car occupants in frontal car accidents had an AIS injury scale of 3+ for the lower extremities but 60 % of them survived. It should be noted that this data does not allow conclusions for fatal injuries because there is no information about multiple injuries and interactions. Nevertheless, these data show that thoracic injuries due to car accidents are quite common, very often severe and life-threatening.

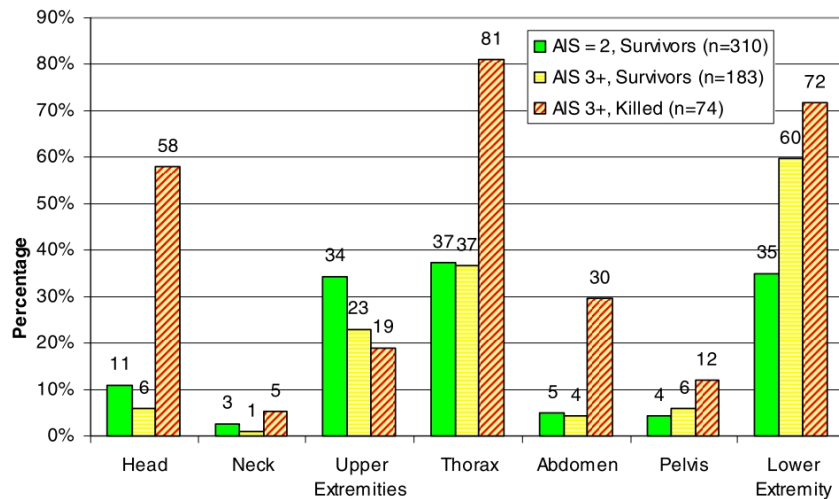
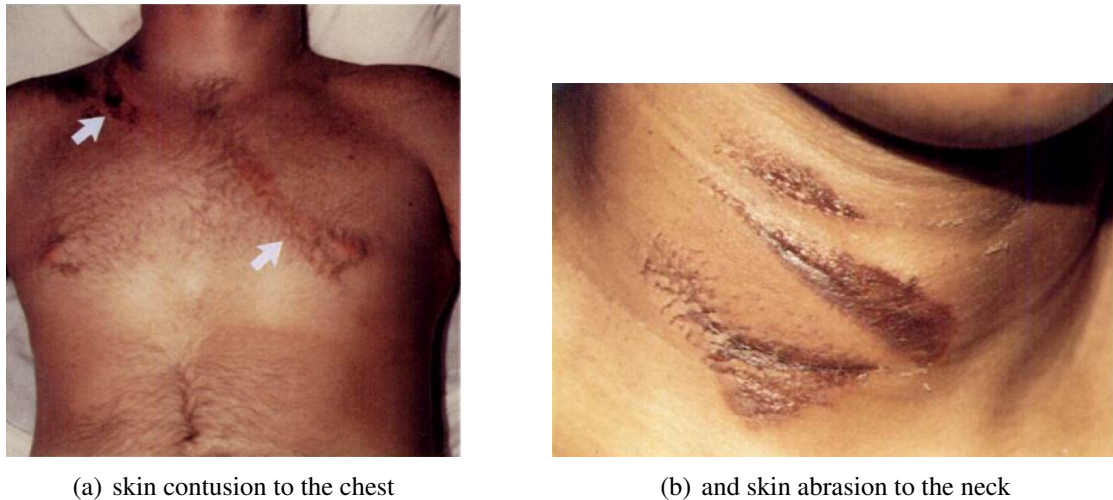


**Figure 2.2:** Injury regions and severe for drivers in frontal car crashes, Cuerden et al. (2007)

Naturally modern three point seatbelts help to protect car occupants in RTC. But despite the enormous advantages seatbelts can cause seatbelt-related injuries. Hayes et al. (1991) called these injuries the seatbelt syndrome and divided them into different groups. The skin abrasion and contusion of the neck, chest and abdomen is called the seatbelt sign and

indicates internal injuries in 30 % of the cases (Figure 2.3). The other groups are skeletal injuries, soft-tissue and visceral injuries and vascular injuries. Injuries of the lungs belong to the group of soft tissue and visceral injuries.



(a) skin contusion to the chest

(b) and skin abrasion to the neck

**Figure 2.3:** Seatbelt signs by Hayes et al. (1991)

In order to analyse and describe injuries in a more detailed way the torso can be subdivided into sternum, shoulder, ribs, lungs, heart, spine and the abdomen. An analysis of the CCIS database showed that a lung injury of  $AIS \geq 3$  was the most common injury of all car occupants who were killed or seriously injured, Carroll (2009).

Lung injuries caused by RTC are mainly Pulmonary Contusion (PC) and pneumothorax. A PC is a non penetrating contusion of the lung caused by a chest trauma. Blood or other fluids can percolate through the lung tissue as a result of a damage to the lung capillaries. This can effect the gas exchange and as a result lead to an inadequate oxygen level.

A pneumothorax due to RTC is also called traumatic pneumothorax and describes the abnormal collection of air or blood in the pleural space between the lungs and the chest wall (cf. Figure 2.1 (a) black arrows). This can result in a lung collapse because the natural vacuum disappears. In contrast to a PC there is a cut or a tear of the lung tissue. This results either from a blunt trauma or a penetrating injury, for example caused by a fractured rib. Both injuries can interfere with the normal breathing and can be fatal.

## 2.4 Human Body Models

The aim of this chapter is to give an overview of HBMs development and the current state of the art. HBMs can be used to study the interaction with restraint systems an to estimate the risk of injuries. For the simulations in this thesis the Total HUMAN Model for Safety version 3.0 (THUMS v3.0) and the thoracic organs from this model have been used. Therefore, a detailed introduction of THUMS v3.0 and modifications that have been done will be given. Caused by the thematic orientation of this thesis on lungs modelling, the focus lies on thoracic models and the material models used for thoracic visceral and lungs.

### 2.4.1 History

Numerical analyses have accompanied experimental investigations since the beginning of the computer age in the 1960s. Limited by computational speed it was necessary to simplify the mathematical model of the experimental system to a small set of derivations. Models were mainly based on lumped-mass models, multi body and Finite Element (FE) models. With the multi body method the kinematic response can be calculated, while with the FEM the dynamic and material response can be calculated. Due to the limited computational speed numerical calculations were focused on an isolated part of the body like the head, neck, thoracic, abdominal and upper and lower extremities.

The highly enhanced performance of information technologies also increased the quality and the amount of details of computer models.

The head was the first part of the body analysed by a numerical model. The first head lumped-mass model was developed by Hodgson et al. (1967) and was used for an investigation of the dynamic response of a cadaveric skull with a simple spring-dashpot-mass model. The first finite element model was published by Chan (1974) and the head was represented by an ellipsoid. This model already contained a brain represented by a viscoelastic material, Yang et al. (2006).

In the following years lots of different models for different experiments and parts of the body were developed and published. Because of the complexity it took nearly a further thirty years until the first real human body model was published in 1995, Yang et al. (2006).

Developed by Huang (1995) this FE-HBM contained 9 308 solid elements and 2 384 shell elements (cf. Figure 2.4 (a)). The model already included bones (e.g. ribs and sternum) and soft tissues like a skin and integrated a pelvis. The model was validated by a side impact test with cadavers.

Several FE-HBMs have been developed in recent years, for example by Happee (1998), Lizee et al. (1998), Van Hoof (2003) and Ruan et al. (2003) (cf. Figures 2.4 (b)-(e)).

The last finite element models were the Total HUMAN Model for Safety (THUMS) (cf. Section 2.4.3) developed by Toyota (Toyota Central R&D abs Inc., Nagekute, Aichi, Japan) and the HUMAN Model for Safety (HUMOS) by Vezin and Verriest (2005). An evaluation study of Holmqvist (2009) showed a better performance of the THUMS v3.0 compared to the HUMOS2 model for side impacts, Toyota (2011); Yang et al. (2006).

The THUMS model is used by several car companies and research institutions, e.g. Chalmers University of Technology.

In 2011 Toyota released an improved version of THUMS (THUMS v4.0) incorporating individual organs parts, Toyota (2011). Currently a new model, the Global Human Body Models Consortium (GHBMC), is being developed by a global consortium of seven car companies and one supplier with the purpose of advancing crash safety technology, Gayzik et al. (2012).

Researchers all over the world are improving the quality and biofidelity of parts or of a whole FE-HBM. Biofidelity is defined by Wismans et al. (2005) as the process where the reliability of a model is assessed against a set of PMHSs tests. The task is to obtain a completely validated model that represents a human body for automotive safety research.

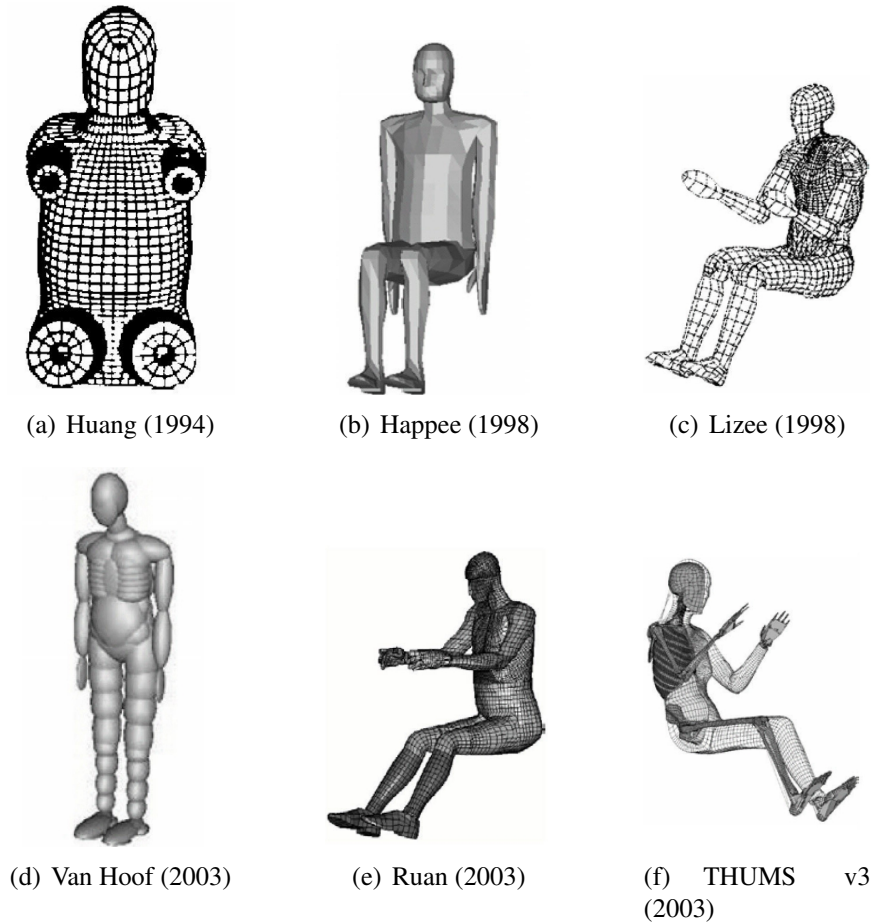


**Figure 2.4:** An overview of recent FE-HBMs, Yang et al. (2006)

Of course, current FE-models have a much higher quality than in the past but still there are a lot of uncertainties. This has different reasons. On the one hand there is still a huge lack of knowledge for the mechanical properties of different parts of the human body, especially for soft tissue (e.g. organs and skin). The mechanism of bone fracture is also not completely understood yet.

On the other hand the understanding of an isolated part of the body is not sufficient. The interaction between different tissues and parts of the body like muscles, bones and organs has to be known as well and need to be implemented in the model.

Usually, the focus lay on whole body response or on validation of parts of the body (e.g. the thorax) and on fractures and ruptures of bones and ligaments. Soft tissue modelling was mainly a means to an end for human body model validation. Yet, the injury mechanism of soft tissue is not well known. Because of these uncertainties referring to soft tissue it was a legitimate way to change the material properties and values of visceral to receive satisfactory results, e.g. Wang (1995).

### 2.4.2 Thoracic Modelling

In the last 50 years several models of the thorax and lungs have been developed. For visceral modelling in general and lungs modelling in particular different material models have been used. The most common material models are pseudo-elastic, viscoelastic and low density foam. For the material properties the authors chose either values randomly or used material properties from experiments with lung tissue (cf. Section 2.6).

All values from the different publications presented in this section are summarized in Tables 3.3 and 6.1.

Numerical simulation of the thorax started in the 1970's with a 2-D spinal column model by Begemann et al. and a model by Lobdell et al. (1973). Lobdell's model was tuned by Kroell (1976) and Viano et al. (1978 and 1987), Wang (1995); Yang et al. (2006).

Four years later Sundaram and Feng (1977) developed a three dimensional model of the thorax using solid elements to represent the internal organs. Sundaram and Feng used non-linear homogeneous material behaviour proposed by Matthews and West (1972) as material properties. Matthews' and West's material data rely on experiments from Radford and Remington (1957).

Huang (1995) developed a human body model to investigate the biomechanics of side impacts. Therefore he compared his model with cadaveric side impact sled tests. The internal organs of the thorax were represented by one volume. He assumed a soft, viscous, isotropic and homogeneous material which was achieved by discrete dampers. The material properties were chosen without reference to literature. Huang argued that a gross representation of the visceral need not be proved.

#### Models Using Pseudo-Elastic Material Models

Vawter (1980) investigated the behaviour of a two dimensional lungs model loaded by its own weight. As material properties he used the pseudo-elastic model represented by a strain-energy function proposed by Fung et al. (1978). For the parameter calculation Vawter used his own experiments summarized in Section 2.6.2, Vawter et al. (1978).

Another FE-HBM which used the strain-energy function was developed by Zhao and Norwani (2004). The experimental data for the coefficient calculation were used from Yen (1999).

Gayzik (2008) developed an FE based injury metric for pulmonary contusion with a rat lung model developed by Stitzel et al. (2005) in a previous study. Therefore Stitzel et al. (2005) used an algorithm to optimize the coefficients for force versus displacement curves from experiments with rats.

#### Models Using Viscoelastic Material Behaviour

For an analytic investigation of driver thoracic response, Plank et al. (1998) exchanged the thoracic part of an existing FE-HBM with a new further developed model of the human thorax. For this experiments Plank et al. chose the material properties proposed by Herrmann and Peterson (1968) which are based on viscoelastic stress analysis (cf. Section 2.8.2). As Young's modulus they used the intermediate values from the heart and lungs proposed by Sundaram and Feng (1977). The density and bulk modulus were taken from Plank et al. (1998) without further literature references.

In the same year Lizee et al. (1998) developed and validated an FE-HBM of a seated 50th percentile adult male. He used viscoelastic material behaviour like Plank et al. (1998) but with different values. Again no reference for the material parameter was given. Ruan et al. (2003) and Roberts et al. (2005) used this viscoelastic material model for non-penetrating ballistic and pendulum impact tests as well.

### Models Using Low Density Foam as Material Model

Wang (1995) developed an FE human thoracic model for side impacts. For the properties of the heart and lungs he used non-linear stress versus strain curves. Wang used the experimental data from Vawter et al. (1979) (cf. Section 2.6.2) as values for the load curve. To approximate the assumed response he increased the values ten times without giving further reasons. He used a highly compressible foam as material model. The same material model was used for the thoracic viscera of THUMS v3.0 as well. The plotted stress versus strain curves can be seen in Figure 2.5, Kimpara et al. (2005).

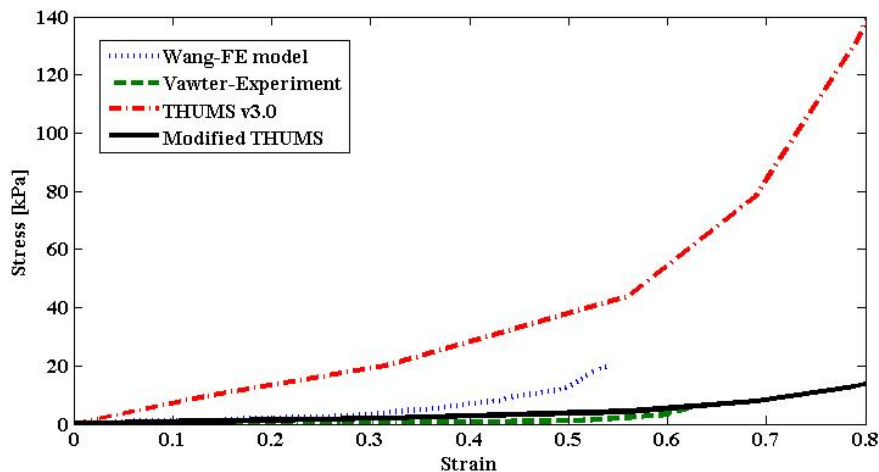


**Figure 2.5:** Stress versus strain curves from experiments and modified curves for low density foam, Mendoza-Vazquez et al. (2012); Vawter et al. (1978); Wang (1995)

### 2.4.3 Total Human Model for Safety

THUMS is an FE-HBM developed by Toyota Motor Corporation and Toyota Central R&D Labs., Inc. The model aims to simulate human body kinetics and injury responses in car crashes. The material properties are defined by constitutive material laws and the geometries of the human body parts are represented by finite element meshes, Toyota (2011).

There are different versions and variations of THUMS. The basis of all THUMS versions is an average sized adult male (AM 50th %-ile) with a height of 175 cm and a weight of 75 kg. A small sized woman (AF 5th %-ile) and a large sized male (AM 5th %-ile) have also been developed. All models exist in a sitting and a standing posture representing a

car occupant and a pedestrian, respectively, Toyota (2011).

THUMS v1, the first version of THUMS was published in the year 2000. The model already contained bones and ligaments but the brain and internal organs were simplified as solid parts. The total amount of elements was around 80 000 with an average mesh size of 15 mm. The aim of the model was to simulate bone fractures and ligament ruptures in car crashes.

The second version (THUMS v2) was completed in 2004 and included a modification of the facial bones.

THUMS v3.0, the third version has been available since 2008 and includes a new brain model for simulating brain injuries. The model consisted roughly of 150 000 elements and 110 000 nodes. Joints were modelled anatomically including the major ligaments and bone to bone contact.

Currently, this version has established itself in several companies and research institutions. Chalmers University of Technology is using this model for research projects in cooperation with different partners for automotive safety research. THUMS v3.0 is the basis model on which the further research is based.

The latest version of THUMS (THUMS v4) was published in 2010 and different internal organs are integrated. The total number of elements is around 2 000 000. The three standing pedestrian versions of a small sized woman, an average sized man and a large sized man can be seen in Figure 2.6. However, this model is not yet established due to the high number of elements that make calculation time high and due to projects still in progress using THUMS v3.0.



**Figure 2.6:** THUMS v4: AF05, AM50 and AM95, Toyota (2011)

### Modifications of THUMS v3.0

Different modifications have been made to improve the biofidelity of THUMS v3.0. Murakami et al. (2006) used the table top tests by Kent et al. (2004) (cf. Section 2.7.2) for an

evaluation study. They found out that changed properties of the rib cartilage can improve the model response compared to the experimental results.

Pipkorn and Kent (2011) modified the mesh and material data and added muscles to THUMS v2.21. Their modified model reacted in a similar way to the PMHS in Kent's table top tests.

An important modification of the THUMS v3.0 was carried out by Mendoza-Vazquez et al. (2012). For a study on the human rib response using an FE-HBM he modified parts of the thorax. The original THUMS v3.0 terminated in some simulations with errors when contact with a seatbelt was involved. To increase the numerical stability and robustness Mendoza-Vazquez deactivated the element elimination and remeshed the intercostal muscles, bones and flesh of the ribcage according to Mroz et al. (2010) and Pipkorn and Kent (2011).

Afterwards the cross sectional width of the ribs seven and eight were changed to increase the elastic stiffness too experimental values. Because the response of the thorax was too stiff compared to Kent's table top experiments the material properties of the flesh and the thoracic organs were changed.

The thoracic organs in THUMS v3.0 were modelled as a highly compressible foam with an input curve of stress versus strain. The original values for the curve stemmed from experiments by Vawter et al. (1978) As mentioned above, manipulated values were used for THUMS v3.0, Kimpara et al. (2005).

Mendoza-Vazquez et al. (2012) decreased this stress versus strain curve again by multiplying the original curve from THUMS v3.0 with  $10^{-6}$ . This stress versus strain curve is plotted in Figures 2.5 and 3.2.

In order to counteract numerical instability by negative element volume due to high compression Mendoza-Vazquez increased the stress versus strain curve by 90 % of strain. This modification increased the stiffness for high deformations. This model is called Total HUMAN Model for Safety version 3.0 Modified (THUMS v3-M). The biofidelity of this modified model was approved by comparing the model response with the table top tests by Kent et al. (2004) summarized in Section 2.7.2. The results for the simulated table top test of the THUMS v3.0-R and THUMS v3-M can be seen in Figure 6.1. This shows that the model response of THUMS v3-R was out of the experimental corridor for three of four load cases. In contrast the model response for THUMS v3-M was almost always inside the experimental corridor for each load case.

This modified version THUMS v3-M has also been used for the biofidelity verification with simulated table top tests in this thesis. The visceral model with the modified material properties of THUMS v3-M was the initial model for further lungs simulations.

## 2.5 ATDs and Injury Prediction

For the evaluation of improved restraint systems or e.g. a new designed interior of cars, tools are required to predict injuries car occupants may sustain in a specific impact. Therefore usually ATDs are used in sled tests or car crash tests. Thus, ATDs are only a gross mechanical representation of the human body, e.g. viscera are not represented in a ATDs.

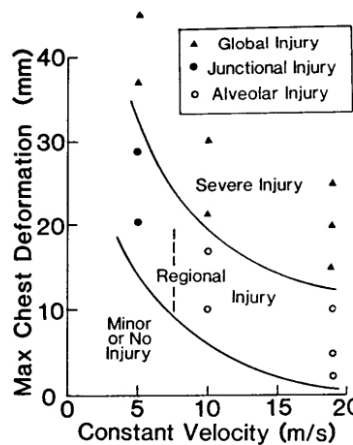
The most commonly used ATDs Hybrid III was validated against pendulum impacts to the mid sternum, e.g. by Foster et al. (1977).

The injury criterion for thoracic injury prediction  $C_{\max}$  was developed by Kroell et al. (1974) and is defined as the ratio of chest deflection to the initial chest depth. This criterion allows prediction about rib fractures.

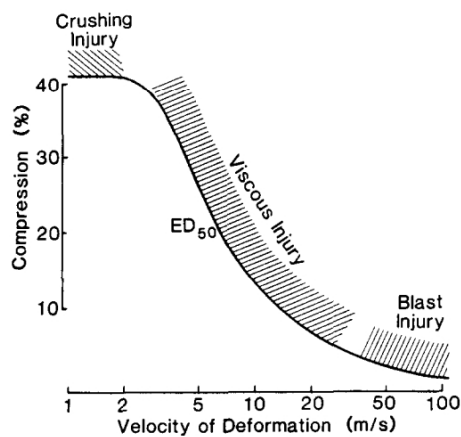
The VC from Lau and Viano (1986) takes beside the deformation the time into account. The VC is a time function generated by the product of the velocity of deformation and the compression of the thorax. According to Lau and Viano (1986) a VC of  $1.0 \frac{m}{s}$  corresponds to a 25 % risk of a severe thoracic injury ( $AIS \geq 4$ ). For soft tissue injuries in general Lau indicates that the VC can be used for deformation velocities below  $3 \frac{m}{s}$ . The deformation velocity for restraint car occupants is usually below  $3 \frac{m}{s}$ .

Lau and Viano (1981) investigated the influence of impact velocity and chest compression to the injury severity of rabbit lungs. For this study they used impact velocities of 5, 10 and  $18 \frac{m}{s}$ . The severity of lung injuries increased with chest compression at a constant velocity (cf. Figure 2.7 (a)). Regions of similar injury severity could be separated by hyperbolas. In addition Lau found out, that the alveolar region of the lungs was more sensitive to the rate of loading than the vascular region, Lau and Viano (1986).

From other experiments with soft tissue Lau and Viano (1986) developed an injury metric in dependency of velocity and compression for soft tissue. As it can be seen in Figure 2.7 (b), velocities smaller than  $3 \frac{m}{s}$  lead to crushing injuries of soft tissue. For velocities smaller  $1 \frac{m}{s}$  than Lau stated that the compression criterion is the best indicator for injuries. The compression velocity of the lungs in frontal crashes is usually  $\leq 3 \frac{m}{s}$  for restraint occupants.



(a) Lung injury severity as function of the impact speed and chest compression



(b) Range of validity for velocity criterion and compression criterion

**Figure 2.7:** AIS injury severity depending to the velocity and compression for lungs and soft tissue, Lau and Viano (1986)

The VC and  $C_{\max}$  injury criteria were developed to be assessed with ATDs. They are validated for the midline sternum chest compression measurements from Hybrid III and

are not sensitive to modern restraint systems. For example modern seatbelts lead to asymmetrical loads of the left and right side of the thoracic cage. Thus there is a need for new tools and criteria which take this specific loadings better under account. To meet these requirements, the intended successor of Hybrid III the Test device for Human Occupant Restraint (THOR) is able to measure three dimensional displacements at four different points of the thorax, Mendoza-Vazquez (2012). Through the availability of more detailed deformation data, Song et al. (2011) recently suggested the Combined Deflection Criterion (DC). This criterion takes the sternal compressions as well as the different deflection in the right and left sides of the ribcage into account.

The dynamic human thoracic responses and injuries associated with frontal impacts, side impacts and belt loadings were investigated by Ruan et al. (2003) using an FE-HBM. He compared the simulated results with PMHS experiments. As injury criterion Ruan used the VC and compared the VC with the occurring pressure. For the velocity and deflection two points were chosen related to the load case. Ruan found out, that the lungs had the lowest pressure of all organs, whereby the left lung had a higher pressure than the right lung. He assumed that a  $VC \geq 1.58$  indicates some tissue damage. This VC correlated well with organ damage seen in the experiments. A comparison of the VC with the pressure showed, that a pressure of 16 kPa indicates a lung laceration injury.

Gayzik et al. (2007) developed an FE based injury metric for PC using CT images of injured rat lungs. Gayzik induced PC on rat lungs through direct impacts with an impact velocity of  $5 \frac{m}{s}$  on in vivo rat lungs. CT scans were taken 24 hours, 48 hours, one week and one month after the impact happened. A numerical simulation was performed of the experiments with the impactor, the rat lungs and surrounding structure. Several injury predictors, like e.g. maximal shear strain and maximum shear stress, were used and compared to the CT images (cf. Figure 2.8). As it can be seen in Figure 2.8 the CT images of the PC and the calculated injury metric correlated well. He obtained the best results for the maximal principle strain \* strain rate ( $\epsilon_{max} * \dot{\epsilon}_{max}$ ) for the PC after 24 hours.

## 2.6 Lung Parenchyma Experiments

The availability of mechanical properties of human lung parenchyma is very limited. Despite reviewing literature extensively it was only possible to identify a few publications with experiments concerning lung tissue. As mentioned in Section 2.4.2 these studies were used from several authors as input for the material properties of their lung models. In this section these experiments are summarized to give an overview of the state of the art and the way these experiments were designed.

### 2.6.1 Hoppin 1975 - Properties of Lung Parenchyma in Distortion

The purpose of the study by Hoppin Jr. et al. (1975) was to provide a basis for comparing analytical models and to provide data for evaluating and developing models for lung dis-

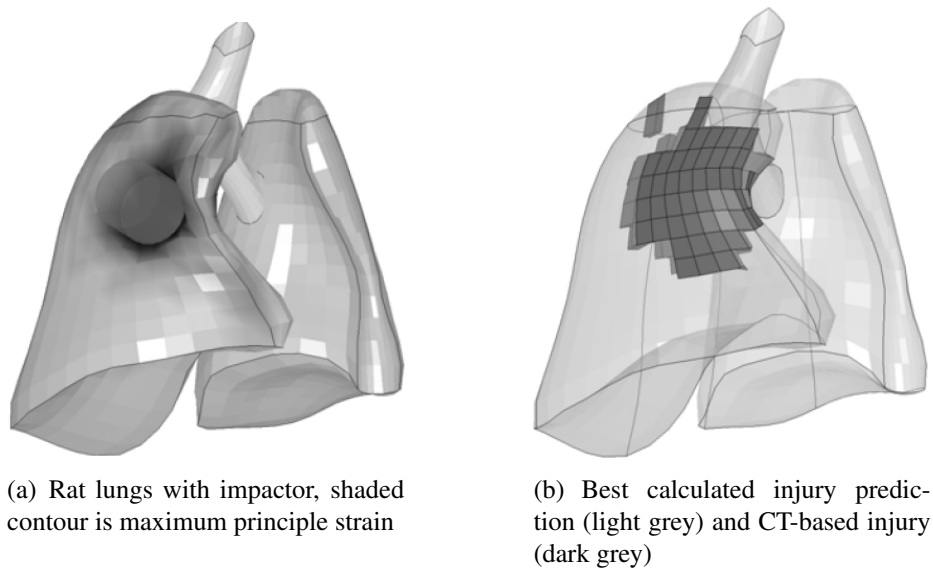


**Figure 2.8:** Rat lung model with maximum strain (a) and best correlation metric (b) for  $\epsilon_{max} * \dot{\epsilon}_{max}$ , Gayzik et al. (2007)

tortion.

Therefore Hoppin cut cubes out of frozen lungs from healthy mongrel dogs' (15 to 25 kg) frozen lungs. The cubes had a side length of 1 cm and masses from 1.2 to 1.4 g. In order to impose nearly uniform stresses they placed sixteen small hooks into each of the six surfaces before loading with different weights. The overall dimensional changes of the specimen were recorded with a Linear Differential Transducer (LDT) and a camera (cf. Figure 2.9 (a)).

The results showed hysteresis behaviour from loading to unloading for symmetrical loading and only moderate differences of extensibility of the axis. Under asymmetrical loading the behaviour of the lung tissue was similar but with greater compliance and less hysteresis (cf. Figure 2.9 (b)).

Hoppin et al. assumed that the lung parenchyma showed elastic and slightly hysteresis behaviour but the experimental data do not allow a prediction about isotropy.

### 2.6.2 Vawter 1978 - Elasticity of Excised Dog Lung Parenchyma

Vawter et al. (1978) used an experimental procedure which had previously been developed by Lanir and Fung (1974) for soft tissue measuring. Vawter et al. measured the stress strain relationship on rectangular slabs of excised dog lungs under different conditions. Thus the group extracted lung tissue from anesthetized mongrel dogs (25-30 kg) and cut it into slabs with a dimension of 5.0 x 5.0 x 0.5 cm. To minimize the effects of boundary conditions and gravity Vawter et al. used slabs and tested them under uni- and biaxial loading conditions (cf. Figure 2.10 (a)). Compared to Hoppin Jr. et al. (1975) these had the advantage that the loads could have been applied easily with clamps. Following the theory of St. Venant the edge effect is limited to the boundary region. The strain rate

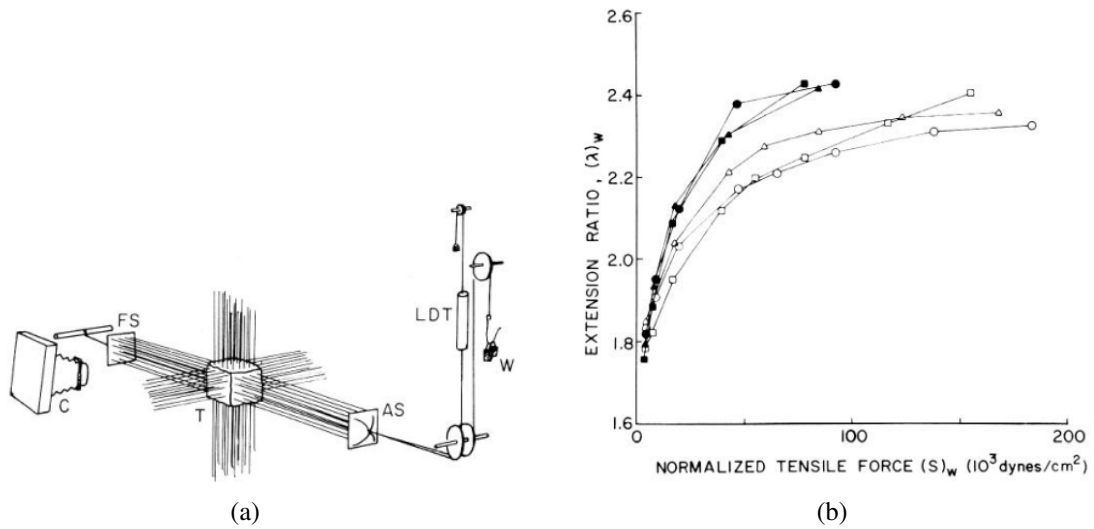


**Figure 2.9:** Schematic drawing of the tissue testing set-up (a); extension ratio under symmetrical loading for all axes against normalized tensile force (b), Hoppin Jr. et al. (1975)

was varied over a factor of 250 with a speed of  $0.03 \frac{cm}{s}$ . Each specimen was stretched for about 100 to 200 times.

Vawter et al. discovered that the dog lung tissue has highly non-linear stress versus strain and slightly hysteresis behaviour. Figure 2.10 (b) shows the stress versus strain curve for uniaxial loading conditions for eleven different specimens.

Vawter et al. also detected a slight effect of biaxial loading conditions. Under uniaxial loading the tissue was stiffer for high tension values than under biaxial loadings.

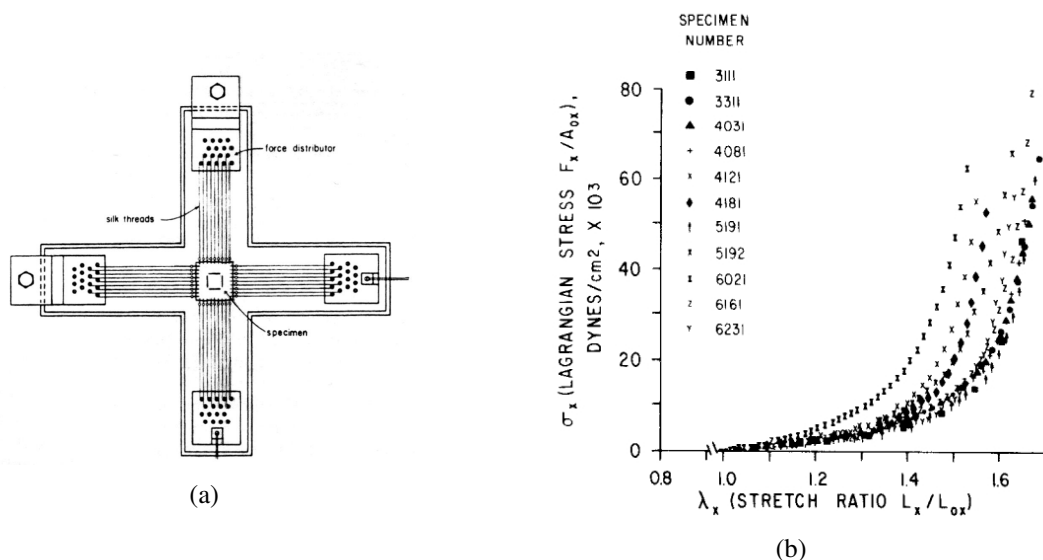


**Figure 2.10:** Slabs specimen testing under uni- or biaxial loading conditions Fung (1993) (a); stress versus strain curve for eleven specimens under uniaxial loading condition (b) Vawter et al. (1978)

### 2.6.3 Zeng 1987 - Measurement of the Mechanical Properties of the Human Lung Tissue

Zeng et al. (1987) measured the mechanical properties of human lung tissue in a state of biaxial tension. The human lungs were obtained through an autopsy within 48 hours after death. After degassing the lungs they were frozen and specimens with a dimension of  $3 \times 3 \times 0.4$  cm were cut out. Force and deformation were measured with an optical device like Vawter et al. (1978) and the forces in x- and y-direction were also recorded with a force transducer. The specimens were loaded with a fixed load in x-direction and with a sinusoidal load with a fixed amplitude and a frequency of 0.04 - 0.002 Hz in y-direction. The stress-strain-relationship was similar to Vawter's et al. with a strong non-linearity and hysteresis (cf. Figure 2.11). Zeng et al. also recorded a rapid creep in the first few seconds to the extent of three to six per cent.

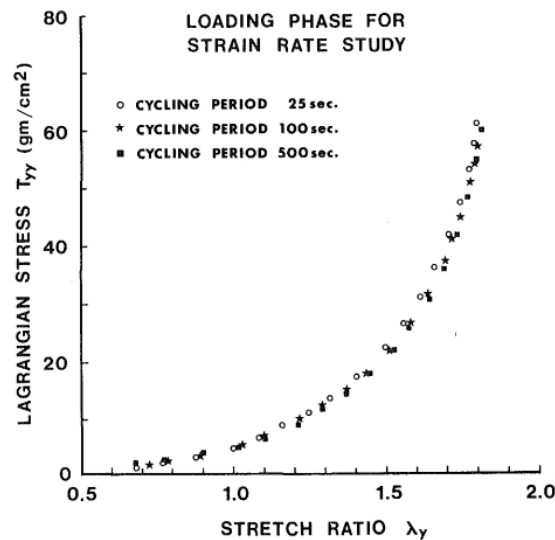


**Figure 2.11:** Stress versus strain curve for a human lung tissue specimen subjected to a fixed load in x-direction and sinusoidally varied stretch in the y-direction, Zeng et al. (1987)

The lung parenchyma gets characterized as a highly non-linear pseudo-elastic material. Zeng et al. also derived a strain-energy function according to Fung et al. (1978) to describe the experimental curves by an equation.

Comparing the constant  $C$ , which determines the overall stress level in the strain-energy function, in the data from Vawter et al. and from Zeng et al. shows that the human lung tissue is stiffer than the dog parenchyma.

## 2.7 Validation Experiments

A lot of different studies for thoracic modelling and validation available (cf. Section 2.4.2) but the focus in them lies on the thoracic response and not on soft tissue and visceral val-

validation.

The only one study which is suitable for validation of a lung model was by Hayamizu et al. (2003). He measured the dynamic response of an impactor on lungs. These experiments were used for lung material model validation. Therefore these experiments are the essential part of this thesis and they are summarized in this section.

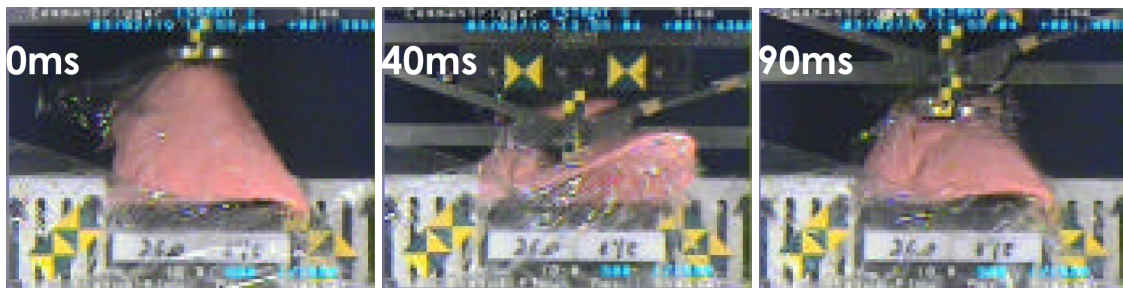
The table top tests by Kent et al. (2004) are frequently used by different authors as validation experiments (e.g. Mendoza-Vazquez et al. (2012); Murakami et al. (2006); Pipkorn and Kent (2011)), cf. Section 2.4.2). These experiments were also chosen for this thesis to prove the biofidelity of the modified lung material model.

### 2.7.1 Hayamizu 2003 - Measurement of Impact Response of Pig Lung

The aim of Hayamizu's experiments was to record swine lungs' dynamic response for lung model validation. For this he placed the lungs on a table and dropped an impactor with a diameter of 80 mm and a weight of 1.7 kg from different heights onto the lungs. Hayamizu et al. chose the heights for dropping the impactor so that the impact speeds were 3.5, 4.4, 5.4 and 6.1  $\frac{m}{s}$ , Hayamizu et al. (2003).

To keep the kinetic impact energy constant the weights of the impactor were changed. For the speeds of 3.5, 4.4, 5.4 and 6.1  $\frac{m}{s}$  the weights were 2.8, 1.7, 1.7 and 0.9 kg, respectively. The initial thicknesses of the lungs were  $129 \pm 16$  mm. Hayamizu et al. recorded the response of the lungs with a high speed camera and measured displacement and force.

Three pictures of the impact process recorded with the high speed camera can be seen in Figure 2.12. The pictures show the lung before the impact happens (a), at the deepest impact point (b) and the state after the impact process (c).



(a) moment before impact happens (b) highest compression after 0.4 s (c) end of impact process after 0.9 s

**Figure 2.12:** High speed impact pictures of a swine lung after different times for 5.4  $\frac{m}{s}$ , Hayamizu et al. (2003)

Unfortunately, the pictures are of poor quality but the principle deformation behaviour of the lung can be seen. The lung is positioned with its lower limb in the front of the picture. The lower limb is moving upwards when the impactor compresses the lung. The highest point of the lower limb is reached at the moment of highest compression through the impactor in the middle of the lung (cf. Figure 2.12 (b)). It can be assumed that the upper limb in the background of the picture is also moving upwards.

The experiments were carried out five times for the impact speed of  $5.4 \frac{m}{s}$ . For the other impact velocities the experiment was carried out only twice each. The graphs for the impact speed of  $5.4 \frac{m}{s}$  can be viewed in Figures 2.13 (a) to (c). The graphs of the other speeds are shown in Figure 2.13 (d).

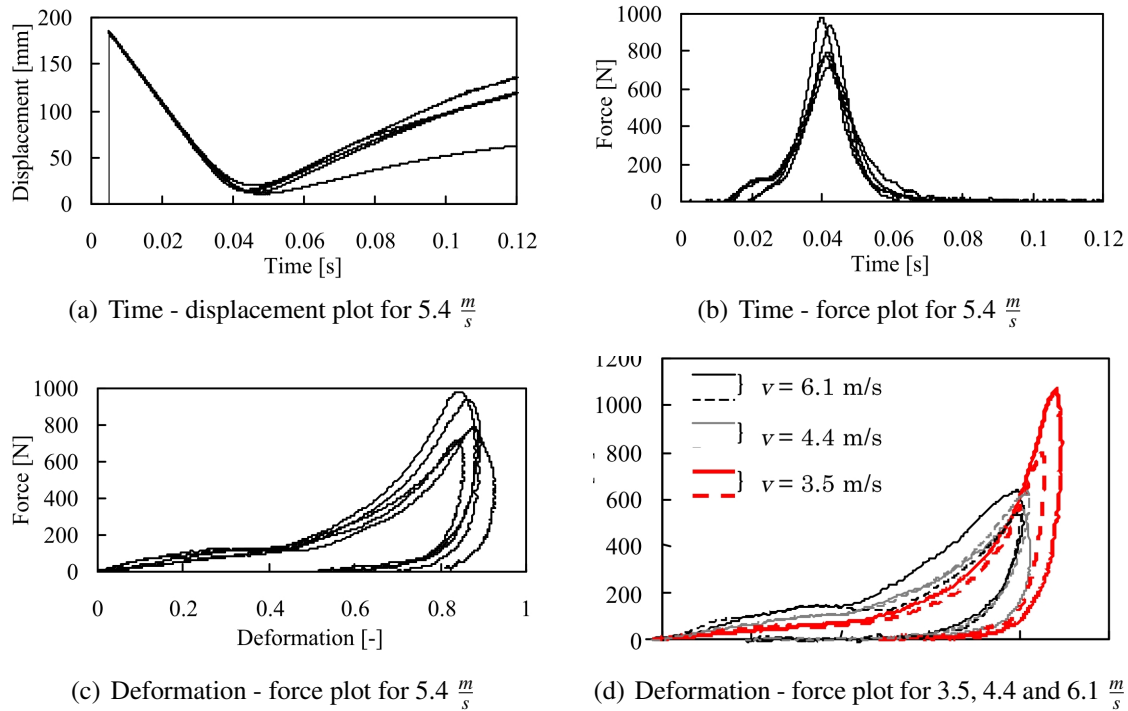


**Figure 2.13:** Experimental results for lung impact experiments by Hayamizu et al. (2003)

Figure 2.13 (a) shows the time displacement curve of the impactor. The displacement starts on a height of approximately 180 mm and decreases continuously down to the lowest point after  $t \approx 0.042 s$  with a displacement of approximately 20 mm. Afterwards the graphs of the different experiments increase to an average displacement of 125 mm, except for one graph which only increases up to 60 mm.

Figure 2.13 (b) shows the time versus force plots of the experiments. It reveals that the first force occurs after  $t \approx 0.018 s$ . With one exception of a short stagnation after 0.02 seconds the graphs increase continuously up to a peak force between 720 N and 980 N after  $t \approx 0.042 s$ . Afterwards all graphs decrease continuously to 0 N after 0.06 to 0.08 seconds.

The deformation over the force is plotted in Figures 2.13 (c) and (d) for the experiments with  $5.4 \frac{m}{s}$  and for the other speeds, respectively. In Figures 2.13 (c) it can be seen that the deformation of the lung is up to 93 %. At a compression rate of approximately 85 % a peak force of nearly 1000 N occur. The lower peak force of 680 N is conspicuously smaller at the same compression rate.

In Figure 2.13 (d) it can be seen that the highest force of  $F \approx 1080 N$  occurs at an impact speed of  $3.5 \frac{m}{s}$ . At  $F \approx 550 N$  the average peak force for 4.4 and  $6.1 \frac{m}{s}$  is clearly less, for  $5.4 \frac{m}{s}$  the forces are between 700 and 990 N. For all speeds the peak forces occur between 80 % and 90 % of deformation.

### 2.7.2 Kent 2004 - Thoracic Response to Dynamic, Non-Impact Loading from a Hub, Distributed Belt, Diagonal Belt and Double Diagonal Belts

Kent et al. (2004) performed table top tests with 15 PMHS to quantify the force deflection response of the same thorax under different loading conditions with dynamic, non-impact, restraint-like loadings. The thoracic response corridors were measured for the four loading conditions single belt, double diagonal belts, distributed and hub loading. The schematic load cases are shown in Figure 2.14.

The subjects were placed on a rigid table and a high speed material testing machine was used to provide controlled chest deflection at a rate of  $1 \frac{m}{s}$  which corresponds to restrained frontal-impact PMHS sled testing experiments at a speed of 48 km/h.

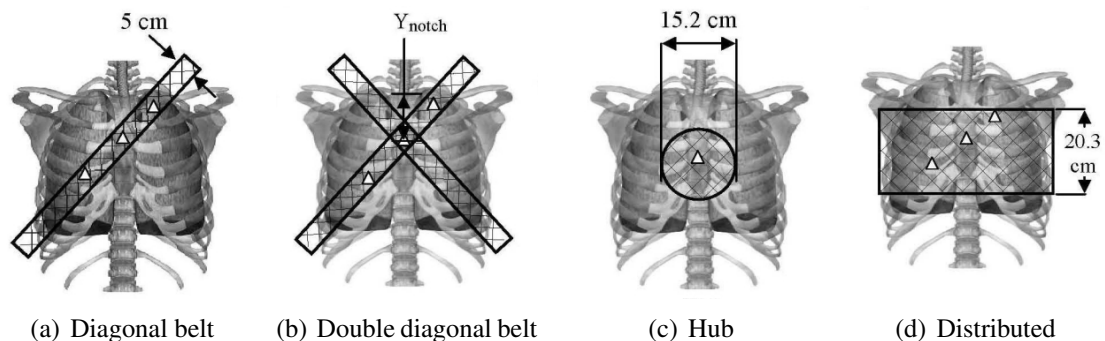


**Figure 2.14:** Load cases for table top tests, Kent et al. (2004)

A load cell was placed between the back of the PMHS and the table to measure the reaction force. The thoracic response was the midline sternum deflection recorded by a string potentiometer attached to the hub, belts or band.

The subjects were tested four times at a nominally non-injurious level. After the non-injurious loading conditions one single loading condition was used for a final, injurious test by nominal 40 % chest deflection.

The recorded mid-sternum deflection and the posterior force were scaled to a 50<sup>th</sup> percentile male-based size and modulus.

The plotted corridors for chest deflection versus reaction force for the four load cases are shown in Figure 2.15. The corridors are showing the  $\pm 1$ -standard-deviation and were developed for 20 % deflection level of the 50<sup>th</sup> percentile male.

## 2.8 Material Models

In Section 2.6 three experiments with lung parenchyma were described. The recorded material behaviour in these experiments was highly non-linear and hysteresis. Also rapid creep was recorded in the first few seconds. To describe this complex material behaviour mathematically is a challenging task.

The three material models most frequently used for lung tissue will be presented in this

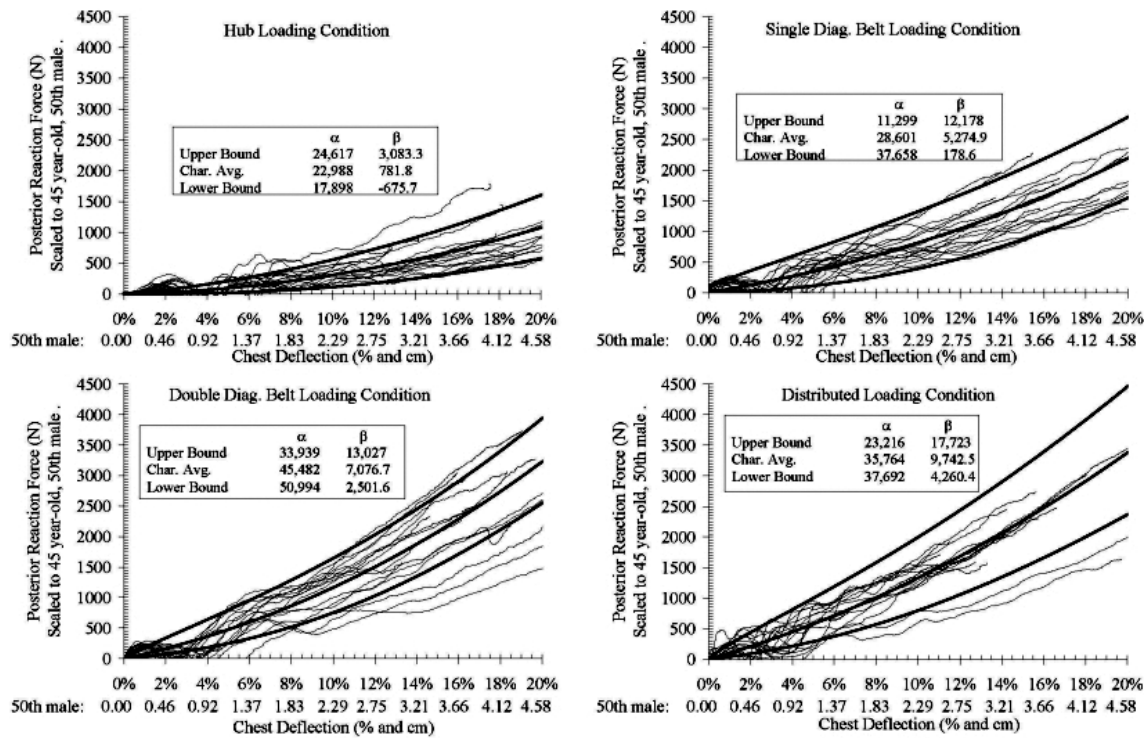


**Figure 2.15:** Force versus deflection and the corridors for hub, single and double diagonal belts and distributed loading conditions; the coefficients shown in each plot refer to the quadratic equation  $y = \alpha x^2 + \beta x$ , Kent et al. (2004)

section. They can describe the experimental stress versus strain curves including hysteresis behaviour recorded in experiments. As mentioned before the values used by different authors for lung modelling are summarized in Table 6.1. Most of them refer to these material models.

These material models were used in this thesis for the simulation of a lung model aiming to figure out which material model represents lung tissue best.

### 2.8.1 Strain-Energy Function

In a publication and later on in his book "Biomechanics - Mechanical Properties of living tissue" Fung et al. (1978) proposed using a pseudo-elastic material model for living soft tissue. The idea behind a pseudo-elastic material is that a material behaves differently for loading and unloading. Therefore the material is treated with the pseudo-elastic material model as an elastic material for loading and another elastic material for unloading. It is a convenient description of the stress versus strain relationship in specific cyclic loadings. Fortunately the advantage of the pseudo-elastic material model is, that the very complex property of tissue is more simply described. This concept describes the hysteresis of living tissue like lung parenchyma easily.

Several authors proposed different analytic expressions to describe the pseudo-elastic material model based on idealized models of the lung structure (e.g. Fung et al. (1978); Hoppin Jr. et al. (1975); Lee and Frankus (1975); Vawter (1980); Vawter et al. (1979)).

The most used equation was the one proposed by Vawter (1980) based on the the theory of strain and surface energy by Fung et al. (1978). For the energy  $W$  applies:

$$W(I_1, I_2) = \frac{C}{2\Delta} e^{(\alpha I_1^2 + \beta I_2)} \quad (2.2)$$

where  $C$ ,  $\alpha$  and  $\beta$  are material constants determined by experiments and  $\Delta$  is the typical alveolar diameter when unstressed.  $I_1$  and  $I_2$  are the known strain invariants. Fung also proposed a relationship for the surface energy density  $E$  given as:

$$E = \frac{12}{\Delta} \int_1^A \gamma(A) dA \quad (2.3)$$

where the surface area  $A$  is given as:

$$A^2 = \frac{4}{3}(I_1 + I_2) - 1 \quad (2.4)$$

The surface tension  $\gamma$  varies with the area, but since the exact variation of  $\gamma$  is not well known, Vawter simplifies the relationship by the following:

$$\gamma = C_1 A^{C_2} \quad (2.5)$$

From Equation 2.3 and 2.5 follows:

$$E = \frac{12C_1}{\Delta(1+C_2)} (A^{1+C_2} - 1) \quad (2.6)$$

where  $C_1$  and  $C_2$  are constants and  $A$  is given in Equation 2.4.

Finally, the strain and surface energy equation for lung parenchyma follows from Equations 2.2 and 2.6 as:

$$W(I_1, I_2) = \frac{C}{2\Delta} e^{(\alpha I_1^2 + \beta I_2)} + \frac{12C_1}{\Delta(1+C_2)} (A^{1+C_2} - 1) \quad (2.7)$$

This equation is used in LS-DYNA (LSTC, Livermore, CA, USA) as material model 129 MAT\_LUNG\_TISSUE, Livermore (2012).

Additionally Fung et al. (1978) proposed an analytic expression for the strain-energy function. This one was also used by some authors (e.g. Lee and Frankus (1975); Vawter et al. (1979); Zeng et al. (1987)) and should be mentioned briefly.

$$\rho_0 W = \frac{1}{2} c e^{(a_1 E_x^2 + a_2 E_y^2 + 2a_4 E_x E_y)} + \frac{1}{2} c e^{(a_1 E_x^2 + a_2 E_z^2 + 2a_4 E_x E_z)} + \frac{1}{2} c e^{(a_1 E_z^2 + a_2 E_y^2 + 2a_4 E_y E_z)} \quad (2.8)$$

Here  $c$ ,  $a_1$ ,  $a_2$  and  $a_4$  are material constants and  $E_x$ ,  $E_y$  and  $E_z$  are short forms of  $E_{xx}$ ,  $E_{yy}$  and  $E_{zz}$ . If the lung tissue is assumed to be isotropic, then:

$$a_1 = a_2 \quad (2.9)$$

and the number of constants gets reduced to three, Zeng et al. (1987)

### 2.8.2 Viscoelastic Material Behaviour

Materials are called viscoelastic when they exhibit both viscous and elastic characteristics when undergoing deformation. Elastic materials strain immediately when stress is applied and return quickly return to their original state when the stress is removed. Contrary, viscoelastic materials strain linearly when stress is applied. Holmes demonstrated that soft-tissue can be described with viscoelastic material behaviour, Holmes (1986).

The equation for viscoelastic materials is given in Equation 2.10, Herrmann and Peterson (1968),

$$G(t) = G_L + (G_S - G_L)e^{-\beta t} \quad (2.10)$$

with  $G$  = shear modulus,  $G_S$  = short term shear modulus,  $G_L$  = long term shear modulus and  $\beta$  = decay constant. Several authors used this material model for internal organs in their finite element analysis (e.g. Lizee et al. (1998); Plank et al. (1998); Roberts et al. (2005); Ruan et al. (2003)). The values for the coefficients were adjusted to experimental results from PMHS impact experiments, Plank et al. (1998), or obtained by the help of an identification process, Lizee et al. (1998).

The Equation 2.10 is the background of the material model 006 MAT\_VISCOELASTIC from LS-DYNA, Livermore (2012).

### 2.8.3 Low Density Foam

This material model was first used by Wang (1995) for the visceral in his FE-HBM (cf. Section 2.4.2) and it is also used in THUMS v3.0 for the internal thoracic organs, Kimpara et al. (2005).

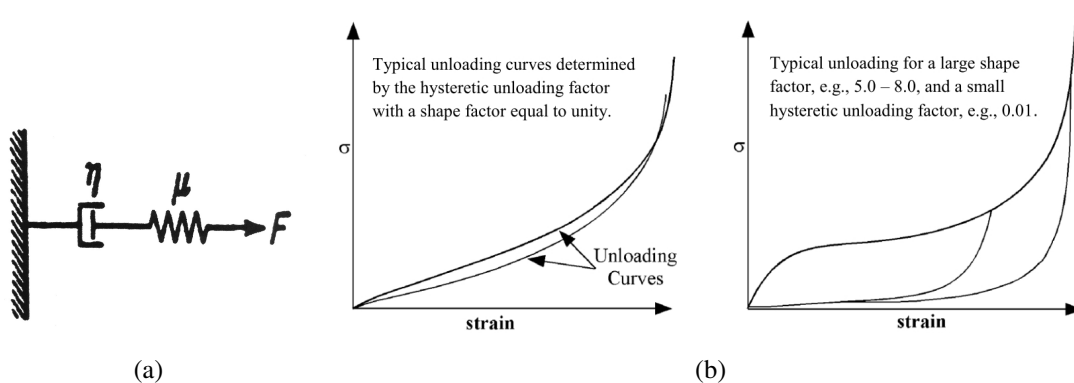


**Figure 2.16:** Kelvin-Maxwell model (a), Wang (1995); behaviour of the low density foam model and the influence of the shape and decay factor (b), Livermore (2012)

Low density foam is a material model of LS-DYNA (057 MAT\_LOW\_DENSITY\_FOAM) and is related to strain-energy material models. This model can be seen as a Maxwell fluid which consists of a damper and a spring in series (cf. Figure 2.16 (a), Livermore (2012)). The influence of the hysteretic unloading factor and the shape factor is illustrated in Figure 2.16 (b). With this factors it is possible to affect the unloading behaviour.

## 3 Methods

The theoretical background given in Chapter 2 is the basis of the simulations which are presented in this chapter.

The thoracic viscera from the FE-HBM THUMS v3.0 modified by Mendoza-Vazquez et al. (2012) was isolated and used for an investigation of the material models presented in Section 2.8. Therefore the experiments of Hayamizu et al. (2003) were modelled with the pre and post processor LS-PrePost (v3.2, LSTC, Livermore, CA, USA) and the finite element solver used was LS-DYNA (R6.0, LSTC, Livermore, CA, USA). To optimize the parameter of the material models the optimization tool LS-OPT (4.2, LSTC, Livermore, CA, USA) were used.

Afterwards, the modified material model was implemented in the FE-HBM THUMS v3-M and the biofidelity was approved with a simulation of the table top test by Kent et al. (2004).

### 3.1 Model

The following two paragraphs depict the models used for the simulation of the experiments to validate the lung model and to prove the thoracic response.

#### 3.1.1 THUMS

The model used for the simulations was originally THUMS version 3.0 presented in Section 2.4.3 in sitting posture from a 50<sup>th</sup> percentile male occupant with a mass of 77 kg and a stature of 1.75 m. The bones were represented by shell elements for the cortical bones and by solid elements for trabecular bones.

The THUMS version AM50 occupant can be seen in Figure 3.1 (a). This model is shown as it was used for the simulation of the table top tests without lower limbs. In this model the skin, flesh and bones were removed partly, to show the inner structure.

As mentioned in Section 2.4.3, this model was modified in some parts by Mendoza-Vazquez et al. (2012) to increase numerical stability and robustness and to improve the biofidelity. This modified model THUMS v3-M was used as the basis for the simulations in this thesis.

#### 3.1.2 Thoracic Organs

For the simulations of the experiments by Hayamizu et al. (2003) the viscera were isolated from THUMS v3-M. As it can be seen in Figures 3.1 (b) and (c) they were modelled by two volumes out of solid elements. These volumes were surrounded with a membrane out of shell elements to apply the contact between the viscera and the thoracic wall.

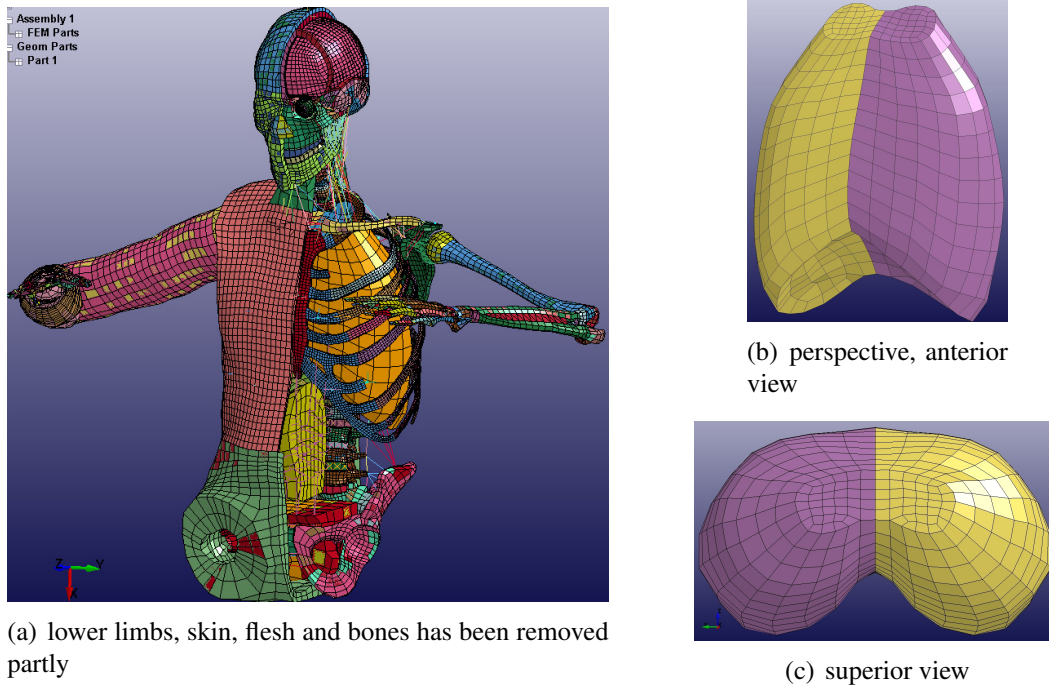


**Figure 3.1:** THUMS v3-M and isolated thoracic viscera

A viscus consists of 1 389 nodes and 962 elements and the volume of each viscus is  $V \approx 3.44 \text{ l}$  with a density of  $\rho = 1 * 10^3 \frac{\text{kg}}{\text{m}^3}$ . Thus, the mass of each viscus is  $m \approx 3.44 \text{ kg}$ . The material model was LS-DYNA MAT\_057 LOW\_DENSITY\_FOAM (cf. Section 2.8.3). The values of the variables of this material can be seen in Table 3.1 and the stress versus strain curve is plotted in figure 3.2.

**Table 3.1:** Low density foam material variables from LS-DYNA for thoracic viscera from THUMS v3-M, Mendoza-Vazquez et al. (2012)

Variable	Description	Value
RO	Density [ $\frac{\text{kg}}{\text{m}^3}$ ]	$1.0 * e^3$
E	Youngs' modulus [ $\frac{\text{N}}{\text{mm}^2}$ ]	0.1
HU	Hysteretic unloading factor	0.1
BETA	Decay constant to model creep in unloading	0
DAMP	Viscous coefficient to model damping effects	0.1
SHAPE	Shape factor for unloading. Values less than 1 reduce, greater than 1 increase energy dissipation	1

## 3.2 Impact Response Tests following Hayamizu

The impact experiments from Hayamizu et al. (2003), summarized in Section 2.7.1, were the only experiments suitable for lung model validation simulations. Therefore these

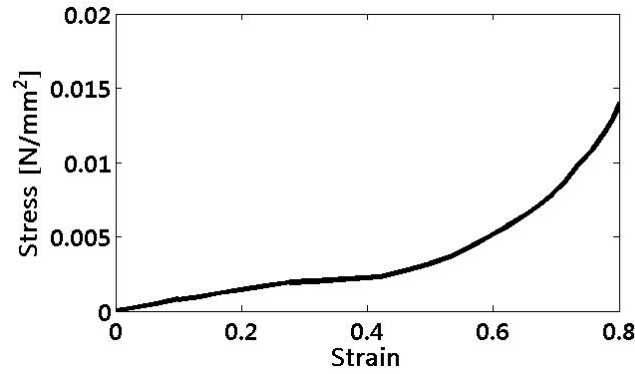


**Figure 3.2:** Load curve for low density foam following Mendoza-Vazquez et al. (2012) for thoracic organs

experiments were used for the comparison and evaluation of material models for lungs. In this section the simulation of the experimental set-up will be explained and a short introduction of the used material properties and the modification process will be given.

### 3.2.1 Experimental Modelling

One of the isolated volumes was placed slightly over a rigid table and loaded with gravity in z-direction to find the contact between the viscus and the table in a steady state. The state when the viscus was in equilibrium with the table was used as the new initial state for the impact simulations.

The impactor was modelled as a cylinder like in the experiments by Hayamizu et al. (2003) with a diameter of  $d = 80 \text{ mm}$  containing of solid elements. The chosen material for the impactor was elastic (LS-DYNA MAT\_ELASTIC\_001) with:  $\rho = 7.85 * e^3 \frac{\text{kg}}{\text{m}^3}$ ,  $E = 40 \frac{\text{kN}}{\text{mm}^2}$  and  $\nu = 0.3$ .

The height for the impactor resulted from the chosen density to fit with the experimental weight. For the main experiments with an impact speed of  $v = 5.4 \frac{\text{m}}{\text{s}}$  the weight was 1.7 kg. The volume of a cylinder is calculated by following equation.

$$V = A * h = \frac{1}{4} \pi * d^2 * h \quad (3.1)$$

In this equation A is the base of the cylinder and h the height. The weight is calculated by:

$$m = V * \rho \quad (3.2)$$

From Equation 3.1 and 3.2 it follows for the height:

$$h = \frac{4}{\pi} * \frac{m}{\rho d^2} \quad (3.3)$$

with the values for  $d$ ,  $\rho$  and  $m$  follows:

$$h = \frac{4}{\pi} * \frac{1.7 \text{ kg}}{7.85 * e^3 \frac{\text{kg}}{\text{m}^3} * (80 \text{ mm})^2} = 43.08 \text{ mm} \quad (3.4)$$

The weights for the other impact speeds were adjusted by changing the density instead of the height. The densities are summarized in Table 3.2.

**Table 3.2:** Impactor densities for adjusted masses

Impact speed [ $\frac{m}{s}$ ]	Impactor mass [kg]	Density [ $\frac{g}{cm^3}$ ]
3.4	2.8	13.145
4.4	1.7	7.85
5.4	1.7	7.85
6.1	0.9	4.225

The model of the experimental set-up can be seen in Figure 3.3. The viscus is already in a steady state and in contact with the table through gravity. In the experiments the impactor was guided on a rail, thus it could only move in z-direction and was fixed for rotating around each axes and translation in x-y-directions. The same boundary conditions were added to the impactor.

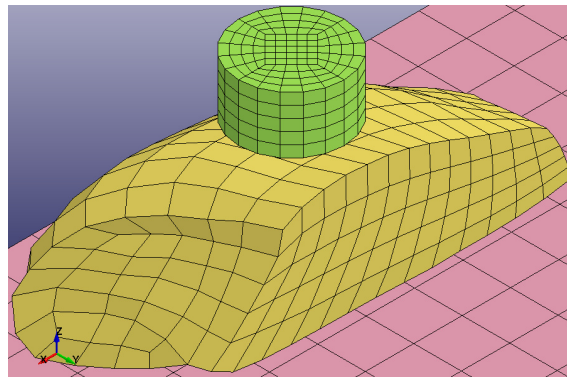


**Figure 3.3:** Model of the experimental set-up by Hayamizu et al. (2003) (isometric view)

According to the densities from Table 3.2 the initial speeds were referred to the impactor. The results from Hayamizu et al. (2003) (shown in Figure 2.13) were digitised with MATLAB (R2012a, The MathWorks Inc., Natick, Ma, USA). As mentioned before, one of the recorded time versus displacement curves from the experiments with  $5.4 \frac{m}{s}$  was much smaller than the others. Therefore this curve was considered as outlier and was ignored for the rating of the simulations.

As it can be seen in Figure 2.13 (a) the time versus displacement curve starts at a height of approximately 180 mm, though the thicknesses of the lungs were only  $129 \pm 16 \text{ mm}$ , which were reached after approximately 0.02 seconds. It can be seen in Figure 2.13 (b) that the first forces occurred after 0.018 - 0.02 seconds. This suggests that the plotted curves already show the displacement of the impactor before the impact on the lungs happens. This hypothesis is also supported by the high speed pictures of the impact procedure in Figure 2.12. The highest compression occurs between 0.3 s and 0.4 s and in contrary to the plotted curves not between 0.4 and 0.5 s. Therefore the data sets needed to be adjusted to the impact time. Furthermore, the displacement height had to be scaled from the thickness of the experimental lungs to the maximum model thickness in the impact

area of 100 mm (thickness in equilibrium after gravity load).

The modified curve is plotted in Figure 3.4. The time versus force curves were also adapted to the changed time. These curves were used for the evaluation of the model response.

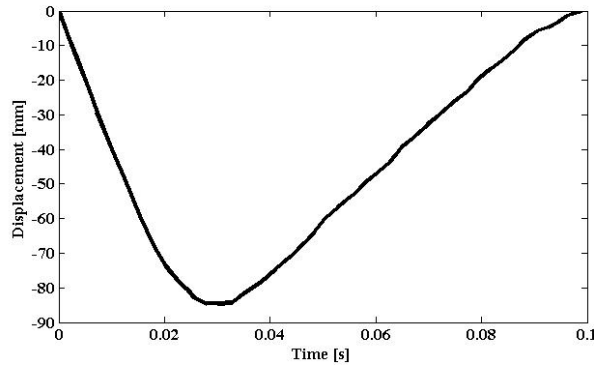


**Figure 3.4:** Time versus displacement curve adjusted to the impact time and scaled to the model size

### 3.2.2 Contact Conditions

As contact conditions between the table and the viscous the contact automatic surface to surface were chosen. The viscous was the slave segment and the table the master segment. To figure out the best contact conditions between the viscous and the impactor several simulations were run. Finally, the contact condition automatic surface to surface was chosen according to Gayzik et al. (2011). For this the viscous were defined as master and the impactor as slave segment. Because there was no lubricant in the experiments between the impactor and the viscous, a high friction coefficient was chosen by Al-Mayah et al. (2008b) and Loring et al. (2005) at 0.3.

To prevent the impactor of penetrating the lung model, it was partly necessary to add a soft constraint formulation with the sub-option pinball edge to edge contact. With this option the calculation of contact stiffness was based on stability consideration and the timestep was taken into account. This prevents penetration when soft materials are in contact with stiff materials.

### 3.2.3 Material Models

The three most common material models presented in Section 2.8 were used as material properties of the lung model for the simulation of the impact experiments by Hayamizu et al. (2003). The initial material parameter were chosen from publications using this material properties for lungs. An overview of different material properties used in literature can be viewed in Table 6.1.

The values for the material models which were used for the simulations are summarized in Tables 3.3 and 6.1. Three different material properties were chosen for viscoelastic

material behaviour, five for the strain-energy function and one for low density foam. It is conspicuously that the values for the materials are widely spread between different publications. E.g. the bulk modulus  $K$  varies from  $0.05 \frac{N}{mm^2}$ , Zhao and Norwani (2004), to  $2880 \frac{N}{mm^2}$ , Roberts et al. (2005).

No values were given for the typical alveolar diameter by Vawter (1980) and Zhao and Norwani (2004), therefore the typical alveolar diameter of a human male were chosen at 0.2 mm after Tenney and Bartlett (1967).

**Table 3.3:** Values for the different material models from literature, Mendoza-Vazquez et al. (2012); Plank et al. (1998); Roberts et al. (2005); Ruan et al. (2003); Stitzel et al. (2005); Vawter (1980); Zhao and Norwani (2004)

Material Model	Symbol [Unit]	Viscoelastic			Strain-energy function			Low d. foam Mendoza
		Plank et al.	Roberts	Ruan	Stitzel et al.	Vawter	Zhao	
Density	$\rho [\frac{kg}{m^3}]$	917	600	600	118	365	700	1000
Bulk modulus	$K [\frac{N}{mm^2}]$	2.875	2880	2.6	0.1124	0.1124	0.05	
Decay constant	$\beta$	100	0.1	0.25				0
Young's modulus	$E [\frac{N}{mm}]$							0.1
<b>Viscoelastic</b>								
Short time shear modulus	$G_S [\frac{N}{mm^2}]$	$7.387 * e^{-3}$	7.39	0.022				
Long time shear modulus	$G_L [\frac{N}{mm^2}]$	$2.358 * e^{-3}$	2.36	0.008				
<b>Strain-energy Function</b>								
Material Coefficient	$C [\frac{N}{mm}]$				$5.035 * e^{-4}$	$2.45 * e^{-3}$	$3.88 * e^7$	
Material Coefficient	$\alpha$				$8.227 * e^{-2}$	0.183	5.85	
Material Coefficient	$\beta$				-2.46	-0.291	-3.21	
Hyperelastic coefficient	$C_1 [\frac{N}{mm}]$				$6.535 * e^{-6}$	$1.93 * e^{-5}$	$1.27 * e^{-8}$	
Hyperelastic coefficient	$C_2$				2.876	2.71	2.71	
Typical alveolar diameter	$\Delta$ [mm]				0.0702	0.2	0.2	
<b>Low density foam</b>								
Tension cut off stress	TC							$1 * e^{14}$
Hysteretic unloading factor	HU							0.1
Viscous coefficient	DAMP							0.1
Shape factor for unloading	SHAPE							1

Most of the material models from literature did not terminate normally. Therefore, the values had to be adjusted manually to find a working model, before a coefficient study for optimizing the model response could be carried out.

### 3.2.4 Coefficient Study

After the first simulation part had been completed and a working model set-up had been found for the different material models, a parameter study was used to optimize the material models.

The simulated material models with values from literature showed a gap to the time versus displacement and force behaviour of the experiments by Hayamizu et al. (2003). Therefore a parameter study was used to optimize the values from the different material models aiming to receive a simulated time versus displacement and force response similar to the experimental results.

For the optimization the software LS-OPT was used. It was necessary to define the material coefficients as variables in the k-file (the LS-DYNA script file of the model), so that LS-OPT was able to identify them as variables. Afterwards the range and starting values

had to be defined for each variable as well as the optimization algorithm and the number of iterations.

The density was partly changed to investigate the influence of all parameter to the model response. Because the weight of the whole THUMS model had to keep constant, the density of the final material model had to be  $\rho = 1000 \frac{kg}{m^3}$  as in the original THUMS version. The optimization argument was the minimization of the Mean Square Error for displacement ( $MSE_{dis}$ ) of the impactor and the modified time versus displacement curve by Hayamizu et al. (2003) as well as the Mean Square Error for force ( $MSE_{force}$ ).

### 3.2.5 Load Curve Study

For the material model low density foam the load curve was a further tuning opportunity besides the material coefficient optimization. Therefore a pre-processor had to be implemented in LS-OPT which calculated the new curve depending on curve variables. A schematic example can be seen in Figure 3.5.

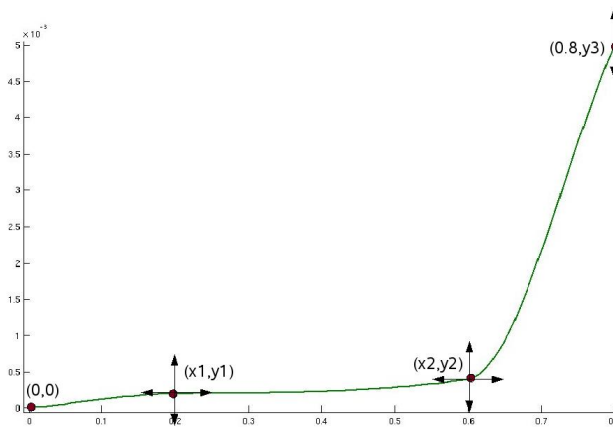


**Figure 3.5:** Schematic drawing of curve optimization with LS-OPT

For the input curve either fixed points (cf. Figure 3.5 point 0,0), points with a fixed x or y-value (point 0.8,  $y_3$ ) or points with flexible x and y-values (e.g. point  $x_1$ ,  $y_1$ ) could be defined.

In addition to the initial load curve of THUMS v3-M by Mendoza-Vazquez et al. (2012) the experimental stress versus strain curves of lung parenchyma (cf. Section 2.6) were digitised and also used as load curves (cf. Figure 5.1). Because Radford's and Remington's (1957) original publication was not available, the stress versus strain curve was obtained from Matthew's and West's (1972) publication. The load curve with the most promising model response was used as the initial curve for the curve optimization.

For the curve optimization only the first point (0, 0) was defined as a fixed one. Four points were defined as alterable in x and y direction, which means eight variables had to be defined.

It should be noted that the number of simulations per iteration and the calculation time increased exponential with an increasing amount of variables. The proposed minimum

simulations for each iteration were already 68 for eight variables. Therefore multiple optimization runs were executed with adjusted ranges for the variables.

### 3.3 Model Validation - Table Top Tests

The optimized material properties were implemented as modified lung material in the THUMS v3-M. With this modified model the table top tests, described in Section 2.7.2 by Kent et al. (2004), were simulated to approve the biofidelity and to investigate the influence of the tuned material to the thoracic response.

Thus the model THUMS v3-M was placed on a table, the pelvic slightly lower than the back and the head 87 mm higher. Gravity was applied until a steady state was reached (cf. Figure 3.6). Belts and the band were applied using the Seatbelt Fitting add-on in LS-PrePost.

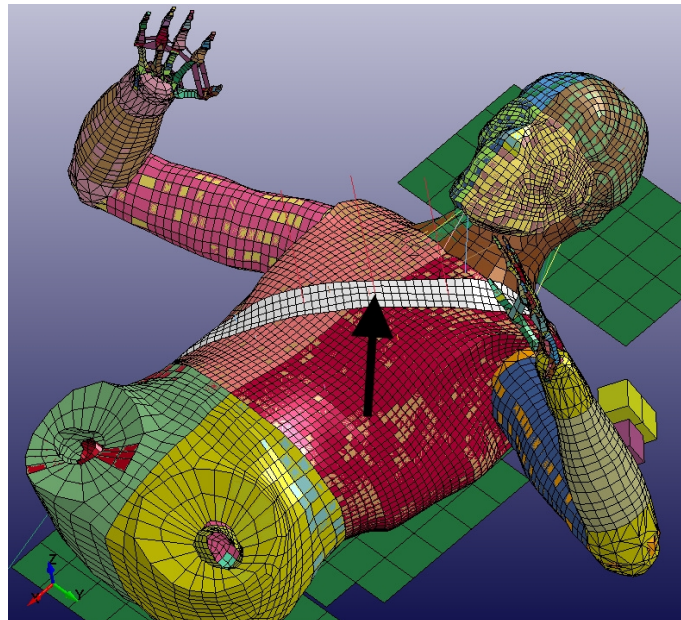


**Figure 3.6:** Experimental set-up of the table top tests by Kent et al. (2004) with a single belt; the arrow points to the place where the displacement was recorded

On both ends of the belts and the hub a displacement was applied, so that the compression rate matched the experimental values. For the force versus compression response, the vertical component of the contact force between the plate and the skin at the back of the model was used. The chest compression was obtained from the displacement of the belts and the band above the sternum in the height of the third rib (cf. black arrow in Figure 3.6).

## 4 Results

In this chapter the results of the simulations described in the chapter before will be given. The focus lies on the model response of different material models to the impact speed of  $5.4 \frac{m}{s}$ . This is due to the limited data for the other impact speeds of the experiments by Hayamizu et al. (2003).

### 4.1 Material Models

In this chapter the results of the simulations of the three different material models will be given. The material models strain-energy function and viscoelastic material behaviour were simulated with different material properties from literature.

#### 4.1.1 Strain-Energy Function

In the simulation of the experiments all material models of strain-energy function terminated with an error. In Figure 4.1 some simulations are shown in the state before termination. The material model according to Vawter (1980) (Figure 4.1 (a)) terminated after 0.019 s because of negative volume in some elements. The viscous was deformed under the impactor 92 mm at the moment of termination. The surrounding of the viscous nearly remained at its initial thickness and a sharp edge was formed between the compressed part under the impactor and the surrounding. The upper and lower limb nearly stayed in their original positions and did not move upwards as observed in the experiments (cf. Figure 2.12).

The material models according to Stitzel et al. (2005), Gayzik et al. (2007) and Gayzik (2008) already terminated after 0.009 s, 0.015 s and 0.011 s, respectively. The progress of deformation of the viscous was not sufficient enough to make a statement about the deformation behaviour.

The simulation with the material model according to Zhao and Norwani (2004) terminated immediately after the calculation was started.

#### 4.1.2 Viscoelastic Material Behaviour

From the three different material data for the viscoelastic material model summarized in Table 3.3, the models from Plank et al. (1998) and Ruan et al. (2003) terminated with an error because of negative volume in some elements. The deformation of the model in the state of error termination can be viewed in Figures 4.2 (a) and (b).

The model according to Plank et al. terminated after 0.006 s. The model was deformed mainly in the area under the impactor since the rest of the viscous was still in its initial state. A sharp edge evolved between the impact area and the rest of the model (cf. Figure 4.2 (a)).

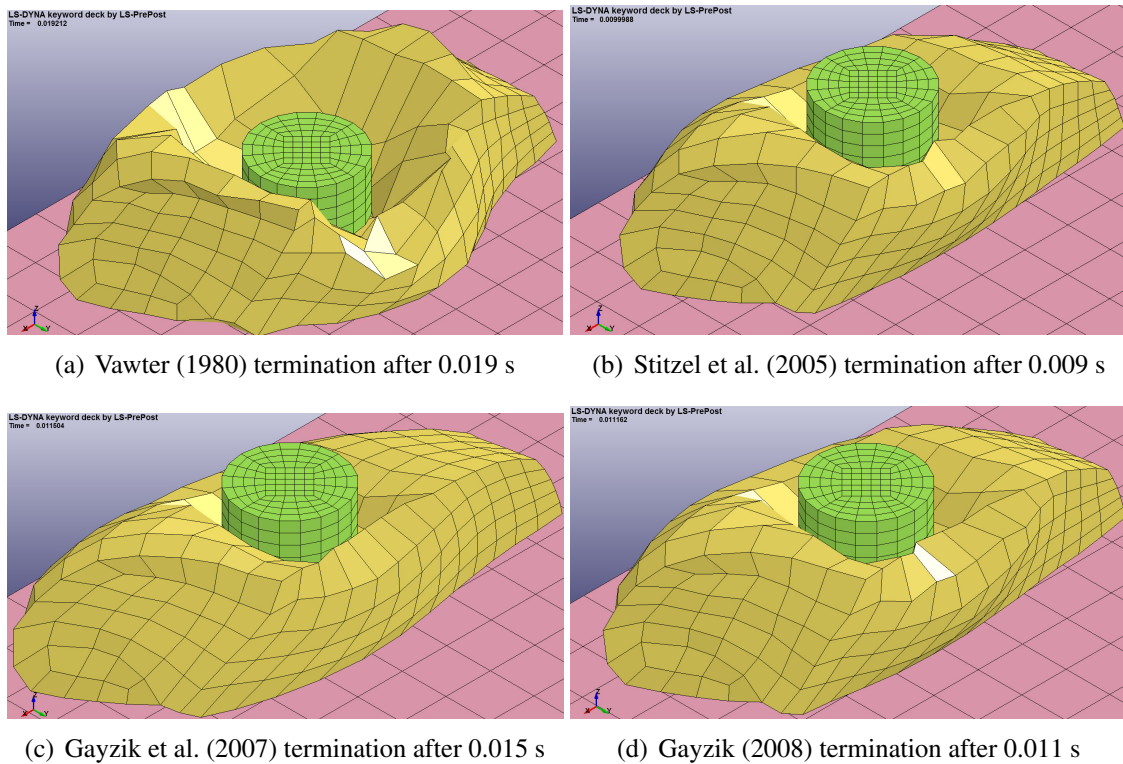


**Figure 4.1:** Simulated experiments for different values of the strain-energy function at the moment of error termination

The model after Ruan et al. terminated after 0.015 s. The impactor deformed the model 62.7 mm before the simulation terminated. Compared to the deformed model of Plank et al. the whole model underwent a deformation through the impactor. The deformation ran continuously from the impact area smoothly to the rest of the model. The upper and lower limbs stayed in their original positions on the table (cf. Figure 4.2 (b)).

The material model according to Roberts et al. (2005) terminated normally. In Figures 4.2 (c) and (d) the model is shown after 0.003 s and after 0.029 s, respectively. The highest compressions already occurred already after 0.003 s with a deformation of only 8.5 mm. Afterwards the impactor was rebounded by the viscous back in z-direction. The viscous also began to bounce off the table through the impact energy (cf. Figure 4.2 (d)).

### 4.1.3 Low Density Foam

The material model low density foam with the material parameters from Mendoza-Vazquez et al. (2012) terminated normally. The model in its initial state can be seen in Figure 4.3 (a). In Figure 4.3 (b) the model is shown after 0.035 s in the state with the highest compression. In the front the impactor is partly covered by the lung tissue. The upper and lower limb moved upwards through the energy of the impactor. In Figures 4.3 (c) and (d) the viscous is shown after 0.1 and 0.2 s. The experiments by Hayamizu et al. (2003) were recorded only for 0.1 s. In the simulation the viscous and the impactor reached a steady state after 0.2 s in which the viscous was still a little bit compressed.

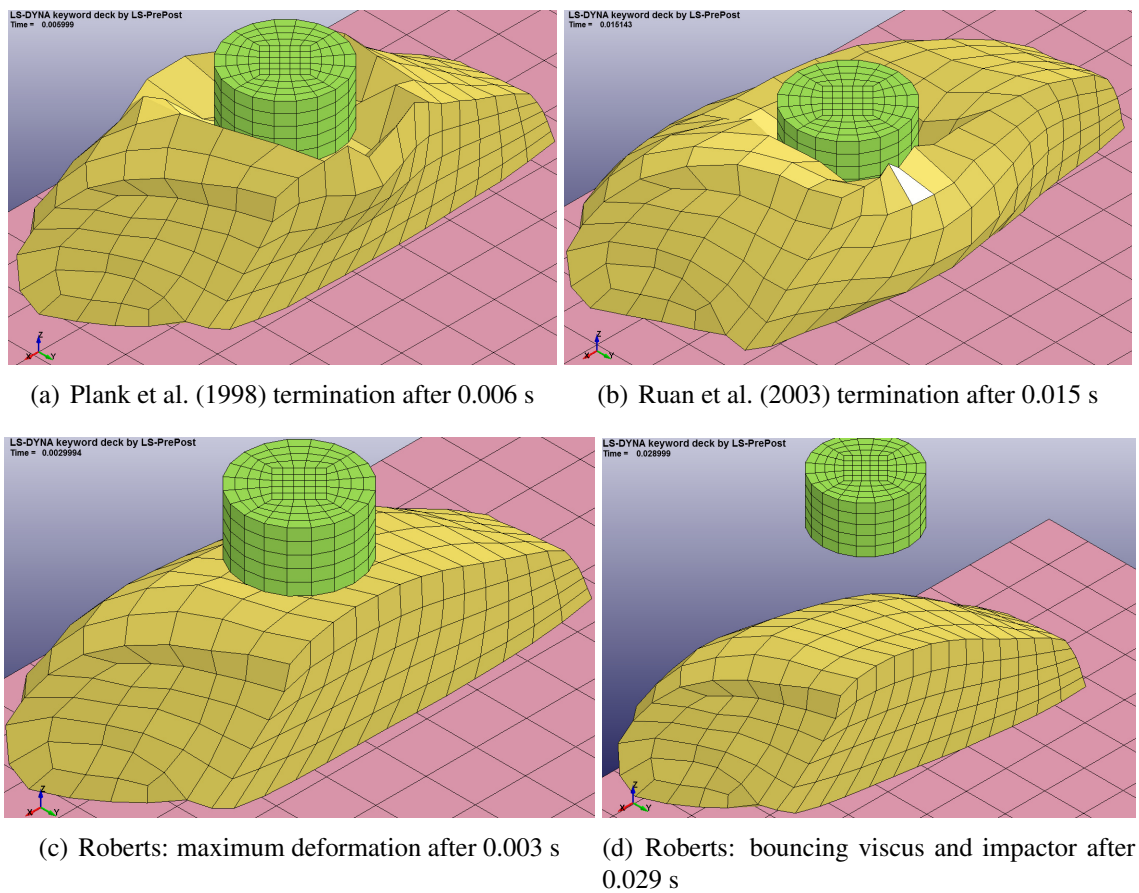


**Figure 4.2:** Simulated experiments for different values of the viscoelastic material model at the moment of error termination (a) and (b) and after some particular elapsed time for normal termination by Roberts et al. (2005) (c) and (d)

The time versus displacement plot of the simulated model with low density foam material properties for an impact speed of  $5.4 \frac{m}{s}$  can be seen in Figure 4.4 (a). Here the displacement is assigned negative because the impactor moved against the z-direction. The impactor compressed the viscus from 100 mm to a minimum of 27.6 mm after 0.035 s. That means the impactor had a displacement of 86.3 mm.

The results of Hayamizu et al. (2003) scaled to the size of the model are also plotted in 4.4 (a). It can be acknowledged that Hayamizu recorded a displacement of the impactor of 85 mm.

In the experiments the impactor was reflected by the lungs up to the original height. Contrary to the experiments, in the simulation the impactor was reflected only to a height of 54 mm after 0.1 s. In the steady state after 0.2 s a maximum reflection to a height of 37 mm was reached (cf. Figures 4.3 (c) and (d)).

In Figure 4.4 (b) the deformation versus force plot of the simulation and the experiments can be seen. In the simulation a peak force of 675 N was reached at a compression rate of 85 %. The peak force was nearly at the height of the experimental peak force at a compression rate of 85 %. The resulting forces between a deformation of 25 % and 60 % were higher than the forces in the experiments.

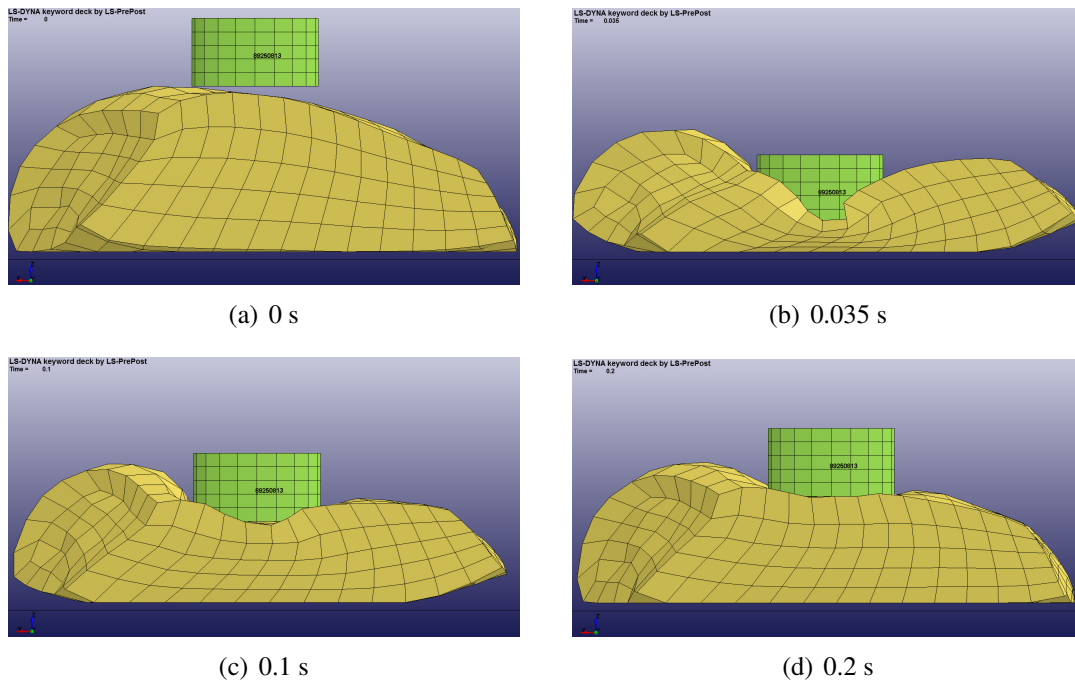


**Figure 4.3:** Thoracic volume deformation behaviour with the low density foam material model after different times with an impact speed of  $5.4 \frac{m}{s}$

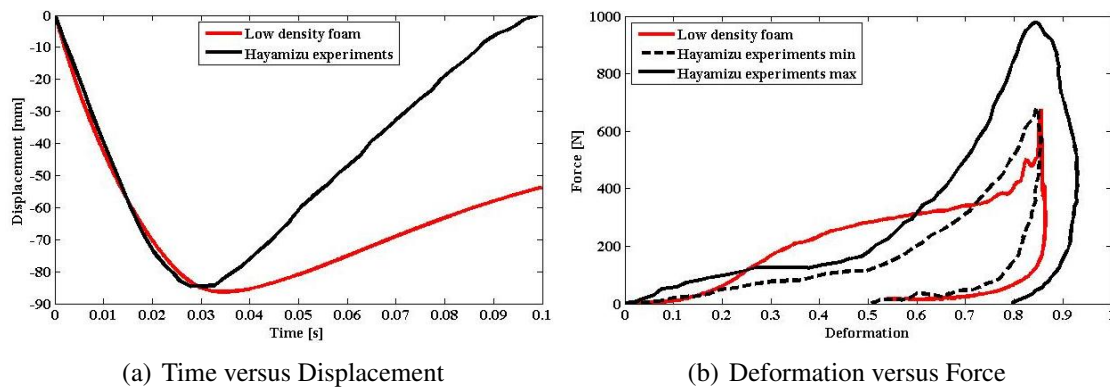


**Figure 4.4:** Experimental data by Hayamizu et al. (2003) and simulation data for an impact speed of  $5.4 \frac{m}{s}$

### 4.1.4 Impact Speed Variation

In Figure 4.5 (a) the deformation versus force plots for the different impact speeds can be seen. The used material model was still low density foam and the plotted curves from Hayamizu are the minimum curves digitised from Figure 2.13 (d).

As can be seen the model response for  $3.5 \frac{m}{s}$  is similar to the experimental data. The force from the simulation is higher in the first part than in the experiments and the peak force at 650 N is less than in the experiments at a rate of nearly 800 N. At 87 % the deformation is slightly higher than in the experiments at 85 %.

The model response for  $4.4$  and  $6.1 \frac{m}{s}$  is quite different to the experimental data. There is

no distinctive peak force and the deformation for  $6.1 \frac{m}{s}$  is less and for  $4.4 \frac{m}{s}$  higher than in the experiments. The maximum resulting forces in the simulations were 250 N for  $4.4$  and  $6.1 \frac{m}{s}$  and in the experiments 630 N and 530 N, respectively.

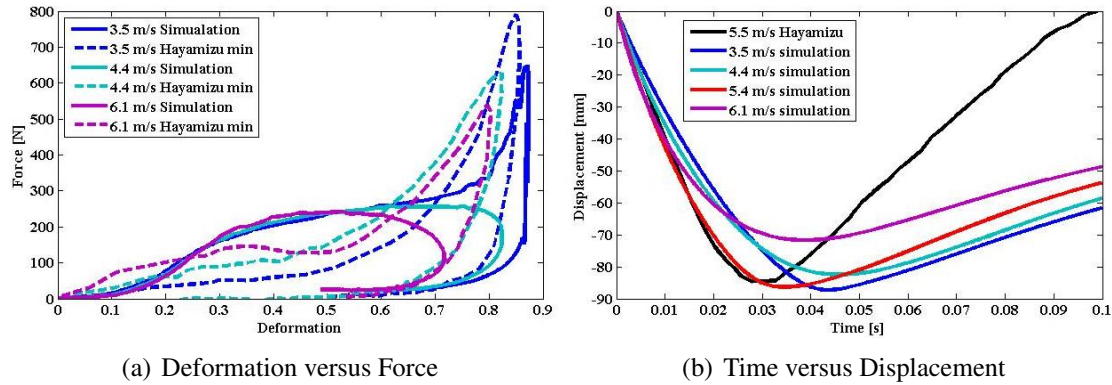


**Figure 4.5:** Model response and experimental data for different impact speeds for low density foam material model

It should be noted that the highest deformation and force appeared in the simulation and in the experiments at the lowest impact speed of  $3.5 \frac{m}{s}$  and the lowest deformation and force at the highest impact speed of  $6.1 \frac{m}{s}$ .

The Figure 4.5 (b) shows the time versus displacement plots for all simulated speeds and for the experiments at  $5.4 \frac{m}{s}$ . Because there are no experimental data available for the time versus displacement behaviour of different impact speeds, this plot does not allow conclusions of the simulated behaviour compared to the experiments.

## 4.2 Coefficient Studies

From the simulations of the three material models with different material properties the best ones were selected and used as initial material models for the coefficient studies. The aim was to enhance the model response and to identify the best material model for the simulation of lungs under impact conditions.

### 4.2.1 Strain-Energy Function

The results of a sensitivity study of LS-OPT are shown in Figure 4.6. It can be seen that the curve fit parameter  $C_1$ ,  $C_2$  and the material constant  $C$  have the highest influence on the Mean Square Error (MSE) with 32.6 %, 24.1 % and 31.5 %, respectively.

In Figure 4.7 (a) the time versus displacement response for an iteration step of the strain-energy function can be seen. The black crosses represent the scaled time versus displacement curve taken from Hayamizu et al. (2003).

A correlation between the displacement and the parameter  $C$  could be observed: the lower the parameter  $C$ , the higher the deformation of the model.

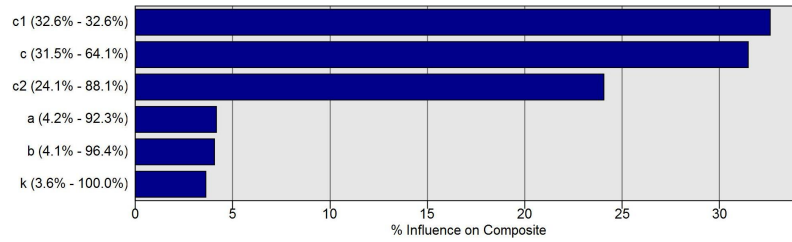


**Figure 4.6:** MSE sensitivity study for the strain versus energy function with  $a = \alpha$  and  $b = \beta$

Figure 4.7 (b) shows the time versus force response from the simulation related to the deformation curves in Figure 4.7 (a). The experimental results are again represented by the black crosses. The lower the parameter C and thus the stiffness, the higher the oscillating of the force.

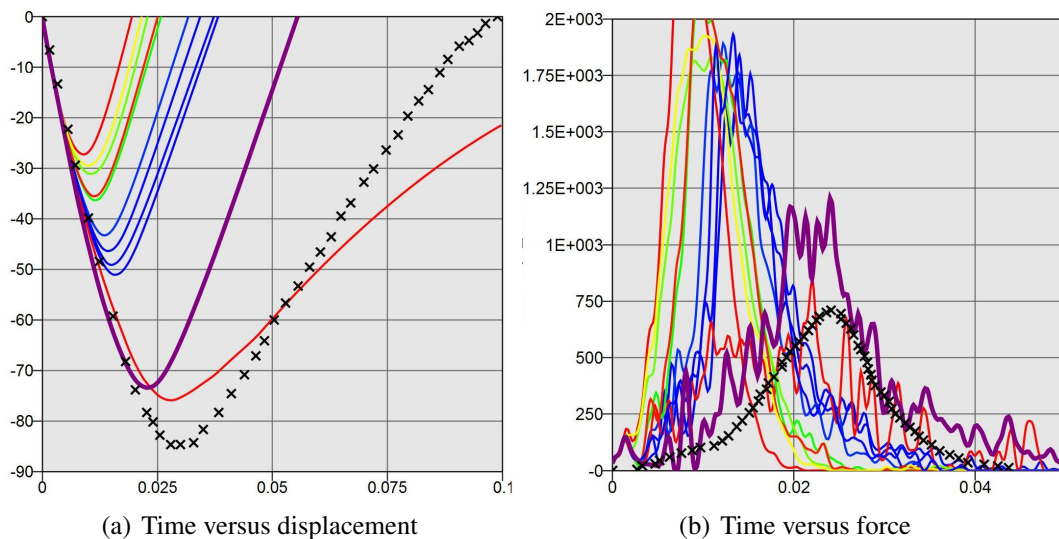


**Figure 4.7:** Model response for a coefficient study for the material model strain-energy function

The highest MSE for the top-most curve was 7.31 and the parameter C was in this case  $0.0172 \frac{N}{mm}$ . The corresponding model can be seen in Figures 4.8 (a) and (b). The highest displacement was reached after 0.006 s with a depth of 22.8 mm. Afterwards the impactor was rebounded by the viscus.

The best time versus displacement and force results were obtained for the curve marked in violet. The corresponding model can be seen in Figures 4.8 (c) and (d). The impactor compressed the viscus 76.2 mm after 0.016 s before the impactor and the viscus were rebounded by the table. The decreased stiffness led to an unstable shape of the viscus. The model behaved completely different compared to the lungs in the experiments shown in Figure 2.12.

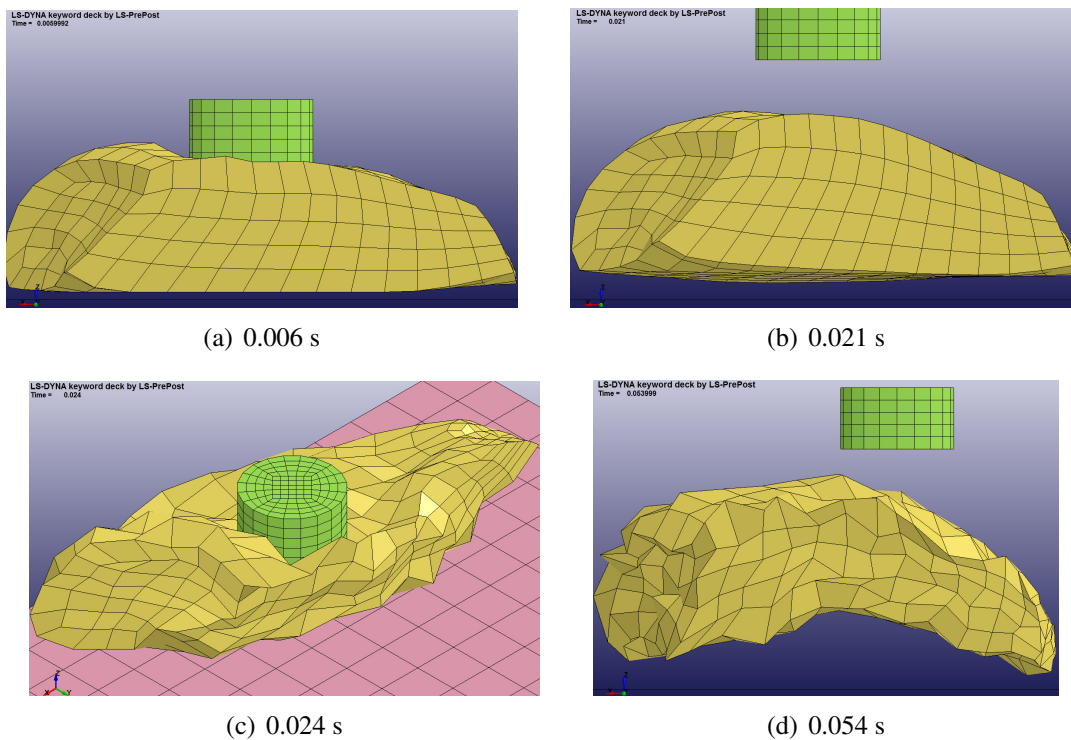


**Figure 4.8:** Stiffest ((a) and (b)) and softest ((c) and (d)) material models from the strain-energy function parameter study shown in Figure 4.7

### 4.2.2 Viscoelastic Material Behaviour

From the models with values from literature only the model according to Plank et al. (1998) terminated normally. This model was used as the basis for the parameter study. In Figure 4.9 it can be seen that the parameter  $\beta$  has with 63.9 % the highest influence on the MSE. The short term modulus  $G_S$  has the second most effect on the MSE. The other parameters, the long term modulus, bulk modulus and density only had a small influence on the model response.

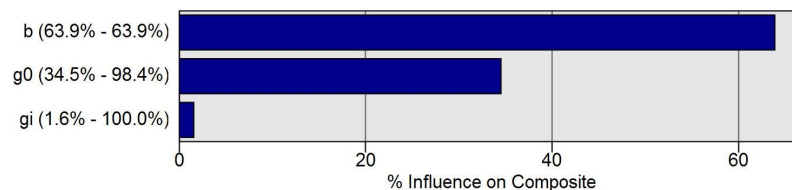


**Figure 4.9:** MSE sensitivity study for the viscoelastic material model, with  $g_0 = G_S$ ,  $g_i = G_L$  and  $b = \beta$

In Figure 4.10 (a) a parameter study is shown for the dependency of  $G_S$  on the time versus displacement model response. A clear correlation between the stiffness and the parameter  $G_S$  was determined. Every simulation with  $G_S \leq 0.03$  terminated with an error. In Figure 4.10 (b) the force time versus force response is shown. As can be seen, the forces highly oscillated for all simulations.

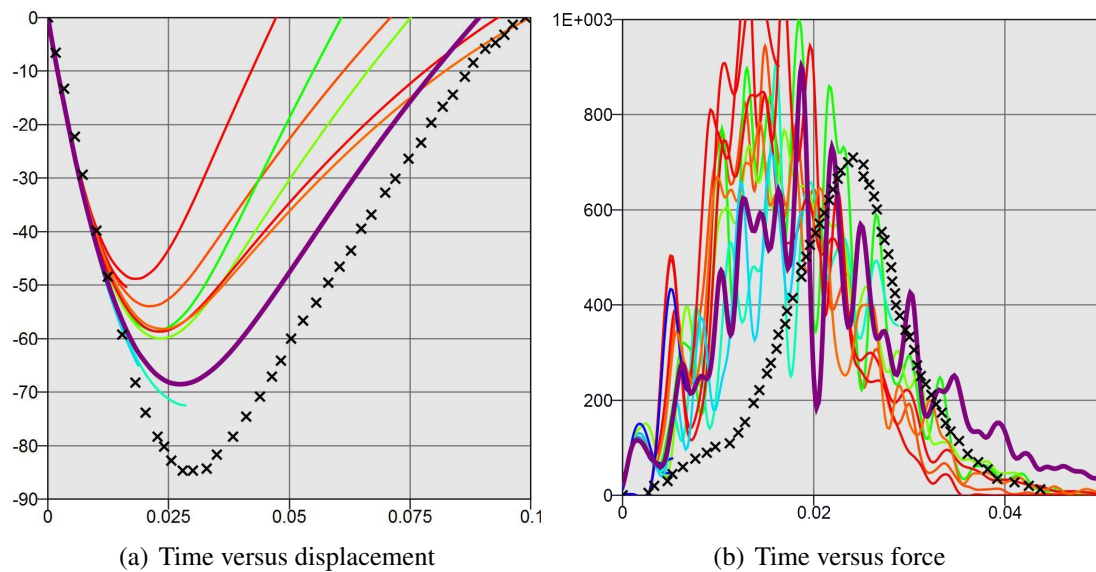


**Figure 4.10:** Model response for a coefficient study of viscoelastic material behaviour

A correlation for the decay constant  $\beta$  and the rebounding intensity could also be determined. The decay constant is a dimension for the energy dissipation, which means for the damping intensity. It should be noted that a lot of simulations of this material model terminated with an error.

The lowest MSE has the curve marked in violet in Figure 4.10 (a) with a  $MSE_{dis}$  of 0.017 and a  $MSE_{force}$  of 0.083. The simulated model for this model parameter can be seen in Figure 4.11. The parameter for the viscoelastic material used in this simulation can be found in Table 4.1.

**Table 4.1:** Viscoelastic material parameter for the best MSE obtained from parameter studies

Parameter	Unit	Value
Density	$\rho$ [ $\frac{kg}{m^3}$ ]	600
Bulk modulus	K [ $\frac{N}{mm^2}$ ]	1112.44
Decay constant	$\beta$	146.7
Short time shear modulus	$G_S$ [ $\frac{N}{mm^2}$ ]	0.03
Long time shear modulus	$G_L$ [ $\frac{N}{mm^2}$ ]	0.0075
$MSE_{dis}$		0.017
$MSE_{force}$		0.083
<b>MSE</b>		<b>0.05</b>

The model is shown in the state of highest compression after 0.023 s with a compression of 63.8 mm.

The principle shape of the viscus remained during the impact procedure and the deformation was continuous from the impact area steady to the rest of the viscus. The upper and lower limb moved slightly upwards.

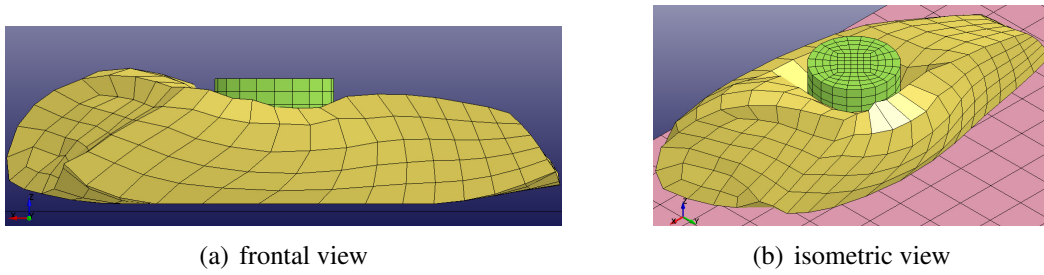


**Figure 4.11:** Simulated thoracic volume with viscoelastic material model with the lowest MSE at the state of highest deformation

### 4.2.3 Low Density Foam

In Figure 4.12 a sensitivity study of parameter for the material model low density foam is shown. The viscous coefficient ( $d$ ) has the highest influence on the MSE with 37.9%. The decay constant  $\beta$  ( $b$ ) influences the outcome as second most with 31.8% followed by the density  $\rho$  with 13.4%.

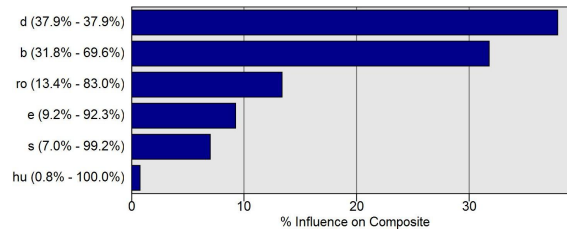


**Figure 4.12:** MSE sensitivity study for the viscoelastic material model with: decay constant  $b = \beta$ , density  $ro = \rho$ , viscous coefficient  $d = DAMP$ , young's modulus  $e = E$ , shape factor for unloading  $s = SHAPE$  and the hysteretic unloading factor  $hu = HU$

Figure 4.13 (a) shows the time versus displacement plots of a multi parameter study for the parameters of low density foam. For this study the decay constant ( $\beta$ ), the viscous coefficient ( $d$ ), the young's modulus ( $E$ ), the shape factor for unloading ( $s$ ) and the hysteretic unloading factor ( $h$ ) have been defined as variables. The upper and lower bounds were chosen corresponding to recommendations of LS-DYNA and to the original values. In Figure 4.13 (a) the coloured scale is for the viscous coefficient  $d$ . A correlation between the rebounding intensity of the impactor and the viscous coefficient can be seen. The damping effect is higher for a high viscous coefficient. In Figure 4.13 (b) the resulting forces of the parameter study can be seen.

The curve marked in violet has the lowest  $MSE_{dis}$  with 0.009 and a  $MSE_{force}$  of 0.37, which means an average MSE of 0.19. The impactor deformed the viscus by 88 mm and a peak force of 1900 N occurred. The parameters for this model are summarized in Table 4.2.

Figure 4.14 (a) depicts the simulated model in the moment of highest compression for the best  $MSE_{dis}$  of the parameter study. The model was highly compressed through the

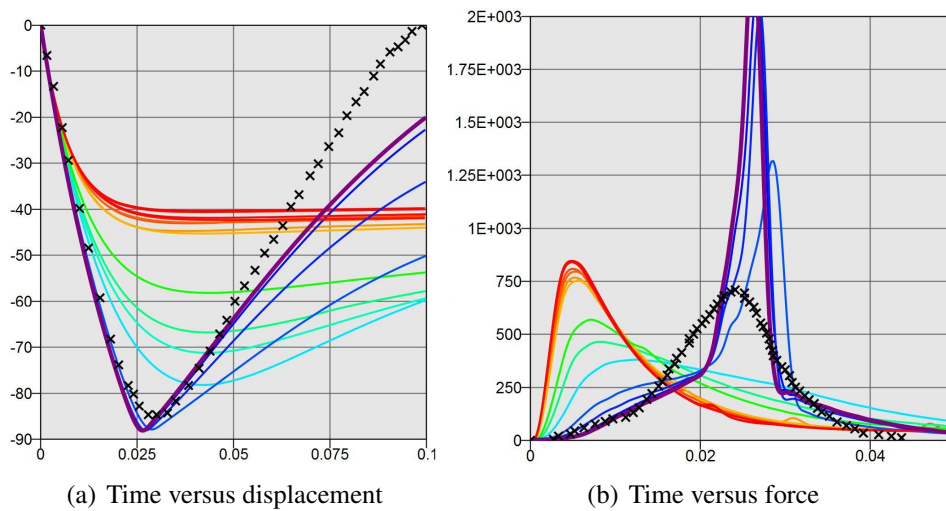


**Figure 4.13:** Model response for a coefficient study of the material model low density foam; colours depending to the viscous coefficient  $d$ .

impactor in the impact area and the upper and lower limbs moved upwards. The deformation behaviour looked similar to the deformed lungs in the experiments by Hayamizu et al. (2003) (cf. Figure 2.12). In this parameter study the density was variable, too.

In Figure 4.14 (b) the simulation with the same parameters but with the original density  $\rho = 1000 \frac{\text{kg}}{\text{m}^3}$  can be seen. The deformation characteristic are similar to the simulation with a lower density.

In Figures 4.14 (c) and (d) the time versus displacement and time versus force responses for both simulations and the experiments are plotted. There it can be seen that the viscous were compressed up to 87.5 mm for both simulations. The curve characteristic at the inflexion point is much harder than in the experiments. The rebounding intensity of the impactor is less for the higher density than for the curve with the best results.

The time versus force plots can be seen in Figure 4.14 (d). The peak force for the simulation of the best parameter for the displacement behaviour is three times higher than in the experiments. For the higher density the peak force is still twice as high as the maximum peak force in the experiments.

### 4.3 Load Curve Study

Despite an extensive parameter study with the different material models a satisfying material model could not be found. The best results were obtained with the material model low density foam, but there was still a gap between the experimental data from Hayamizu et al. (2003) and the model response in the simulations. Therefore a curve verification study with the load curve of low density foam was performed with LS-OPT.

In the first step the digitised stress versus strain curves of the experiments with lung tissue, plotted in Figure 5.1, were implemented as load curves in the material model low density foam.

The model response of the simulation with the experimental stress versus strain curves

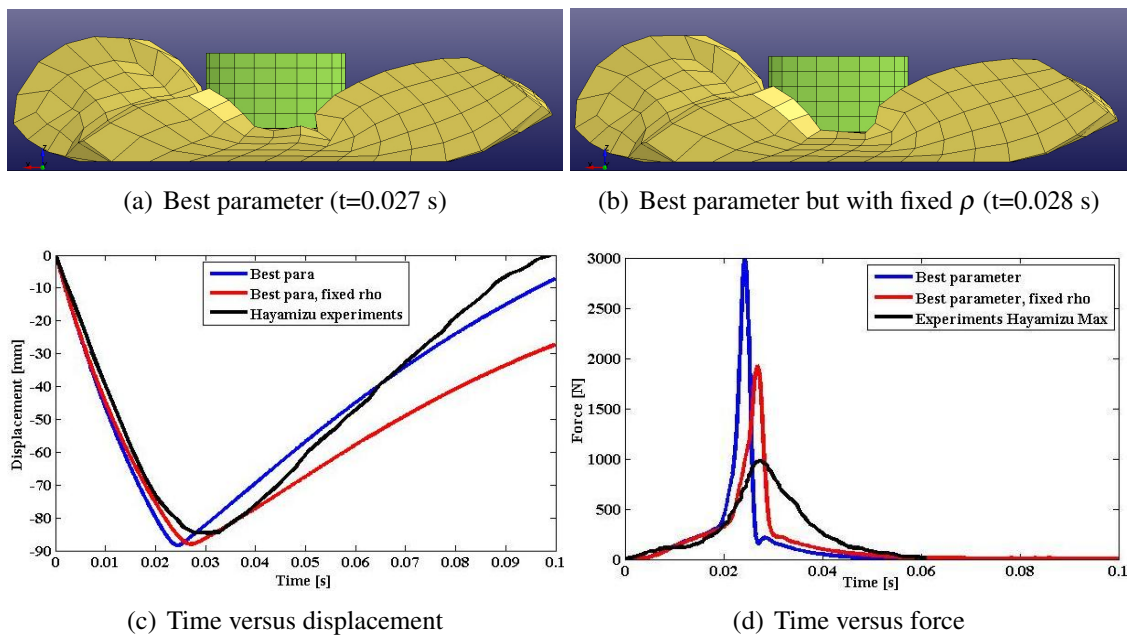


**Figure 4.14:** Model response for the the material model low density foam at the moment of highest compression ((a) and (b)) and model response plots ((c) and (d)) for the best results of the coefficient study

was much stiffer than with the original one from Mendoza-Vazquez et al. (2012). The best results were obtained with the load curve from Hoppin Jr. et al. (1975), but the viscus was only compressed up to 63 mm.

Therefore the further investigations were based on the load curve from THUMS v3-M from Mendoza-Vazquez et al. (2012) as the initial curve. In Figure 4.15 a curve study for time versus displacement and time versus force response is shown. As can be seen, there is no clear correlation between the displacement and force behaviour. Most of the plotted curves have, for example, a similar displacement behaviour but totally different time versus force responses.

It should be noted that already small changes of the load curves could lead to completely different model responses. A clear correlation between the model response and the load curve could not be identified.

For the most promising load curve a parameter optimization was also carried out. The final parameter of this model can be seen in Table 4.2. The final model has a  $MSE_{dis}$  of 0.004 and a  $MSE_{force}$  of 0.06. The average MSE is 0.032. The  $MSE_{dis}$  is twenty times lower than the  $MSE_{dis}$  from the original material parameter from Mendoza-Vazquez et al. (2012). The  $MSE_{force}$  is with 0.06 the same as from the original material model and four times lower than the  $MSE_{force}$  of the parameter study. Finally the average MSE is with 0.032 less than half the original MSE.

The final load curve and the load curves of other simulations and experiments can be seen in Figure 4.16. Figure 4.16 (a) shows that the final curve, the modified curve by Mendoza-Vazquez et al. (2012) and the curve from the displacement optimization are very similar compared to the load curve from THUMS v3.0 and from Wang (1995). In Figure 4.16

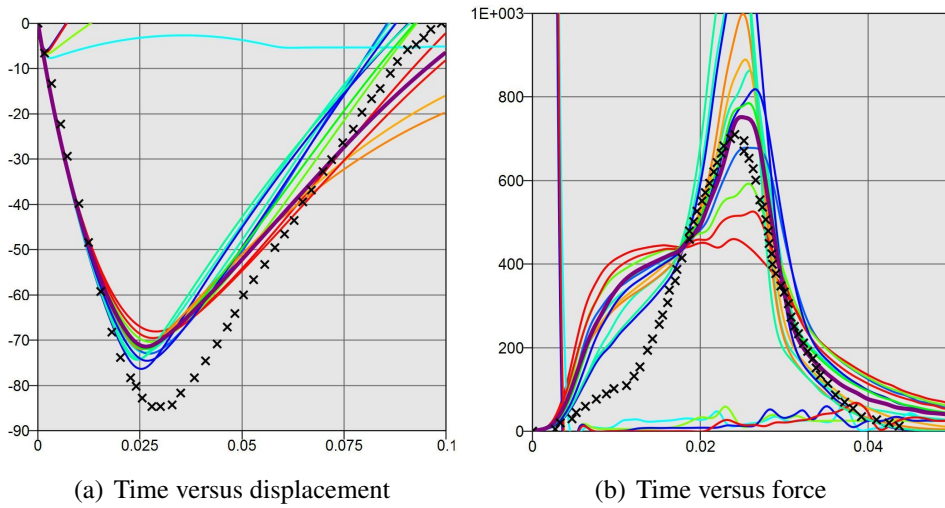


Figure 4.15: Model responses for different load curves

Table 4.2: Parameter for low density foam from parameter and curve studies and the corresponding MSE

Parameter	Unit	Mendoza-V.	Parameter Study	Final model
Density	$\rho$ [ $\frac{kg}{m^3}$ ]	1000	1000	1000
Decay constant	$\beta$	0	0.001	0
Young's modulus	$E$ [ $\frac{N}{mm^2}$ ]	0.1	0.968	0.1
Hysteretic unloading	HU	0.1	0.0347	0.1
Viscous Coefficient	DAMP	0.1	0.056	0.3
Shape factor for unloading	SHAPE	1	5.638	1
$MSE_{dis}$		0.081	0.022	0.004
$MSE_{force}$		0.06	0.25	0.06
<b>Average MSE</b>		<b>0.07</b>	<b>0.136</b>	<b>0.032</b>

(b) the stress is scaled to show the differences between these load curves. Especially the modified THUMS curve and the load curve for the best MSE are very similar.

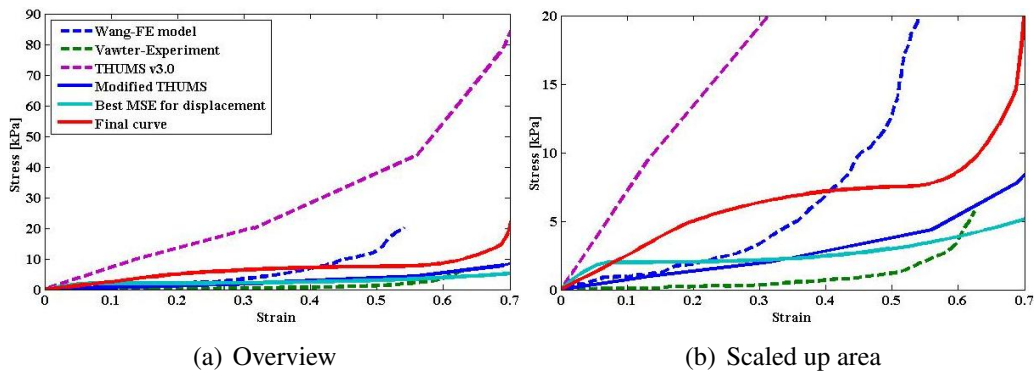
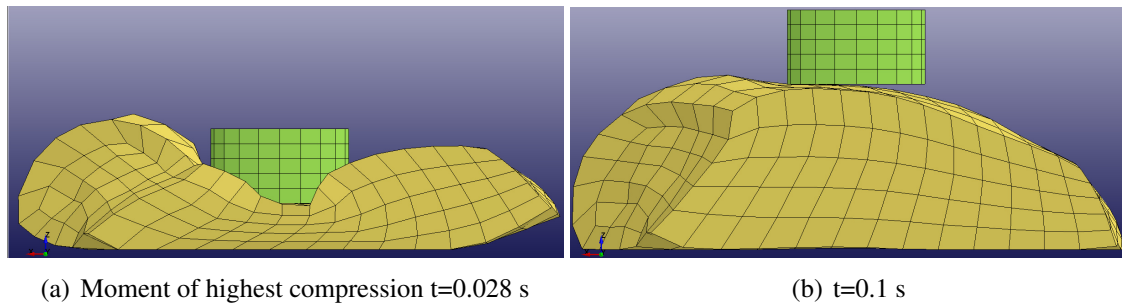


Figure 4.16: Stress versus strain curves from curve optimization and from literature

## 4.4 Final Model Response

The model deformation and expansion characteristics of the final model can be seen in Figure 4.17. The moment of highest compression was reached after 0.028 s with a compression of 78.5 mm. The upper and lower limbs were moved upwards through the impact energy as in the experiments by Hayamizu et al. (2003) in Figure 2.12. The curvature of the deformed model smoothly continues from the impact area to the rest of the model.



**Figure 4.17:** Model response for the final material model

In Figures 4.18 (a) and (b) the time versus displacement and time versus force plots of the final material model, the original material model and the experiments are plotted. It can be seen that the highest compression of the final model is with 78.5 mm slightly smaller than in the experiments with 84.6 mm. The remaining compression after 0.1 s is with 8 mm slightly less than in the experiments, but much better than in the original model with 54 mm.

In Figure 4.18 (b) it can be seen that the final material model similar to the original model has too high forces between 0.05 s and 0.02 s of the simulation. Except for the time between 0.3 s and 0.4 s, where the force is slightly under the minimal forces of the experiments, the force remains inside the corridor of the experiments until the end. The peak force is with 800 N perfectly in the average of the experimental results. The original model is, contrary to the modified model, most of the time outside the experimental corridor.

In the Figures 4.18 (c) to (f) the deformation versus force plots of the different impact speeds are shown for the final model, the original model and the experiments. As can be seen, the force versus deformation behaviour of all impact velocities is similar for the original and modified material model for the first approximately 30 % of deformation. Afterwards the occurring forces are higher for the modified model.

The force is between  $\sim 24\%$  and  $60\%$  over the forces recorded in the experiments for all velocities and both material models.

For  $3.5 \frac{m}{s}$  and  $5.4 \frac{m}{s}$  the shape of the model response curve is similar to the experimental results. The highest deformation is approximately eight per cent less than in the experiments and the forces are slightly higher in the first deformation part. The height of the peak forces is inside the corridor of the experiments at  $5.4 \frac{m}{s}$  and slightly under it at  $3.5 \frac{m}{s}$ .

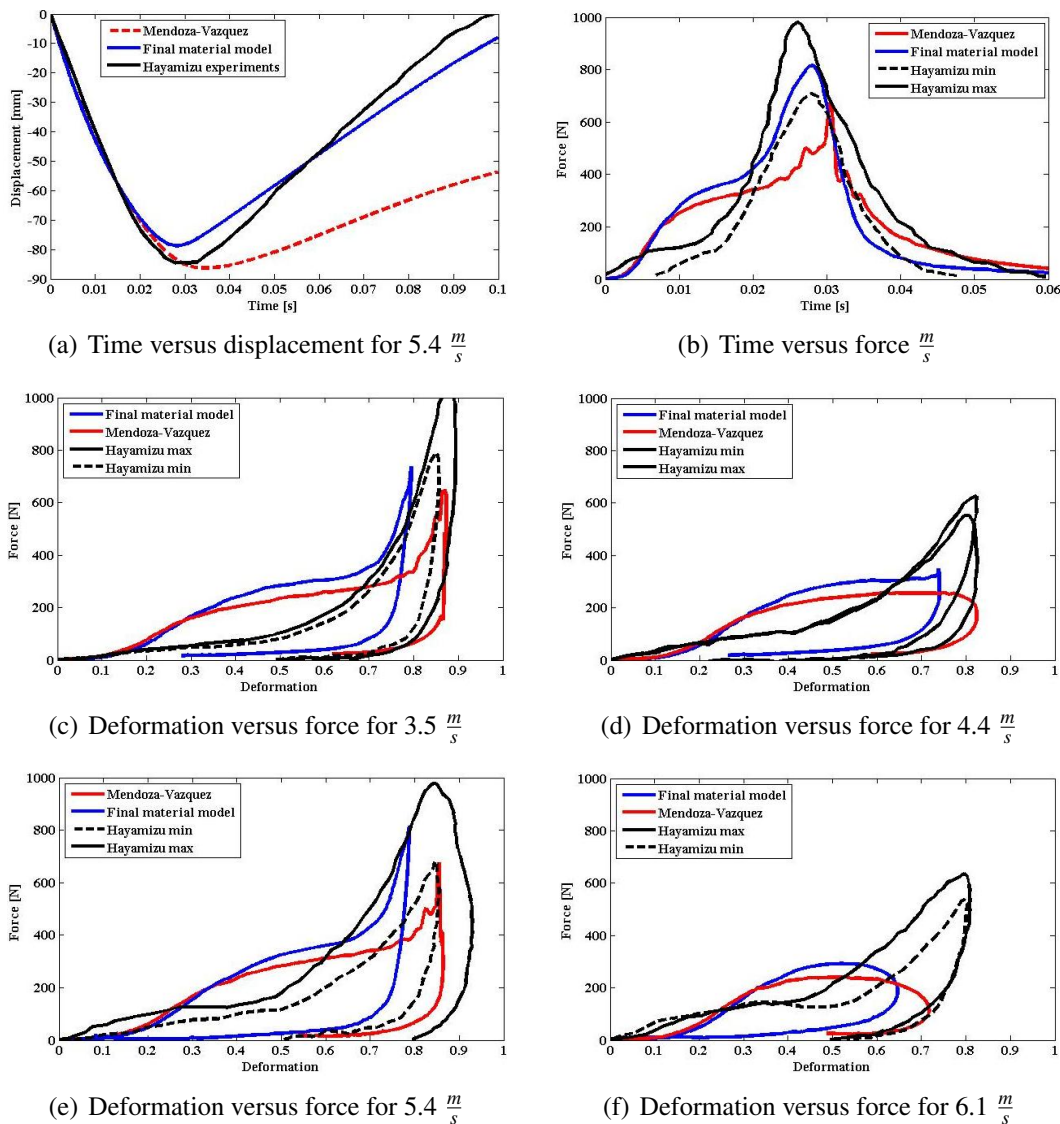


**Figure 4.18:** Model response of the viscus for the final material model

For the impact speeds of  $4.4 \frac{m}{s}$  and  $6.1 \frac{m}{s}$  the model response is quite different to the experiments. The deformation is 10 to 20 % less than in the experiments. In both simulations no real peak forces occur and the maximum force is roughly half the size of the forces in the experiments with approximately 320 N.

## 4.5 Model Validation

The optimized material model with the modified load curve was implemented as material model for the thoracic viscera in THUMS v3-M. With this modified model and the original model the table top tests of Kent et al. (2004) were simulated.

In Figure 4.19 the THUMS v3-M model can be seen in the initial state before the simulation began and after 0.1 s in the moment of highest compression. The left part of the

model was removed to make the compression of the viscera visible. As can be seen, the belt compressed the thoracic cage and the deformation was transformed through the ribs and the sternum to the viscera.

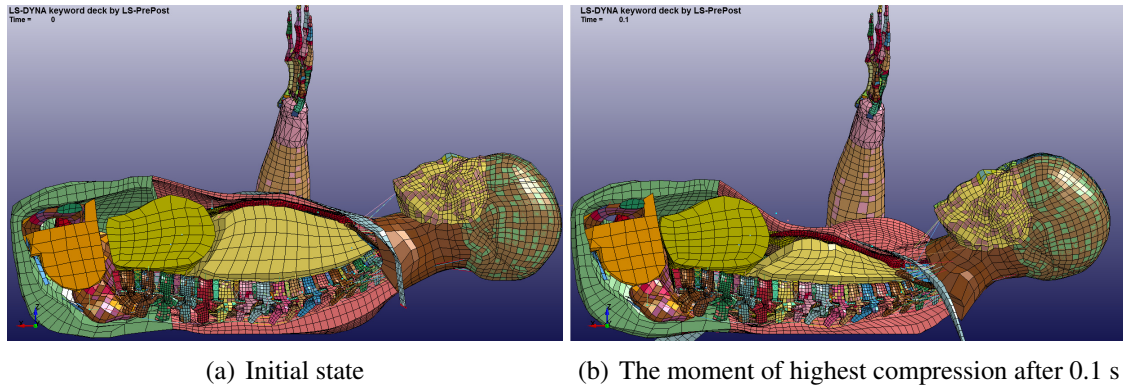


**Figure 4.19:** THUMS v3-M with the modified lung material model under single belt loading conditions, the left part of the body had been removed

The results of the chest deflection versus reaction force from the simulations are plotted in Figure 4.20. The results are shown for the four load cases: hub loading, belt loading, double belt loading and distributed loading.

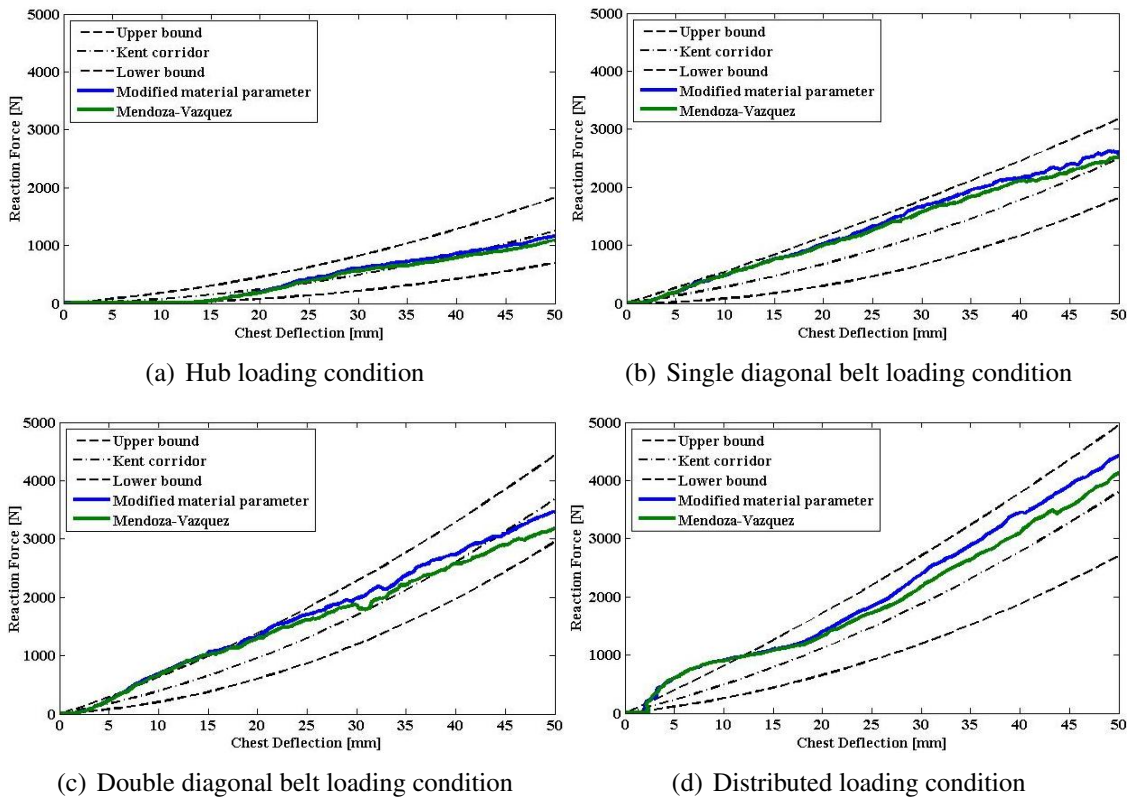


**Figure 4.20:** Force versus compression response for THUMS v3-M

For each load case the results of the simulation of THUMS v3-M with the material parameter according to Mendoza-Vazquez et al. (2012), the results with the modified material model and the experimental corridors from Kent et al. (2004) are plotted.

As can be seen, the results of the THUMS v3-M and the results of THUMS v3-M with modified lung properties are similar for the roughly first 20 mm of chest deflection. Afterwards, the reaction force of the modified material model increases slightly faster than the reaction force of the original THUMS v3-M. The highest difference in the reaction force is reached for all loading conditions at the highest point of chest deflection after 50 mm. At this point, the reaction force is approximately 70 N (hub loading), 150 N (single belt) and 300 N (double diagonal belt and distributed) higher than the original THUMS v3-M. The original model response is only outside the corridor for the double diagonal belt and the distributed loading conditions in the first part of chest compression. In this region the modification of the lung material has no influence on the model response. The influence increases with a higher chest deflection but the reaction force of the modified THUMS v3-M remains clearly inside the experimental corridor.

# 5 Discussion

## 5.1 Experimental Discussion

A summary of experiments with lung parenchyma is given in Section 2.6. In this chapter a short discussion of these experiments will be given to rate the quality of the available material data for lung tissue.

The validation experiments by Hayamizu et al. (2003) and the table top tests by Kent et al. (2004) will be discussed afterwards.

### 5.1.1 Lung Tissue Experiments

Hoppin Jr. et al. (1975) performed experiments with triaxial test conditions on cubes out of dog lung tissue. The loads were applied on the specimens with sixteen hooks on each side. This is also the limitation of the experiments, because 96 hooks in a small cube have a huge influence on the outcome. In the publication, Hoppin et al. did not discuss the influence of these boundary effects on the results. Furthermore, Hoppin et al. tested only two specimens which is a too little scope to receive valid results.

Contrary to these experiments, Vawter et al. (1978) used slabs out of dog lung tissue from eleven dogs and tested them with uni- and biaxial loading conditions. The deformations were measured in some distance to the clamps with the advantage of minimized boundary effects on the results. Furthermore, the scope was much higher with eleven specimens than in the experiments by Hoppin et al.

Zeng et al. (1987) was the only author who used human lung tissue for the experiments. The experimental setup was similar to Vawter et al. and thirteen specimens were used.

As mentioned before, the publication for the experiments by Radford and Remington (1957) was not available. From the title of the publication "Recent studies of mechanical properties of mammalian lungs" it can be assumed that mammalian, but non human specimens were used. The curve data were digitised by Matthews and West (1972).

The presented experiments are the state of the art and the material models for several FE-simulations were based on these results, e. g.:

- **Vawter et al.:** Gayzik et al. (2007); Kimpara et al. (2005); Mendoza-Vazquez et al. (2012); Wang (1995)
- **Radford et al.:** Matthews and West (1972); Plank et al. (1998); Ruan et al. (2003); Sundaram and Feng (1977)
- **Zeng et al.:** Al-Mayah et al. (2008a)
- **Hoppin et al.:** Lee and Frankus (1975).

These emphasize the key role of these experiments in recent and current investigations and simulations of lungs.

In Figure 5.1 the digitised, average stress versus strain curves of the four experiments are plotted. The curve of Radford and Remington (1957) increases up to a maximum stress of 7.5 kPa at 0.8 % of strain. It can be seen that the curve of Radford et al. looks quite similar to the curve of Zeng. He measured a maximum stress of 6 kPa at 0.8 % of strain. The stress versus strain curve of Vawter et al. increases up to 6 kPa after 0.7 % of strain. Contrary to these three stress versus strain curves, the curve in the experiments by Hoppin et al. first starts to increase at 0.8 % of strain up to a maximum stress of 9 kPa at 1.4 % of strain.

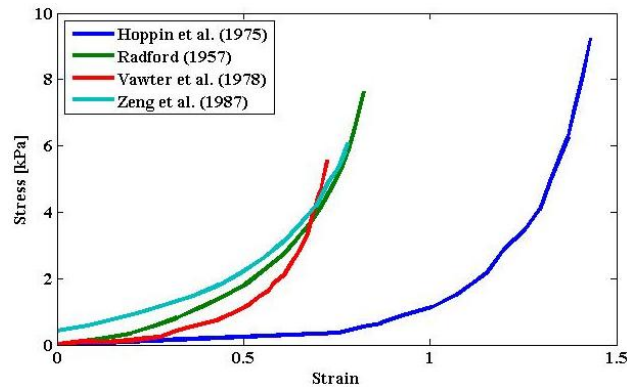


**Figure 5.1:** Stress versus strain curves from experiments, Hoppin Jr. et al. (1975); Radford and Remington (1957); Vawter et al. (1978); Zeng et al. (1987)

A comparison of these stress versus strain curves shows that there are huge differences in the experimental results of the different authors. First, it is conspicuous that Hoppin's curve first starts increasing first after 0.8 % of strain. In contrary to Vawter and Zeng, Hoppin measured the specimens under multi-dimensional loading conditions. As mentioned before, he neglected the influence of his boundary conditions. This could explain the gap between the stress versus strain curves of Hoppin et al. compared to the other authors.

Contrary to the the other authors, Zeng et al. used human lung tissue in his experiments. The experimental setup was the same Vawter et al. used for his experiments with dog parenchyma. Therefore, in his discussion Zeng compared the results of Vawter et al. with his results. He concluded that human lungs have a stiffer material behaviour than dog lungs. This conclusion is only reasonable for the first strain part, the stress versus strain curve of dog lungs increases faster after 5 % of strain. Already at a strain of 0.7 % the dog lungs' curve has a higher stiffness than the human lungs' curve.

The results of Radford and Remington (1957) can be described as an average of Vawter et al. and Zeng et al. Because of the missing publication, these results can not be taken into account in this discussion.

It should be noted, that all of the specimens in these experiments were tested in tension and only with cubes or slabs cut out of lungs. Therefore the significance of these experiments for the simulation of a whole lung model is limited because a small slab or a cube do not represent the inhomogeneous lung structure and the deformation behaviour of the whole organ. Furthermore in RTC lungs are being compressed, thus it would be a matter of interest how lung parenchyma behave under pressure.

### 5.1.2 Impact Response Tests

The impact response tests with swine lungs by Hayamizu et al. (2003) were carried out with impact velocities higher than they usually occur in frontal RTC and some information is missing. Furthermore, the scope of the experiments is very small with only five specimens for the impact speed of  $5.4 \frac{m}{s}$  and with only two specimens for the other impact speeds. Further information, e.g. about the specimen's size, are missing and the time versus displacement and time versus force results are only published for the impact speed of  $5.4 \frac{m}{s}$ .

In addition, detailed information to the results is missing. As already mentioned in Section 3.2.1, the time versus displacement curves obviously already begin before the impact on the lungs happens. This assumption is supported by the delayed force occurrence and the different time scale of the impact pictures (cf. Figures 2.13 and 2.12).

The next point which is worthy of discussion is the chosen mass for the different impact speeds. Hayamizu declared that the mass of the impactor was adjusted depending on the impact speeds to keep the kinetic energy in the moment of impact equivalent. The kinetic energy is calculated by the Equation 5.1. Table 5.1 shows the calculated kinetic energy for the different impact speeds. The corrected mass is the mass the impactor should have had to keep the kinetic energy equal to the kinetic energy of  $5.4 \frac{m}{s}$  for all impact speeds.

$$W_{kinetic} = \frac{1}{2} * m * v^2 \quad (5.1)$$

As can be seen in Table 5.1, the kinetic energy for the impact speeds of  $3.5 \frac{m}{s}$ ,  $4.4 \frac{m}{s}$  and  $6.1 \frac{m}{s}$  was more or less in the same dimension at 17.15 J, 16.46 J and 16.74 J, respectively. For the impact speed of  $5.4 \frac{m}{s}$  the kinetic energy was at clearly higher 24.79 J. This could be expected, because the same mass was used for  $4.4 \frac{m}{s}$  and  $5.4 \frac{m}{s}$ . Hayamizu did not explain this oddity further.

**Table 5.1:** Kinetic energy for different impact speeds

Velocity $v$ [ $\frac{m}{s}$ ]	Mass $m$ [kg]	Kinetic Energy $T$ [J]	Corrected Mass [kg]
3.5	2.8	17.15	4.05
4.4	1.7	16.46	2.56
5.4	1.7	24.79	1.70
6.1	0.9	16.74	1.33

In the Figures 2.13 (c) and (d) the deformation versus force responses of the experiments are plotted. The principle shape of the curves looks similar for all impact speeds. The lowest force occurs at roughly 600 N for the impact speeds  $4.4 \frac{m}{s}$  and  $6.1 \frac{m}{s}$ . The average force occurs with 800 N at the impact speed of  $5.4 \frac{m}{s}$  and the highest force occurs with 1000 N at  $3.5 \frac{m}{s}$ .

It is conspicuous that the highest force occurs with the lowest impact speed and that the highest kinetic energy leads to the average force. These unexpected results were again not mentioned or discussed by Hayamizu.

The thickness of the lungs has a huge variation with  $129 \pm 16 \text{ mm}$ . The displacement results had to be scaled to the size of the used model. Because no further information

was given, the average thickness was used as scaling size for the deformation and for the adjustment of the time.

In summary it can be said that the impact response tests by Hayamizu et al. (2003) have a large room for the interpretation of the results because some information and a discussion of the results are missing. Nevertheless, the experimental setup and procedure by Hayamizu et al. can be applied perfectly for validation simulations with FEM. Furthermore, in absence of alternatives these experiments were chosen for the investigation of different material models for lungs.

### 5.1.3 Table Top Tests

The table top tests by Kent et al. (2004) can be used as validation experiments for thoracic models and HBM. Previously, several models were validated against pendulum impact tests with PMHS. Pendulum impact experiments to the sternum load the chest symmetrically and only in a narrow area. In contrast restraint systems like seatbelts lead to quite different, asymmetrical loads over the whole chest. Among others the PMHS were tested in these table top experiments with the specific load condition of a seatbelt.

A further advantage is, that different load cases were tested with the same PMHS and the results were scaled to the 50<sup>th</sup> percentile male. This simplifies the simulation for different load cases and the comparability of the results between the experiments and an FE-HBM is ensured.

## 5.2 Discussion of the Simulations

As mentioned before, no investigation has been done to validate a human lung model for frontal car crashes. Only one publication was published with experiments under loading conditions similar to frontal car crashes suitable for the validation of a human lung model. These experiments were first published in 2003 and only in Japanese language, Hayamizu et al. (2003).

Furthermore, no publication could be found in which different material models for lungs or thoracic organs were compared with each other.

The aim of the simulations in this thesis was to figure out the best material model for lung tissue and to enhance the model response of a human lung to experimental data. In the last fifty years several simulations of the thorax and thoracic organs were done. Different material models were developed and used for thoracic viscera in general or lungs in particular. An overview of thoracic modelling is given in Section 2.4.2.

From the literature three common material models were chosen for closer investigation of the material behaviour (cf. Section 2.8). Therefore, the experiments by Hayamizu et al. (2003) were simulated and the models were rated and optimized on the basis of their impact response.

As already mentioned before, the experimental data of Hayamizu had to be edited to the impact time and scaled to the size of the model. Because of the limited data the material models were rated on the basis of the time versus displacement and time versus force

response to an impact speed of  $5.4 \frac{m}{s}$ . Furthermore, the model deformation characteristic was used as a further argument for the quality of the material model.

### 5.2.1 Strain-Energy Function

The material model strain-energy function is the most commonly used material model for soft tissue of lungs. The material model is defined by two mechanical parameter (density and bulk modulus), three material coefficients ( $C$ ,  $\alpha$  and  $\beta$ ), the hyperelastic coefficients  $C_1$  and  $C_2$  as well as the anatomic coefficient delta ( $\Delta$ ). Herein the coefficient  $C$  determines the overall stress level.  $C$ ,  $\alpha$  and  $\beta$  were determined by experiments and therefore they are also called curve fit parameters, Zeng et al. (1987).

The parameter  $\Delta$  is the typical alveolar diameter and depends on the specimen. Gayzik et al. (2007) used e.g. for their investigation with rat lungs the typical alveolar diameter of rats with 0.0702 mm according to Tenney and Remmers (1963). Some authors like Vawter (1980) or Zhao and Norwani (2004) did not publish the alveolar diameter they used. In the simulation of their material properties the typical alveolar diameter of a human male were used with a thickness of 0.2 mm as in Tenney and Remmers (1963).

All five material models that have been simulated executed with an error. This could be explained by different model designs, mesh sizes or boundary conditions. Zhao and Norwani (2004) for example, developed a human body model and validated the thoracic response including viscera against pendulum impact experiments. The material parameter for the lungs were determined by using the experiment data of Yen (1999). A further validation of the isolated lungs was not performed.

Stitzel et al. (2005) and Gayzik (2008) developed and validated a model for an FE based injure metric for pulmonary contusion of rat lungs (cf. Section 2.5). They optimized the material model for the deformation versus force response of rat lungs to an impactor with low kinetic energy ( $8.74 \pm 2.5$  mJ versus 25 J in the experiments by Hayamizu et al. (2003)).

Thus, the simulated material parameter were originally used for divergent simulations with different boundary conditions. In the simulated experiments in this thesis, the lungs were hit by the impactor with high kinetic energy and were highly deformed. This explains why the simulation with material data from other experiments aborted.

Hence, the parameter of the strain-energy material model were optimized for the model response compared to the experiments by Hayamizu et al. As a basis for the parameter study the model of Stitzel et al. (2005) was used. To obtain a higher numerical stability of the model, the initial stiffness was increased with a higher material parameter  $C$ . A coefficient study with a varying typical alveolar diameter showed that the influence on the time versus displacement outcome was very small. For a varied  $\Delta$  from 0.07 mm (alveolar diameter of a rat) to 5 mm (alveolar diameter of a whale), the deformation changed by a maximum of 10 mm. Because of this limited influence and the anatomic background, the alveolar diameter were excluded from the parameter optimization.

As can be seen in Section 4.2.1 the parameter study did not lead to a satisfying model response. Also the model deformation behaviour for soft material behaviour looked unnatural (cf. Figures 4.8 (c) and (d)). Thus, the optimization of this material model was abandoned to focus on the other material models.

### 5.2.2 Viscoelastic Material Behaviour

The initial material properties for the simulation of viscoelastic material behaviour were chosen from three publications which used this material model for lungs in their simulations. Ruan et al. (2003) and Plank et al. (1998) used the material properties in their publication for the validation of a thoracic model's response to different car crash loading conditions. Roberts et al. (2005) investigated the model's response of a thoracic FE-model to non-penetrating ballistic impacts. Hence, all publications only investigated the response of a thoracic model with implemented lungs, a validation of the isolated lungs was not carried out.

From the three simulated material models with different parameter, the models of Ruan et al. (2003) and Plank et al. (1998) terminated with an error because of negative element volume. The model of Roberts et al. (2005) terminated normally. Unfortunately, the material showed a very stiff behaviour. The impactor compressed the model only up to 8.5 mm. Nevertheless, this parameter of the material model according to Roberts et al. were used as initial values for the parameter study to tune the model response.

The material model viscoelastic is defined by the parameter  $G_S$  = short term shear modulus,  $G_L$  = long term shear modulus and  $\beta$  = decay constant as well as the bulk modulus  $K$  and the density  $\rho$ . The density is a fixed value which is defined by the weight of the human body model. The bulk modulus  $K$  varied greatly in the publications and had nearly no influence on the model response. Therefore, only the three parameter  $G_S$ ,  $G_L$  and  $\beta$  were used for the parameter study.

As can be seen in Figure 4.9 the parameter  $G_L$  had nearly no influence on the MSE. The parameter  $\beta$  influenced the dumping characteristic and  $G_S$  the stiffness. Unfortunately, all simulations with a value of  $G_S \leq 0.04$  terminated with an error. Therefore, the maximum deformation that could be reached was 18 % less than in the experiments and measured 69 mm (cf. Figure 4.10 (a)). Furthermore, the force oscillated highly for all simulations (cf. Figure 4.10 (b)). Hence, the material tuning for the viscoelastic material model was not successful.

### 5.2.3 Low Density Foam

For the simulation of the material model low density foam the parameter of the THUMS v3-M from Mendoza-Vazquez et al. (2012) were used. As apparent in Figure 4.4 already the model response with the original values was much better than the optimized models of strain energy function and viscoelastic material model. The deformation characteristic (cf. Figure 4.3) also looked similar to the pictures of the experiments from Hayamizu et al. (2003).

To improve the expanding characteristic a parameter study was carried out. The material model low density foam is defined by six material parameter, which means a huge range of modification opportunities. Nevertheless, an optimized deformation behaviour led to a deteriorated force response. The best model response for time versus deformation led to a peak force twice the size of the experimental forces. Thus, this modified material was not convenient and could not be used.

The modification of the stress versus strain curve was a second tuning opportunity. Originally, the experimental stress versus strain curve from Vawter et al. (1978) was used. Wang (1995) increased this curve by multiplying the stress with ten to validate the thoracic model response against cadaver impact experiments. This curve was doubled and used as the load curve for the thoracic organ properties of the original THUMS v3.0, Kimpara et al. (2005). In turn, Mendoza-Vazquez et al. (2012) decreased the curve by multiplying it with  $10^{-6}$ . These modified curves can be seen in Figure 2.5. Finally, it can be said that it was a common procedure to modify the experimental stress versus strain curve to obtain a valid thoracic response. Therefore, a modification of this curve can doubtlessly be used as a tuning opportunity.

First of all, the experimental stress versus strain curves of Hoppin Jr. et al. (1975), Radford and Remington (1957), Vawter et al. (1978) and Zeng et al. (1987) were implemented as load curves for low density foam to check the model response with curves justified by the help of experiments. Because the model response for all experimental curves was much stiffer than with the load curve of Mendoza-Vazquez et al. this approach was discarded and the curve of THUMS v3-M was used for the curve optimization.

Surprisingly, already small changes in the load curve can lead to completely different model responses and also have a huge influence on the resulting forces (cf. Section 4.3). The final material model was a little bit stiffer than the experimental results. The impactor deformed the lung model by seven per cent less but the expansion characteristic was quite similar to the experimental results. The  $MSE_{dis}$  was with 0.004 much better than the original  $MSE_{dis}$  with 0.022 and with a steady  $MSE_{force}$ . Also the deformation characteristic of the model looked similar to the pictures of the experiments (cf. Figure 4.17).

The final material model was also simulated with the different impact speeds and the deformation versus force responses were compared to the experimental results (cf. Figure 4.18). It can be seen that the reaction force for all impact speeds for the first 60 % to 75 % of deformation is higher than in the experiments. This anomaly could not be eliminated with the parameter and curve modifications. Because of missing data the time versus displacement characteristic could only be evaluated for an impact speed of  $5.4 \frac{m}{s}$ .

The completely different model responses for the impact speeds of  $4.4 \frac{m}{s}$  and  $6.1 \frac{m}{s}$  might be explained by the inconstant kinetic impact energies. The impact energies of  $4.4 \frac{m}{s}$  and  $6.1 \frac{m}{s}$  were with 16.46 J and 16.74 J the lowest of the experiments, respectively. These contradict, that despite completely different kinetic energies the model responded similar to the impactors with  $5.4 \frac{m}{s}$  and  $3.5 \frac{m}{s}$ .

For the high impact speed of  $6.1 \frac{m}{s}$  the conspicuous model behaviour might also be explained by the dumping effect which is sensitive to velocity. But this explanation can not reason that the model responded for  $4.4 \frac{m}{s}$  on the same way.

### 5.2.4 Model Validation

The tuned material model with the optimized load curve was implemented as the material model for the thoracic viscera in the THUMS v3-M. To verify the biofidelity of the THUMS v3-M with the new material model the table top tests by Kent et al. (2004) were used.

The results showed that the changed material parameter had a small influence on the deformation versus force response of the model. For the first 15 mm to 20 mm of chest deflection the modified THUMS v3-M model behaved like the original THUMS v3-M. Afterwards the reaction force increased slightly higher.

This could be explained by the changed material model. In the validation simulation, the modified material model behaved a little bit stiffer than the original one. The model was compressed by nine percent less which resulted in a 36 % higher peak force. In the first part of compression the modified material had the same deformation versus force response than the original material model. At an impact speed of  $3.5 \frac{m}{s}$  the force was first higher after 29 mm of compression.

The deformation velocity in the table top tests was with  $1 \frac{m}{s}$  less than in the experiments of Hayamizu et al. (2003).

### 5.2.5 Summary

The experiments by Hayamizu et al. (2003) were simulated with a thoracic organs from THUMS v3.0. Three common material models were chosen from literature and the material parameter of several publications were implemented in the model.

All of the tested material models were only validated for thoracic responses against different load cases. Only Gayzik et al. (2007) validated the material model of an impact on a rat lung model against experiments.

All simulations of the material model strain-energy function terminated with an error and only one of the simulated viscoelastic material models terminated normally but with a stiff material characteristic. The best material model from literature was doubtlessly low density foam with the load curve according to Mendoza-Vazquez et al. (2012).

The parameter study enhanced the model response of the strain-energy function model and the viscoelastic material model, but both material models could not reach the quality of the material model of THUMS v3-M.

The parameter study of low density foam enhanced the deformation characteristic but worsened the force response. Therefore an optimization of the load curve was carried out. The final model had an enhanced deformation and force response and the deforming characteristic of the model was also similar to the experiments. The biofidelity of the THUMS v3-M with the tuned viscera material properties was validated with the table top tests after Kent et al. (2004).

Finally, it can be said that the material model low density foam is best suitable as a material model for the simulation of lungs. This model outclassed the other material models in all aspects.

Unfortunately, it was not possible to modify this material model so that the response refers to the deformation and force data of the experiments. For a valid time versus deformation response too high forces occurred. Therefore a compromise between the deformation and force behaviour had to be found. Furthermore, the response for the impact speeds of  $4.4 \frac{m}{s}$  and  $6.1 \frac{m}{s}$  was not satisfactory.

## 5.3 Classification of the Results

In this section it will be discussed how the findings of the simulations of impact experiments with swine lungs can be compared with human lungs. Furthermore it will be discussed why a model of the thoracic viscera of THUMS v3.0 was used and where the limitations of a lung models are.

### 5.3.1 Comparability Between Human Lungs, Swine Lungs and the Lungs Model

For the simulations in this thesis, it was assumed that the experimental results of swine lungs can be compared with human lungs. Kramer et al. (2012) measured the size of human lungs inside the body by using computer tomography images. According to his results, the total average size of human male lungs is  $5.858 \pm 1.094$  l ( $2.738 \pm 0.533$  l for the left lung and  $3.121 \pm 0.605$  l for the right lung). With a capacity of 3.443 l the size of one modelled lung volume is bigger than the left lung including the upper boundary but inside the volume span of the right lung. With 6.886 l the total volume of both thoracic contents is also within the span of the total average size of male human lungs. Thus, the viscera approximately has the size of a human lung and can therefore be used for the validation of lung materials.

According to Schulte and Schumacher (2012) the volume of a deflated right lung is 1.5 l and 1.4 l for a left lung. With a volume of 2.7 l the volume of the visceral model after loading with gravity is clearly bigger. This can be explained by the different structure of an anatomic lung and the model. An anatomic lung is filled with air and the volume reduces when the lung deflates. If the air deflating is inhibited, the lung would only be compressed through its own weight. A modelled lung consists only of volume elements and no air can stream out.

The maximum thickness of the impact area of the swine lungs in the experiments by Hayamizu et al. (2003) was  $129 \pm 16$  mm. The thickness of the swine lungs was kept constant to the in vivo size over air insufflation. These conditions could not be modelled in the simulations. Thus, the model thickness was reduced through gravity to a thickness of 100 mm in the impact area. The original model inside the chest has a maximum thickness of 153 mm and a minimum thickness of 111 mm. With 132 mm the average thickness is close to the experimental swine lungs thickness.

Among other parameter, the strain-energy function takes the typical alveolar diameter into account. The typical alveolar diameter for a human male is 0.2 mm. According to Lum and Mitzner (1987), the typical alveolar diameter of a swine is smaller with a length of 0.133 mm. However, this was the biggest diameter of all mammals investigated in the publication of Lum and Mitzner (1987). From this point of view, swine lungs appear suitable for animal experiments with the aim of transferring the results to human lungs.

For their lung tissue experiments Hoppin Jr. et al. (1975) and Vawter et al. (1978) used dog lung parenchyma. Only Zeng et al. (1987) used human lung parenchyma for his experiments. The resulting stress versus strain curves of Vawter et al. (1978) and Zeng et al.

(1987) are more similar than the curve from Hoppin Jr. et al. (1975). Consequently, it can be said that the experimental set up has a much higher influence of the experimental outcome than the used specimen.

In conclusion, the size, the alveolar diameter and the experimental results of Hoppin Jr. et al. (1975), Vawter et al. (1978) and Zeng et al. (1987) support the conclusion, that experiments with animal lungs, especially with swine lungs, can be compared with human lungs.

### 5.3.2 THUMS v3.0 Lung Model

The target of this thesis is to compare different material models for lungs and to modify and validate a material model with experimental data. Thus a model of the thoracic viscera from THUMS v3.0 was used. The thoracic viscera are modelled out of two volumes filling out the chamber inside the thoracic cage. These volumes represent the lungs, trachea and bronchi as well as the heart and great vessels. The lungs taking up by far the most volume of all viscera in the thoracic cage.

In THUMS v4.0 and also some other FE-HBMs the thoracic organs are already separately modelled. There is one main reason why the latest models were not used. The current model is used for the THORAX project at Chalmers University of Technology and by several companies for automotive safety research. Therefore, it was necessary to validate the lung model of THUMS v3.0 so that the results can be used for current research projects. There are several aspects and different parts in the THUMS v3-M that can be optimized. To validate further modifications of the thorax it is important to have a valid response of the viscera. The lungs are the biggest organ in the thoracic cage and therefore they can influence the thoracic response substantially.

Furthermore, the comparison and evaluation of different material models is not connected to a specific model. The material model low density foam was clearly identified as the best material model for lungs. This knowledge can easily be transferred to different lung models.

## 5.4 Injury Prediction

Injury prediction with ATDs on the basis of detected deformation with the VC is widely accepted, especially for bones. The VC was developed for ATDs and their limitations of instruments. With new ATDs like THOR the availability of more detailed deformation data has increased and new injury criteria need to be developed. In their publication Song et al. (2011) proposed with the Collision Deformation Classification (CDC) a new criterion which is taking the higher information rate like multidimensional deformation information into account.

The advantage of bone injury prediction compared to lung injuries is, that an fractured bone can easily be detected in experiments. To develop a new kind of injury criterion for hard and soft tissues the measurement of injury related parameters, like stress, strain,

bending, shear and torsion, during experiments is necessary.

The difficulty of developing a valid soft tissue injury criteria is that the detection of stresses and strains related to soft tissue damage in cadaver impact tests, may be difficult, if not impossible, Ruan et al. (2003). Furthermore, only lung laceration injuries can easily be detected in cadaver experiments. Detecting contusion injuries in cadavers is very challenging. In a contusion capillaries are damaged and blood can seep into the tissue. Because blood does not circulate in cadavers, the damaged tissue is hard to identify. Pulmonary contusion leads to lung dysfunction and can be fatal.

An advantage of FE-HBMs over the ATDs is that HBMs offer a more detailed description of the human anatomy. In FE models stresses and strains can be calculated but tissue damage can not be estimated unless valid tissue failure criteria are established.

Finding an injury criteria for lung contusion Gayzik et al. (2007) impacted lungs of living rabbits and the occurring PC were detected with CT images 24 hours after the impact happened. Gayzik found a high correlation between the calculated maximal principle strain multiplied with the strain rate ( $\epsilon_{max} * \dot{\epsilon}_{max}$ ) and the pulmonary contusion caused by the impactor.

The material parameters Gayzik et al. (2007) used for the rat lungs were validated against the force versus displacement response to the impactor at a speed of  $5 \frac{m}{s}$ . The results are limited by the lack of validation for more than a single loading scenario. The possibility of transforming the injury metric to human lungs also needs to be investigated.

The material parameters from Gayzik et al. (2007) were simulated in this thesis, but the simulation terminated after 0.015 s with an error (cf. Section 4.1.1). However, after 0.015 s the lung was already deformed 10 mm more than in the experiments. Thus, the material behaved more softly than the swine lungs in the experiments by Hayamizu et al. (2003).

The injury threshold Ruan et al. (2003) identified in his publication took only the visible lung laceration damages of cadaver experiments into account. The simulation in this thesis with the material properties from Ruan et al. (2003) also terminated after 0.015 s. In this moment the deformation was 4 mm higher than the swine lungs in the experiments by Hayamizu et al. (2003), which means a slightly softer material behaviour.

Finally it can be said, that the injury prediction for lungs is a challenging task. It is not possible to measure stresses and strains of the lungs in cadaver experiments which are related to tissue damage. Also in cadaver experiments only laceration damages can be detected.

Usually PC occur before lungs lacerate which means at a lower deformation level or deformation speed. A PC can already lead to several or fatal injuries, therefore it is very important to develop an injury criterion which can also reliably predict lung laceration and PC. However, to identify PC in vivo further experiments are necessary and the transformation of the results to human lungs need to be investigated.

# 6 Conclusions

In this chapter it will shortly be summarized what was done in this thesis, which results were obtained due to the simulations and which knowledges were gained in context with the literature research.

In the second part suggestions for prospective experiments and for further investigations on lung models will be given.

## 6.1 Summary

The purpose of this study was to compare and to improve the model response of a lung model to enhance the quality of a current HBM. Therefore impact experiments with swine lungs by Hayamizu et al. (2003) were used.

For the validation the thoracic organs from the THUMS v3-M were used. The material model with the best results was low density foam. This material model was improved by modifying the stress versus strain curve and adapting the material parameter. The final model was implemented in THUMS v3-M and the biofidelity of the thoracic response was validated against table top tests.

At the beginning of the thesis extensive literature research was carried out. The state of the art of FE-HBM and of thoracic models in general and of lung models in particular was identified. Three different material models were mainly used for lung modelling but not even one publication compared or rated the quality of these material models.

The quality, level of details and biofidelity of HBM is increasing continuously. For example, the number of elements increased from THUMS v1 to THUMS v4 from 80 000 elements to 2 000 000 elements. In THUMS v4 internal organs like heart and lungs are already anatomically represented. Single parts, like an isolated rib or a ligament, were improved and validated against experiments.

So far the thoracic organs were mainly used to optimize the thoracic response for the validation of the whole thorax against PMHS experiments. No validations of an isolated human lung model under frontal car crash like conditions were performed.

The availability of experiments with whole lungs for the validation of a human lung model for frontal car crashes is very limited. Only two publications measured the deformation and force response of impact experiments with animal lungs. One of these publications used in vivo rat lungs and the other post mortem swine lungs. Because of the different size compared to human lungs and the specific experimental procedure of the rat lungs experiments, only the experiments of Hayamizu et al. (2003) suited for the validation of a human lung model.

These experiments by Hayamizu et al. (2003) were simulated for this thesis with the thoracic organs of THUMS v3.0. Several material models used for lung modelling in different publications, which were identified in the first part of the thesis, were implemented

in the lung model. Most of the models terminated with an error, showed a too soft or too stiff material behaviour or the model deformed peculiarly.

To improve the model response a coefficient study with the material parameter of the different material models was conducted. The most promising material model was low density foam with the load curve from Mendoza-Vazquez et al. (2012). This material model was modified and a new load curve was implemented to enhance the model response compared to the impact experiments.

The deformation and force response of the optimized material model was much better compared to the best model from literature. The deformation characteristic and the resulting forces were close to the experiments at an impact speed of  $5.4 \frac{m}{s}$ . For an impact speed of  $4.4 \frac{m}{s}$  and  $6.1 \frac{m}{s}$  the responses of the modified model could not be improved. The deformation versus force responses were quite different to the experimental results. This conspicuous behaviour was unexpected and might be explained by the varying impact energy or the dependency of dumping to velocity.

The optimized material model was implemented in the thoracic viscera in THUMS v3-M and the table top tests by Kent et al. (2004) were simulated to verify the biofidelity. Furthermore the influence of modified material properties of the thoracic organs on the thoracic response was investigated.

No differences were seen for the first 20 mm of chest compression. A slightly stiffer behaviour was determined later. Nevertheless, the thoracic response remained clearly in the experimental corridor of Kent et al. (2004) for all load cases.

To enhance the quality of restraint systems the influence of improvements needs to be investigated. Therefore ATDs and HBMs are used. The advantage of HBMs is, that e.g. organs are represented and more detailed information like stresses and strains can be obtained for different parts of the body. By the help of this information it is possible to predict injuries if a valid injury criterion is available.

A valid lung injury criterion is not available yet. This is due to the difficulty of measuring the stresses and strains causing injuries and the detection of PC in cadaver experiments. In a HBM with validated thorax and lungs it might be possible to detect the stresses and strains causing injuries.

The investigation of the force and deformation behaviour of a lung model, done in this study is a remarkable first step on the way to a validated lung models.

## 6.2 Future Work

The availability of experiments for the validation of a human lung model is very limited. Only the experiments by Hayamizu et al. (2003) are applicable for the validation of a lung model for frontal car crash investigations. However, the experiments were carried out with a higher velocity than the chest is compressed in RTCs and some further information, e.g. about the deformation characteristic are missing. Therefore it is absolutely essential that new experiments are designed and carried out.

The experimental realization of dropping an impactor on a lung by Hayamizu et al. (2003) is basically a good idea. Also the choice of using swine lungs is reasonable because of the similarity to human lungs. Despite the ethic concerns, to carry out at least some further investigations should be carried out with human subjects to investigate the comparability of human lungs and swine lungs. Additionally, some parts of the experiments need to be revised.

In a RTC high decelerations and forces occur due to high velocities. Two thirds of all accidents happen between  $36 \frac{km}{h}$  EES and  $65 \frac{km}{h}$  EES. The risk of a moderate thorax injury (AIS 2+) is already nearly 30 % for an EES speed of  $56 \frac{km}{h}$  to  $65 \frac{km}{h}$ , Carroll (2009).

The chest deflection speed measured with PMHS in a sled test at  $48 \frac{km}{h}$  is  $1 \frac{m}{s}$ , Kent et al. (2004).

Therefore the impact speed should be adjusted to the lower impact speeds to obtain valid information for the lungs behaviour in frontal RTCs with lower speeds as well. Furthermore either the impact speed should be varied with a fixed impactor weight or the impactor weight should be changed adequately to the impact velocity. Also, the scope of the experiments should be increased because two specimens per impact speed is too little to obtain valid information.

Hayamizu et al. (2003) inflated the lungs to the in vivo lungs height for the whole experiments. In further experiments it might be reasonable to open a valve at the moment of impact to allow the air to escape.

Finally, the injuries of the lungs should be studied after the experiments to gain more information for injury prediction, at least for lung laceration damages. Because no blood circulates in ex vivo lungs PC is very difficult, if not impossible to detect.

The simulation of the experiments should also be repeated with the new experimental data. Furthermore, in future simulations a lung model which anatomically represents the lung should be used. If swine lungs are used for the experiments, it also might be recommendable to use a swine lung model as well to investigate the comparability of swine lungs and human lungs.

# References

- Alaa K. Abbas, Ashraf F. Hefny, and Fikri M. Abu-Zidan. Seatbelts and road traffic collision injuries. *World J Emerg Surg*, 6(1):18, 2011. doi: 10.1186/1749-7922-6-18. URL <http://dx.doi.org/10.1186/1749-7922-6-18>.
- A. Al-Mayah, J. Moseley, and K. K. Brock. Contact surface and material nonlinearity modeling of human lungs. *Phys Med Biol*, 53(1):305–317, Jan 2008a. doi: 10.1088/0031-9155/53/1/022. URL <http://dx.doi.org/10.1088/0031-9155/53/1/022>.
- A. Al-Mayah, J. Moseley, M. Velec, and K. K. Brock. Effect of friction and material compressibility on deformable modeling of human lung. *Springer-Verlag Berlin Heidelberg*, pages 98–106, 2008b.
- J. D. Bean, C. J. Kahane, M. Mynarr, R. Rudd, C. J. Rush, and C. Wiacek. Fatalities in frontal car crashes despite seat belts and air bags - review of all cds cases - model and calendar years 2000 - 2007 - 122 fatalities. *Office of Vehicle Safety National Highway Traffic Safety Administration*, 2009.
- Statistisches Bundesamt. Accidents and casualties covered, Sep 2012. URL [https://www.destatis.de/DE/ZahlenFakten/Wirtschaftsbereiche/TransportVerkehr/Verkehrsunfaelle/Tabellen\\_/Strassenverkehrsunfaelle.html](https://www.destatis.de/DE/ZahlenFakten/Wirtschaftsbereiche/TransportVerkehr/Verkehrsunfaelle/Tabellen_/Strassenverkehrsunfaelle.html).
- J. A. Carroll. Matrix of serious thorax injuries by occupant characteristics, impact conditions and restraint type and identification of the important injury mechanisms to be considered in thorax and thomo; consisting of one main summary report and three annexes. *COVER D5 Main Summary Report*, 1:55, 2009.
- R. Cuerden, R. Cookson, P. Massie, and M. Edwards. A review of the european 40configuration. *Proceedings of the 20th international technical conference on the Enhanced Safety of Vehicles (ESV)*, 2007.
- Patrick A. Forbes. Development of a human bod model for the analyses of side impact automotive thoracic trauma. Master's thesis, University of Waterloo, 2005.
- J. Foster, J. Kortge, and M. Wolanin. Hybrid iii - a biomechanically based crash test dummy. *Stapp Car Crash J*, (21):975–1014, 1977.
- Y. C. Fung. *Biomechanics - mechanical properties of living tissues*. Springer Verlag New York, 2 edition, 1993.
- Y. C. Fung, Tong Pin, and Paul Patitucci. Stress and strain in the lung. *Journal of the Engineering Mechanics Dicision*, page 23, 1978.
- F. S. Gayzik. *Development of a finite element based injury metric for pulmonary contusion*. PhD thesis, Virginie Tech - Wake Forest University School of Biomdical Engineering & Sciences, Aug 2008.

- F. S. Gayzik, J Jason Hoth, Melissa Daly, J Wayne Meredith, and Joel D. Stitzel. A finite element-based injury metric for pulmonary contusion: investigation of candidate metrics through correlation with computed tomography. *Stapp Car Crash J*, 51:189–209, Oct 2007.
- F. S. Gayzik, J Jason Hoth, and Joel D. Stitzel. Finite element-based injury metrics for pulmonary contusion via concurrent model optimization. *Biomech Model Mechanobiol*, 10(4):505–520, Jul 2011. doi: 10.1007/s10237-010-0251-5. URL <http://dx.doi.org/10.1007/s10237-010-0251-5>.
- F. S. Gayzik, D. Moreno, N. Vavalle, A. Rhyne, and J. Stitzel. Development of a full human body finite element model for blunt injury prediction utilizing a multy-modality medical imaging protocol. *12th International LS-DYNER Users Conference, Dearborne, Michigan*, 2012.
- Quentin Grimal, Salah Naili, and Alexandre Watzky. A high-frequency lung injury mechanism in blunt thoracic impact. *J Biomech*, 38(6):1247–1254, Jun 2005. doi: 10.1016/j.jbiomech.2004.06.010. URL <http://dx.doi.org/10.1016/j.jbiomech.2004.06.010>.
- Norwiyuki Hayamizu, Isao Watanabe, Toshikazu Ishihara, and Kazuo Miki. Measurement of impact response of pig lung. *Toyota Central R&D Labs., Inc. Japan*, page 2, 2003.
- C. W. Hayes, W. F. Conway, J. W. Walsh, L. Coppage, and A. S. Gervin. Seat belt injuries: radiologic findings and clinical correlation. *Radiographics*, 11(1):23–36, Jan 1991.
- L. R. Herrmann and F. E. Peterson. A numerical procedure for viscoelastic stress analysis. *Seventh Meeting of ICRPG Mechanical Behaviour Working Group, Orlando, FL*, (177), 1968.
- M. H. Holmes. Finite deformation of soft tissue: Analysis of a mixture model in uni-axial compression. *J. of Biomechanical Engineering*, 8:372–381, 1986.
- K. Holmqvist. Chest injury in heavy vehicle frontal collisions - evaluation and adaptation of the hybrid iii dummy instrumentation and injury reference values by means of human body modeling. thesis for the degree of licentiate, applied mechanics, traffic safety, chalmers university of technology, gothenburg, sweden. 2009.
- F. G. Hoppin Jr., G. C. Lee, and S. V. Dawson. Properties of lung parenchyma in distortion. *J Appl Physiol*, 39(5):742–751, Nov 1975.
- Yue Huang. *Automotive side impact protection: Biomechanical issues*. Dissertation, Wayne State University, 1995.
- Richard Kent, David Lessley, and Chris Sherwood. Thoracic response to dynamic, non-impact loading from a hub, distributed belt, diagonal belt, and double diagonal belts. *Stapp Car Crash J*, 48:495–519, Nov 2004.
- Hideyuki Kimpara, Jong B. Lee, King H. Yang, Albert I. King, Masami Iwamoto, Isao Watanabe, and Kazuo Miki. Development of a three-dimensional finite element chest model for the 5(th) percentile female. *Stapp Car Crash J*, 49:251–269, Nov 2005.

- W. Klanner. Status report and future development of the euro ncap programm. *International Technical Conference in the Enhanced Safety Vehicle Conference*, page 6, Jun 2001.
- Gary H. Kramer, Kevin Capello, Brock Bearrs, Aimee Lauzon, and Lysanne Normandeau. Linear dimensions and volumes of human lungs obtained from ct images. *Health Phys*, 102(4):378–383, Apr 2012. doi: 10.1097/HP.0b013e31823a13f1. URL <http://dx.doi.org/10.1097/HP.0b013e31823a13f1>.
- C. K. Kroell, D. C. Schneider, and A. M. Nahum. Impact tolerance and response of the human thorax ii. *Society of Automotive Engineers*, (741187):383–457, 1974.
- Y. Lanir and Y. C. Fung. Two-dimensional mechanical properties of rabbit skin. i. experimental system. *J Biomech*, 7(1):29–34, Jan 1974.
- I. V. Lau and D. C. Viano. The viscous criterion - bases and applications of an injury severity index for soft tissues. *J Biomech*, (5):123–142, 1986.
- V. K. Lau and D. C. Viano. Influence of impact velocity and chest compression on experimental pulmonary injury severity in rabbits. *J Trauma*, 21(12):1022–1028, Dec 1981.
- G. C. Lee and A. Frankus. Elasticity properties of lung parenchyma derived from experimental distortion data. *Biophys J*, 15(5):481–493, May 1975. doi: 10.1016/S0006-3495(75)85832-2. URL [http://dx.doi.org/10.1016/S0006-3495\(75\)85832-2](http://dx.doi.org/10.1016/S0006-3495(75)85832-2).
- Livermore. *LS-DYNA Keyword User's Manual Volume II Material Models*. Livermore Software Technology Corporation (LSTC), Livermore Software Technology Corporation P. O. Box 712, 971 r6.1.0 edition, Aug 2012.
- Emmanuel Lizee, S. Robin, Eric Song, Nicolas Bertholon, and Jean-Yves Le Coz. Development of a 3d finite element model of the human body. *42nd Stapp Car Crash Conference Proceedings (P-337)*, page 25, 1998.
- Stephen H. Loring, Richard E. Brown, Andrew Gouldstone, and James P. Butler. Lubrication regimes in mesothelial sliding. *J Biomech*, 38(12):2390–2396, Dec 2005. doi: 10.1016/j.jbiomech.2004.10.012. URL <http://dx.doi.org/10.1016/j.jbiomech.2004.10.012>.
- H. Lum and W. Mitzner. A species comparison of alveolar size and surface forces. *J Appl Physiol*, 62(5):1865–1871, May 1987.
- F. L. Matthews and J. B. West. Finite element displacement analysis of a lung. *J Biomech*, 5(6):591–600, Nov 1972.
- Manuel Mendoza-Vazquez. *Rib and Thoracic Response in Frontal Car Crashes: A study Using a Finite Element Human Body Model*. Thesis for the degree of licentiate of engineering, Chalmers University of Technology Department of Applied Mechanics, Vehicle Safety Division, 2012.

- Manuel Mendoza-Vazquez, Karin Brodin, and Johan Davidsson. Human rib response to different restraint systems in frontal impacts: a study using a human body model. *International Journal Crashworthiness*, 2012.
- Krystoffer Mroz, Ola Bostrom, Bengt Pipkorn, Jac Wismans, and Karin Brodin. Comparison of hybrid iii and human body models in evaluating thoracic response for various seat belts and aribag loading conditions. *IRCOBI Conference Hannover*, page 16, 2010.
- Daisuke Murakami, Seiichi Kobayashi, Toshikazu Torigaki, and Richard Kent. Finite element analysis of hard and soft tissue contributions to thoracic response: sensitivity analysis of fluctuations in boundary conditions. *Stapp Car Crash J*, 50:169–189, Nov 2006.
- A. M. Nahum and Melvin. Accidental injury biomechanics and prevention. *Springer-Verlag Inc., New York*, 2002.
- NHTSA. Seat belt use in 2008 - use rates in the states and territories. *National Center for Statistics & Analyses*, Apr 2009. URL <http://www-nrd.nhtsa.dot.gov/Pubs/811106.PDF>.
- NHTSA. Drivers involved in fatal crashes by vehicle type, and restraint use - state : Usa, year : 2010. *National Center for Statistics & Analyses*, 2010. URL <http://www-fars.nhtsa.dot.gov/People/PeopleRestrains.aspx>.
- M. Peden, R. Scurfield, D. Sleet, and C. Mathers A. Hayder, E. Jarwan. World report on road traffic injuries prevention. *World Health Organization Geneva*, 2004. URL [http://www.who.int/violence\\_injury\\_prevention/publications/road\\_traffic/world\\_report/summary\\_en\\_rev.pdf](http://www.who.int/violence_injury_prevention/publications/road_traffic/world_report/summary_en_rev.pdf).
- B. Pipkorn and R. Kent. Validation of a human body thoax model and its use for force, energy ad strain analyses in various loading conditions. *International IRCOBI Conference on the Biomechanics of Impact, Krakow, Poland*, pages 210–223, 2011.
- Gordon R. Plank, Michael Kleinberger, and Rolf H. Eppinger. Analytical investigation of driver thoracic response to out of position airbag deployment. *42nd Stapp Car Crash Conference Proceedings (P-337)*, page 16, 1998.
- E. P. Radford and J. W. Remington. Recent studies of mechanical properties of mammalian lungs. *Tissue Elasticity*, pages 177–190, 1957.
- Jack C. Roberts, James V. O'Connor, and Emily E. Ward. Modeling the effect of non-penetrating ballistic impact as a means of detecting behind armor blunt trauma. *J Trauma*, 58(6):1241–1251, Jun 2005.
- Jesse Ruan, Raed El-Jawahri, Li Chai, Saeed Barbat, and Priya Prasad. Prediction and analysis of human thoracic impact responses and injuries in cadaver impacts using a full human body finite element model. *Stapp Car Crash J*, 47:299–321, Oct 2003.
- M. Schuenke, E Schulte, and U. Schumacher. *Atlas of Anatomy - Neck and Internal Organs*. Thieme, 2006.

- E. Schulte and U. Schumacher. *Prometheus - LernAtlas der Anatomie, Innere Organe*, volume 3. Thieme, 2012.
- Kenji Shigeta, Yuichi Kitagawa, and Tsuyoshi Yasuki. Development of next generation human fe model capable of organ injury prediction. *Toyota Central R&D Labs., Inc. Japan*, (09-0111):20, 2009.
- E. Song, E. Lecuyer, and X. Trosseille. Development of injury criteria for frontal impact using a human body fe model. *International Technical Conference in the Enhanced Safety Vehicle Conference, June 13-16, Washington, D.C., USA*, 2011.
- Susan Standring, H. Ellis, J. C. Hely, D. Johnson, and A. Williams. *Gray's Anatomy - The Anatomical Basis of Clinical Practice*, volume 39. Elsevier, 2005.
- John D. States. Abbreviated injury scale (ais) revision. *American Association for Automotive Medicine*, 1990.
- Joel D. Stitzel, F Scott Gayzik, J Jason Hoth, Jennifer Mercier, H Donald Gage, Kathryn A. Morton, Stefan M. Duma, and R Mark Payne. Development of a finite element-based injury metric for pulmonary contusion part i: model development and validation. *Stapp Car Crash J*, 49:271–289, Nov 2005.
- S. H. Sundaram and C. C. Feng. Finite element analysis in the human thorax. *J Biomech*, 10(8):505–516, 1977.
- S. M. Tenney and D Bartlett, Jr. Comparative quantitative morphology of the mammalian lung: trachea. *Respir Physiol*, 3(2):130–135, Oct 1967.
- S. M. Tenney, S. M. and J. E. Remmers. Comparative quantitative morphology of the mammalian lung: diffusing area. *Nature*, 197:54–56, Jan 1963.
- Toyota. Total human model for safety (thums) - am50 pedestrain/occupant model academic version 4.0-20111003. Technical report, Toyota Motor Corporation, 2011.
- D. L. Vawter. A finite element model for macroscopic deformation of the lung. *J Biomech Eng*, 102(1):1–7, Feb 1980.
- D. L. Vawter, Y. C. Fung, and J. B. West. Elasticity of excised dog lung parenchyma. *J Appl Physiol*, 45(2):261–269, Aug 1978.
- D. L. Vawter, Y. C. Fung, and J. B. West. Constitutive equation of lung tissue elasticity. *Biomechanical Engineering*, 101:8, 1979.
- P. Vezin and J. Verriest. Development of a set of numerical human models for safety. *International Technical Conference in the Enhanced Safety Vehicle Conference, Washington, D.C., USA*, 2005. URL <http://www-nrd.nhtsa.dot.gov/pdf/esv/esv19/05-0163-O.pdf>.
- Hui-Chang K. Wang. *Development of a side impact finite element human thoracic model*. Dissertation, Wayne State University, Detroit, Michigan, 1995.

- J. Wismans, R. Happee, and J. A. W. Dommelen. Computational human models for safety. *International Technical Conference in the Enhanced Safety Vehicle Conference, Washington, D.C., USA*, pages 417–429, 2005.
- King H. Yang, Jingwen Hu, Nicholas A. White, Albert I. King, Clifford C. Chou, and Priya Prasad. Development of numerical models for injury biomechanics research: a review of 50 years of publications in the stapp car crash conference. *Stapp Car Crash J*, 50:429–490, Nov 2006.
- Michael R. T. Yen. *Development of Thorax Model Sub-project-C: Mechanical Properties of Human Heart, Lung and Aorta*. PhD thesis, Department of Biomedical Engineering of University of Memphis, 1999.
- Y. J. Zeng, D. Yager, and Y. C. Fung. Measurement of the mechanical properties of the human lung tissue. *J Biomech Eng*, 109(2):169–174, May 1987.
- Jay Zhao and Gopal Norwani. Development of a human body finite element model for restraint system r&d applications. *TAKATA - Automotive System Laboratory, Inc.*, page 13, 2004.

# Appendix A

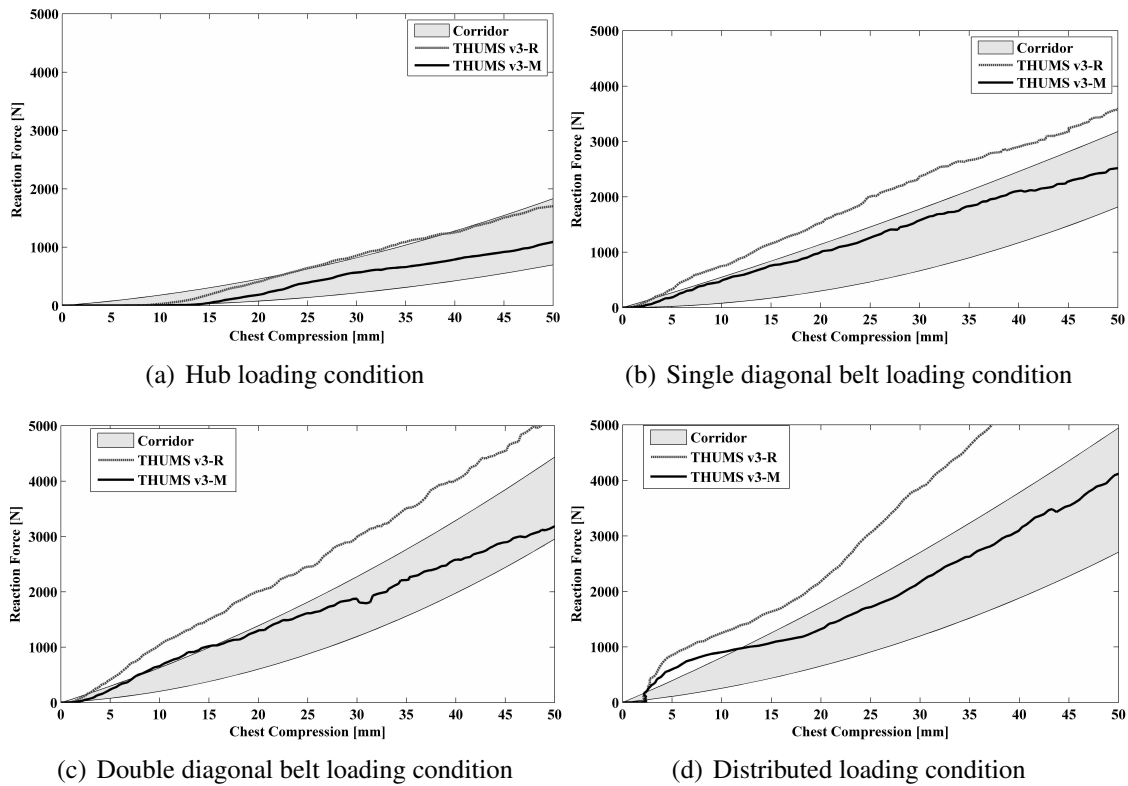


**Figure 6.1:** Force versus compression response for THUMSv3-R and THUMS v3-M, Mendoza-Vazquez et al. (2012), and the experimental table top corridors by Kent et al. (2004)

# Appendix B

**Table 6.1: Material properties for lung tissue**

Author (Year)	material behaviour	Poisson's r. $\nu$	Density $\rho$ [ $\frac{kg}{m^3}$ ]	Young's mod. $E$ [ $\frac{N}{mm^2}$ ]	Bulk mod. $K$ [ $\frac{N}{mm^2}$ ]
Matthews and West (1972)	non-linear homogenous	0.2 - 0.4	230		
Lee and Frankus (1975)	strain-energy function	0.46			
Sundaram and Feng (1977) Vawter et al. (1979)	non-linear homogenous strain-energy function	0.45		0.0017	
Zeng et al. (1987)	strain-energy function				
Huang (1995) Wang (1995)	soft viscous isotropic homogenous non-linear stress-strain curve	0.47	1000 600	0.0084	
Lizee et al. (1998)	viscoelastic				
Grimal et al. (2005)	homogenous, isotropic linear-elastic	0.3	600	0.7130	
Al-Mayah et al. (2008a)	strain-energy function		430	0.0078	
Al-Mayah et al. (2008b)	strain-energy function	0.35 - 0.4		0.0037	
Gayzik et al. (2007)	strain-energy function		118		0.1384
Gayzik (2008)	strain-energy function		118		0.1124
Shigeta et al. (2009)	LS-DYNA: Mat_elastic_fluid		129		1.4

Author (Year)	Coefficients and curve fit parameter	Reference
Matthews and West (1972)		Mead (1961), Setnikar (1955) Radford and Remington (1957) Hoppin Jr. et al. (1975)
Lee and Frankus (1975)	$a_1 = -21.06; a_2 = 19.76; a_3 = -7.88; a_4 = 1.062;$ $b_1 = 2.673; b_2 = -0.350; c_1 = 1.324; c_2 = -1.94; c_3 = 0.943$	
Sundaram and Feng (1977) Vawter et al. (1979)	$c = 3.51; a_1 = 1.69; a_2 = 2.77; a_4 = 0.62$ (loading) and $c = 0.45; a_1 = 2.71; a_2 = 9.13; a_4 = 1.23$ (unloading)	Matthews and West (1972)
Zeng et al. (1987)	$c = 11.8; a_1 = 0.43; a_2 = 0.56; a_4 = 0.32; a = 0.5$ (loading) $c = 8.8; a_1 = 0.53; a_2 = 0.69; a_4 = 0.39; a = 0.63$ (unloading)	Fung et al. (1978)
Huang (1995) Wang (1995) Lizee et al. (1998)		Vawter (1979) Plank et al. (1998)
Grimal et al. (2005)	$c_p = 40 \frac{m}{s}; c_s = 21 \frac{m}{s}$	
Al-Mayah et al. (2008a) Al-Mayah et al. (2008b)	$c = 11.8; a_1 = 0.43; a_2 = 0.56; a_4 = 0.32$ $c = 1.187e^{-3}; c_1 = 1.949e^{-5}; c_2 = 1.918;$ $\alpha = 0.4451; \beta = -3.95; \Delta = 0.0702$	Zeng et al. (1987) Vawter (1978 & 1980)
Gayzik et al. (2007)	$c = 5.035e^{-4}; c_1 = 6.535e^{-6}; c_2 = 2.876;$ $\alpha = 8.227e^{-2}; \beta = -2.46; \Delta = 0.0702$	
Gayzik (2008)		
Shigeta et al. (2009)	Nominal Strain [%] - Nominal Stress [kPa]: 10% = 5.4kPa; 20% = 12.4kPa; 30% = 28kPa; 50% = 374.9kPa; $\nu_c = 0.1$	Hayamizu (2003)

# Declaration

I hereby declare that I am the sole author of this thesis. I have only used the resources given in the list of references.

Rostock, 26<sup>th</sup> of March 2013

---